ORGANIC ENRICHMENT AT AQUEOUS INTERFACES STUDIED WITH NON-LINEAR SPECTROSCOPY: COOPERATIVE ADSORPTION OF SOLUBLE SACCHARIDES TO LIPID MONOLAYERS

by

Katie Ann Link

A dissertation submitted in partial fulfillment
of the requirements for the degree

of

Doctor of Philosophy

in

Chemistry

MONTANA STATE UNIVERSITY
Bozeman, Montana

May 2019

DEDICATION

This thesis is dedicated to my family. Your love and support were essential. I would not be here if it were not for your sacrifices.

To my mom for always being there and for encouraging and nurturing my reading habit.

To my dad for never getting too angry when I took apart his solar powered lawn lights to power my video games, encouraging my interest in computers, and making me work for what I wanted.

To my grandmother for introducing me to crafting and making.

To my grandfather and uncle for introducing me to baseball, Star Wars, and Star Trek. If not for their choosing Thursday night television, filled heavily with a female scientist Star Trek captain, I do not know if I would have considered becoming a scientist "cool".

To my siblings for putting up with me and to my brother especially for the constant competition that pushed us both to great heights.

To Dr. Joe, for letting me be a normal kid. I think this degree is at least partially his fault.

ACKNOWLEDGEMENTS

First, I would like to thank my graduate advisor, Dr. Rob Walker. His guidance, support, and sense of humor were essential for my growth as a scientist and as a person. Working for Rob has been a wicked good time—I could not ask for a better PI and I am sad to move on from this gnarly adventure. I also want to thank my committee members, Dr. Erik Grumstrup, Dr. Aleks Rebane, and Dr. Timothy Minton, for their insight and support. I would like to thank Dr. Doreen Brown for her support throughout this degree.

Thank you to the members of the Walker Research Group—both past and present. Specifically, Dr. Melissa McIntyre and Grace Purnell for creating a safe environment to ask any (even basic) questions and for thoughtful discussions on virtual states and pulse overlap. To Gabrielle Spurzem for being a fantastic research assistant.

I am also thankful for the friends I have made in graduate school. To Jac Miller—even if you do not count as my plus one, I never would have made it through graduate school without your friendship. To Aoife Casey, my roommate, who cooked many of the potatoes that fueled this thesis writing, for her support.

To Camp Rising Sun (CRS)—I never could speak in public until I became a clown at CRS. I am indebted to the loving and safe environment of CRS for my success as an adult. To Dr. Elizabeth Christophy who first got me excited about chemistry. To Dr. Nancy Breen for mentoring me through college. To Dr. Lynetta Mier, for teaching me the ways of laser alignment and convincing me that I belonged in graduate school.

TABLE OF CONTENTS

TABLE OF CONTENTS CONTINUED

TABLE OF CONTENTS CONTINUED

LIST OF TABLES

Table Page

LIST OF FIGURES

Figure Page

LIST OF FIGURES CONTINUED

Figure Page

LIST OF FIGURES CONTINUED

Figure Page

NOMENCLATURE

DPPC:	1,2-dipalmitoyl-*sn*-glycero-3-phosphocholine
DMPE:	1,2-dimysistoyl-*sn*-glycero -3-phosphoethanolamine
GA:	Glucosamine
GU:	Glucuronic Acid
Tre:	Trehalose
Phe:	Phenylalanine
DMS:	Dimethyl sulfide
VSFG:	Vibrational Sum Frequency Generation
DSC:	Differential Scanning Calorimetry
FTIR:	Fourier Transform Infrared Spectroscopy
SSML:	Sea Surface Microlayer
SSA:	Sea Spray Aerosol
CCN:	Cloud Condensation Nuclei
IN:	Ice Nuclei
OCEANFILMS:	Organic Compounds from Ecosystems to Aerosols: Natural Films and Interfaces via Langmuir Model Surfactants

ABSTRACT

Field measurements of sea spray aerosols have reported high concentrations of soluble organic material that are in excess of the concentration of soluble organics in the ocean. The studies described in this dissertation investigated a possible mechanism for this increase deemed cooperative adsorption. The cooperative adsorption mechanism describes an interaction between an insoluble Langmuir monolayer at the aqueous/vapor interface and soluble organic molecules that would not normally be enriched at the surface. In this model, the soluble organics are drawn to the surface through non-covalent interactions with the lipid surfactant. This mechanism was investigated with the surface specific nonlinear optical technique, vibrational sum frequency generation spectroscopy. These optical measurements were coupled with surface tension measurements and differential scanning calorimetry measurements.

To study cooperative adsorption, model systems were used; these were composed of a phosphatidylcholine lipid surfactant, DPPC, and soluble saccharides including glucosamine, glucuronic acid, and trehalose. Glucosamine, in both a positive and neutral state, induced ordering in both expanded and condensed DPPC monolayers, supporting cooperative adsorption as a mechanism. Glucuronic acid, an anion, ordered lipid monolayers in the limits that the lipid DPPC was moderately packed and there were no competing ions in solution. Trehalose, a larger, uncharged saccharide showed, through ordering the DPPC monolayer, indications of cooperative adsorption in moderately packed DPPC when the trehalose concentration was sufficiently high. These results support cooperative adsorption as a mechanism for the accumulation of soluble organics in sea spray aerosols with some limitations.

CHAPTER ONE

INTRODUCTION

1.1 Motivation

"…there's one issue that will define the contours of this century more dramatically than any other, and that is the urgent threat of a changing climate." Barack Obama, September 23, 2014, U.N. Climate Change Summit

Climate change is a wicked problem[1-2]—since the 19th century, the average global temperature has increased by ~0.9°C, with 5 of the warmest years on record occurring in this decade.[3-5] Snow cover in the Northern Hemisphere is decreasing and melting earlier,[6-7] glaciers are retreating,[8-9] the thickness and amount of Artic sea ice is declining,[10-14] and the global sea level is rising.[15] Even more troubling is that the rates of these processes are accelerating: the global sea level has been rising at a rate of ~3 ± 0.025 mm/y since 1993 resulting in a rise of ~7 cm over the last 25 years, but satellite altimeter data extrapolations predict an acceleration of this rate by 0.084 ± 0.025 mm/y^2.[15] In addition to sea level changes, global warming is also increasing ocean surface temperature and affecting ocean precipitation, wind, nutrient, and circulation patterns.[16]

Understanding climate change's impact on weather, agriculture and ecosystems requires accurate, predictive models.[16] Currently, these models are used to make climate projections that try to capture a broad range of possible scenarios including emissions, speciation, temperature changes and human choices. To increase the reliability of climate

models and develop more accurate predictive capabilities, researchers systematically add new processes to these models based on field research and observations from sources including polar ice sheets, terrestrial ground cover, and ocean ecosystems.[17-18]

Climate models that incorporate contributions from ocean ecosystems require knowledge about molecular and biochemical behavior for accurate parameterization. For example, dimethyl sulfide (DMS) is produced by marine organisms and DMS contributes to sulfates in sea spray aerosols (SSA).[19] Changes in marine ecosystems, including phytoplankton physiology and community structure, impact DMS transfer to the atmosphere that subsequently affects the quantity of sulfates in aerosols and the number of cloud condensation nuclei (CCN). Despite extensive field studies and sophisticated models, numerous questions remain about relationships between ocean biology and climate science. In particular, researchers have noted that SSA often show enriched organic content well above what would be predicted based on simple oceanic abundance. Even allowing for enhanced concentrations of surface active solutes in the sea surface microlayer (SSML), the amount of organic matter in SSA can be 10-100x greater than expected.[20]

This increase in soluble organics in SSA has pronounced and far reaching effects on the Earth's radiative budget and therefore is an important parameter in climate studies.[21] SSA serve as CCN,[22-24] ice nuclei (IN),[25-28] and affect cloud formation,[29-30] cloud albedo (proportion of incident light that is reflected),[29, 31-32] and precipitation cycles.[33-34] Furthermore, clouds have a greenhouse effect; the Earth receives, on average, 175 PW of energy from the sun. Clouds and the surface reflect approximately 31% of this

energy back into space.[35] Sea salt particles may make up as much as 90% of cloud condensation nuclei in marine regions.[36] With the oceans making up to 72% of the Earth's surface, changes in sea spray content will alter cloud composition and result in changes in cloud albedo, which will impact atmospheric heating.

Understanding the possible mechanisms responsible for organic accumulation in SSA requires knowledge about the SSML and the formation of aerosols from this boundary. The SSML is a thin film at the ocean surface ranging from 20-400 μm in thickness that is chemically distinct from seawater because of the high organic matter content as compared to bulk ocean conditions.[37-38] This SSML is enriched with saccharides relative to sodium by as much as a factor of 16. Despite this enrichment, however, organic content in the SSML still lags the ~10^2-10^3-fold enrichment measured in fine ($PM_{2.5}$) and coarse ($PM_{10-.25}$) SSA.[20] SSA can be produced via several mechanisms at the sea surface.[39] The smallest particles (< 1 μm diameter) are called film droplets and are produced from bubbles bursting at the ocean surface. This bubble bursting event leaves behind a void, that can produce a jet that produces jet drops with a diameter typically between 2 and 20 μm. These two mechanisms produce particles in the size range that is the most effective in creating long-lived aerosols, as larger particles have short lifetimes. Other SSA production mechanisms include larger particles such those formed from spume torn off of wave crests, usually in high winds, and splash drops that can propagate the formation of more SSA by bursting bubbles and forming jets when they recombine with the ocean surface.

That these SSA have anomalously high organic content is not in doubt. A multitude of independent, boat-based field measurements that include analysis by FTIR, Quadrupole Aerosol Mass Spectroscopy, and Scanning Transmission X-ray Microscopy with Near Edge X-ray Absorption Fine Structure (STXM-NEXAFS), all report unusually high organic content in fresh SSA.[36, 40] The origin of these high concentrations is not obvious. Potential enrichment mechanisms have included marine colloidal particles being swept to the surface by rising bubbles coupled with Langmuir adsorption behavior, but field measurements find that the organic accumulation is more efficient than a Langmuir adsorption model.[37] Determining the underlying mechanism of this accumulation is important because higher organic content in SSA leads to more effective cloud nucleation that directly effects radiative forcing.

Recently, climate modelers introduced a mechanism to describe how highly soluble organic molecules could be drawn to the surface and driven into SSA.[18, 37] This mechanism, termed cooperative adsorption (Figure 1.1), describes interactions between an insoluble Langmuir monolayer adsorbed to the aqueous/vapor interface and soluble organics that would not normally be enriched at the surface. In this mechanism, lipids and other insoluble organics at the surface draw soluble species to the surface predominantly through noncovalent interactions including simple dipolar coupling, hydrogen bonding, and Coulombic attraction. The cooperative adsorption mechanism differs from the traditional picture of molecular adsorption from the gas phase onto solid surfaces in that the Langmuir adsorption model for gases assumes a fixed number of equivalent surface sites that can only adsorb one molecule per site. This Langmuir adsorption is in a

dynamic equilibrium and full adsorption results in monolayer coverage. The cooperative adsorption mechanism examined in this dissertation does not require fixed and/or uniform adsorption sites. Instead, soluble saccharides are drawn to an insoluble monolayer already adsorbed to the aqueous/vapor interface. The saccharides are attracted to the insoluble monolayer by noncovalent interactions and create a sublayer with distinctively higher local concentrations and anisotropic structure relative to bulk solution species. The cooperativity between the lipid and saccharide is a relatively mild effect and has been found to be on the order of single to tens of kJ/mole.

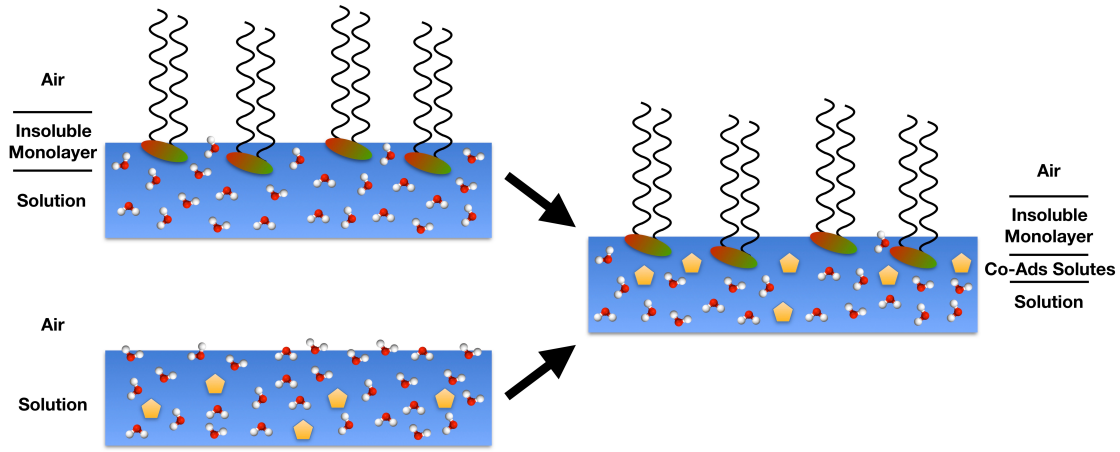

Figure 1.1 Schematic of cooperative adsorption. A film of insoluble molecules is at the air/aqueous interface (left top and right). Soluble saccharides (pentagons) remain dispersed in solution without the insoluble monolayer (left bottom). When the insoluble monolayer is on a solution containing the soluble saccharides (right) the soluble organic molecules are drawn to the insoluble film, displacing water molecules from the lipid solvation shell, and enriching organic content at surface.

An early version of the cooperative adsorption model was incorporated into the OCEANFILMS (Organic Compounds from Ecosystems to Aerosols: Natural Films and Interfaces via Langmuir Model Surfactants) package, a computational model used to predict SSA composition.[18] This package was updated to OCEANFILMS-2 with the

incorporation of vibrational sum frequency generation (VSFG) data from a tightly packed phosphocholine on an aqueous solution of glucosamine (GA) to improve agreement of the modeled sea spray aerosol composition with field measurements of SSA. This experimental study correlated a decrease in hydrogen-bound water with increasing GA accumulation at the surface. Data were fit with a Langmuir adsorption model with a $C_{1/2}$=0.00126 ± 0.00045 M. This experimental result was incorporated into OCEANFILMS-2 with the inclusion of a two-layer adsorption cooperative adsorption model. Work described in the following chapters tests the limits of this model by investigating the tendency of other soluble saccharides with different charges to cooperatively adsorb to aqueous interfaces covered with lipid films that vary in surface coverage and headgroup identity. The work presented utilizes non-linear vibrational spectroscopy, surface tension measurements, and differential scanning calorimetry to examine and clarify mechanisms responsible for saccharide/lipid interactions.

The following sections provide a description of the experimental methods used in these studies of cooperative adsorption with particular emphasis placed on VSFG. Additional methods described include surface tension measurements and differential scanning calorimetry (DSC). The chapter concludes with brief descriptions of the individual studies conducted in our laboratory at Montana State University (MSU) as well as experiments performed at the Environmental Molecular Science Laboratory (EMSL) user facility at Pacific Northwest National Laboratory (PNNL) in Richland, WA.

1.2 Model Systems

To test the cooperative adsorption hypothesis, model systems of surfactants and soluble saccharides were used. Glucosamine (GA) was chosen as an ocean-relevant saccharide because this saccharide is the monomer unit of chitosan. GA has a pKa of 7.58; in Millipore solutions with pH 5.8, GA is predominately positively charged. In buffer solutions with pH 9.0, GA is neutral. To further study charged-based cooperative adsorption effects, glucuronic acid, pKa 3.3,[41] was selected because of this anionic saccharide's ocean relevance as a monomer unit of alginate. To study the cooperative effects of a neutral, disaccharide, trehalose was chosen. Trehalose is found in the blood of shrimp and some insects as well as a component in some plants. Trehalose has also drawn attention for its ability to serve as a cryoprotectant for lipid membranes. For the lipid surfactant, the zwitterion DPPC was used, because this lipid is the main component of mammalian cells and lung surfactant and is prevalent in the ocean. Structures of these molecules appear in Figure 1.2.

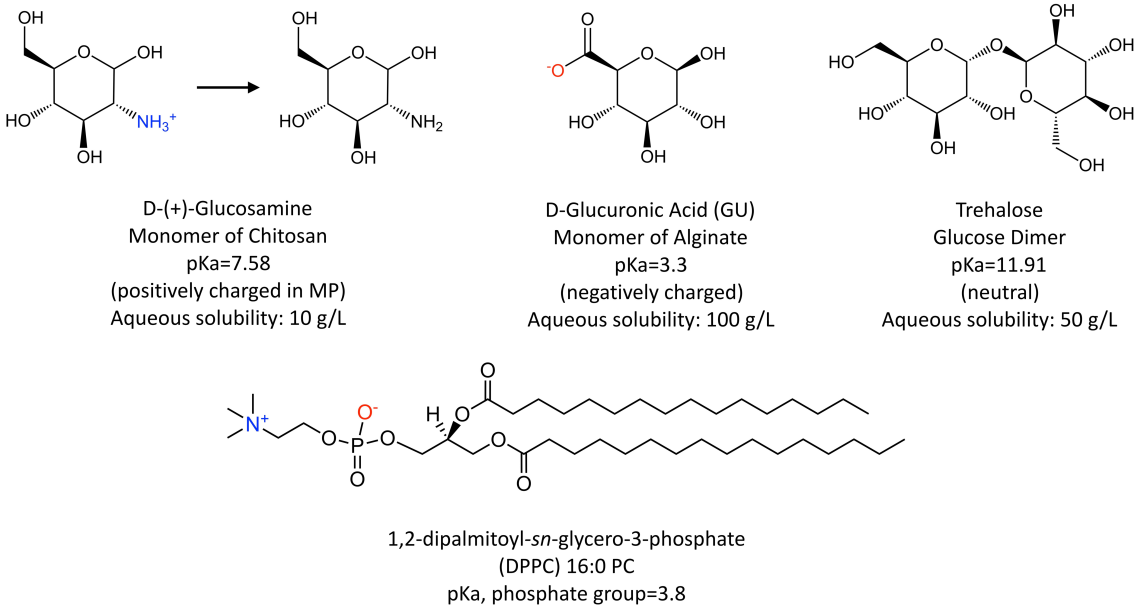

Figure 1.2 Molecular structures of the soluble saccharides (top row) and the lipid (bottom row) used to study the cooperative adsorption hypothesis. Glucosamine has a pKa of 7.58 and is positively charged in Millipore solutions and neutral in buffer.[42] Glucuronic acid has a pKa of 3.3 and is negatively charged in all studies in this work.[41] Trehalose, with a pKa of 11.91, is neutral.[43-44] The lipid surfactant, DPPC, is zwitterionic in the Millipore and buffer conditions in this work.[45]

1.3 Vibrational Sum Frequency Generation

The primary experimental technique used in these studies testing cooperative adsorption mechanisms is vibrational sum frequency generation (VSFG) spectroscopy. Within the electric dipole approximation, VSFG is a surface specific technique used to acquire vibrational spectra from liquid-vapor, solid-liquid, and liquid-liquid interfaces. In 1987, results from the first experiments using VSFG were published Shen and coworkers. This seminal work probed C-H vibrations from methanol and pentadecanoic acid adsorbed on glass (air/solid) interfaces and water (air/liquid) interfaces.[46] A decade later,

Walker *et. al.* published the first VSFG data acquired from lipid monolayers.[47] This work marked the first use of surface specific vibrational spectroscopy to link conformational order in biologically relevant systems with film composition and temperature. Related work was conducted by the Allen group in 2006 and investigated structural differences between expanded and condensed monolayers composed of DPPC, the main lipid component of lung surfactant.[48] Currently, VSFG lipid research has expanded include interactions with cations,[49-50] interactions via cooperative adsorption,[18, 51-52] and interactions of environmentally relevant systems.[18, 51, 53-55]

1.3.1 VSFG Theory

Vibrational sum frequency generation is a coherent, second order nonlinear, surface specific spectroscopy technique that is well described in literature.[56-69] This technique arises from the nonlinear effects that accompany the interaction of intense optical fields with molecules and materials. The nonlinear effects can be described starting with fundamentals.[64, 70] Light, as it travels through a medium, has an electric field that induces an electric dipole (**μ**) in the valence electrons of molecules. In an isotropic medium **μ** is given by:

$$\boldsymbol{\mu} = \boldsymbol{\mu}_o + \alpha \mathbf{E} \quad (1.1)$$

where is $\boldsymbol{\mu}_o$ is the static dipole and α is the polarizability of the electrons. In the condensed phase, the sum of the molecular electric dipoles results in the bulk polarization **P**. The polarization induced by the oscillating electric field is:

$$\mathbf{P} = \varepsilon_o \chi^{(1)} \mathbf{E} \quad (1.2)$$

where ε_o is the vacuum permittivity and $\chi^{(1)}$ is the average of α and is also known as the linear first-order susceptibility.

With a higher energy electric field, the molecular dipole moment's higher order terms become significant.[28] For these additional terms, β and γ are the coefficients for the second order and third order hyperpolarizabilities, respectively.[64]

$$\boldsymbol{\mu} = \boldsymbol{\mu}_o + \alpha\mathbf{E} + \beta\mathbf{E}^2 + \gamma\mathbf{E}^3 \quad (1.3)$$

Likewise, the polarization contains higher order terms for non-linear susceptibilities: [56, 64]

$$\mathbf{P} = \varepsilon_o\left(\chi^{(1)}\mathbf{E} + \chi^{(2)}\mathbf{E}^2 + \chi^{(3)}\mathbf{E}^3\right). \quad (1.4)$$

When the applied electromagnetic field is on the order of the field experienced by the electrons in a molecule, these higher order, nonlinear terms become important. Sum frequency generation is one consequence that results from the second order nonlinear susceptibility, $\chi^{(2)}$.[64]

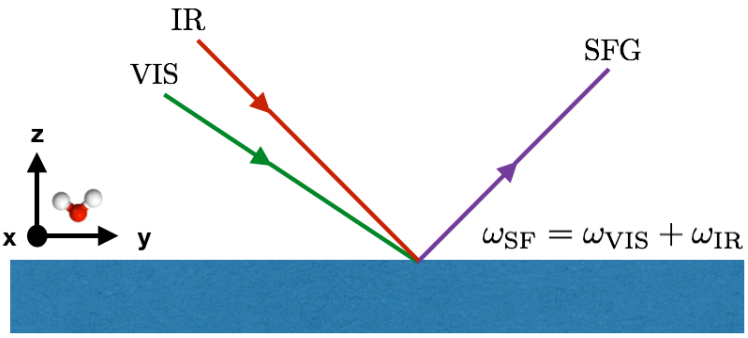

Figure 1.3 The fixed frequency visible beam and the tunable infrared beam are overlapped in space and time to induce a coherent polarization in the interfacial molecules. This generates a beam with a frequency that is the sum of the two incident frequencies.

Sum frequency generation is a two-pulse technique. Two laser pulses of different frequencies (ω_1 and ω_2) are matched in space and time at the surface of interest. Typically,

one pulse is at a visible frequency and the other is at an IR frequency. The surface electric field **E** is given as a sum of the two incident oscillating electric fields:[64]

$$\mathbf{E} = \mathbf{E}_1 \cos\omega_1 t + \mathbf{E}_2 \cos\omega_2 t \quad (1.5)$$

The second order polarization can be written as:

$$\mathbf{P}^{(2)} = \varepsilon_o \chi^{(2)} (\mathbf{E}_1 \cos\omega_1 t + \mathbf{E}_2 \cos\omega_2 t) \quad (1.6)$$

The second order polarization, when expanded becomes:

$$\mathbf{P}^{(2)} = \varepsilon_o \chi^{(2)} \left[(\mathbf{E}_1^2 + \mathbf{E}_2^2) + (\mathbf{E}_1 \cos\omega_1 t + \mathbf{E}_2 \cos\omega_2 t) + \left(\frac{1}{2} \mathbf{E}_1 \mathbf{E}_2 \cos(\omega_1 - \omega_2)\, t \right) + \left(\frac{1}{2} \mathbf{E}_1 \mathbf{E}_2 \cos(\omega_1 + \omega_2)\, t \right) \right] \quad (1.7)$$

The two incident fields create a DC field (the first piece, $\mathbf{E_1^2 + E_2^2}$), sum harmonic generation ($\mathbf{E_1^2}\cos 2\omega_1 t + \mathbf{E_2^2}\cos 2\omega_2 t$), difference frequency generation ($1/2\ \mathbf{E_1 E_2}\cos(\omega_1 - \omega_2)t$), and sum harmonic generation ($1/2\ \mathbf{E_1 E_2}\cos(\omega_1 + \omega_2)t$). In SHG, two photons share the same frequency and combine to produce photons with a frequency equal to the sum of the two incident frequencies. In DFG, light is emitted at the difference between the two input frequencies and in SFG the light is emitted at the sum of the incident frequencies.[64]

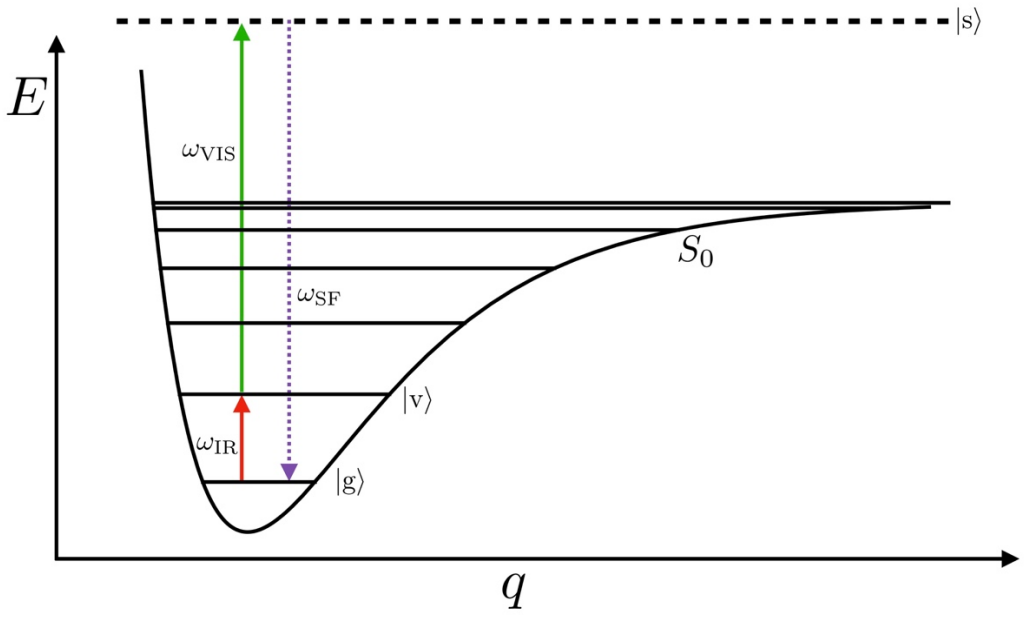

Figure 1.4 Energy level diagram for resonant enhanced SFG. When the frequency of the infrared light is near a vibrational mode of an interfacial molecule the second order non-linear susceptibility approaches zero (see Equation 1.11).

In this second order polarization equation, only the second order non-linear susceptibility, $\chi^{(2)}$, changes significantly when the IR frequency is resonant with allowed vibrational transitions.[64] Thus, this is the term that contains the vibrational information from a sum frequency spectrum. This is evident when examining the equation for the molecular hyperpolarizabilities, β, the term for which $\chi^{(2)}$ is the average of. This equation is applicable in the limit that the IR frequency is near a vibrational resonance and the visible frequency is not energetic enough to induce an electronic transition. In this equation, ω_v is the visible frequency, ω_{IR} is the IR frequency, and Γ^{-1} is the relaxation time of the vibrationally excited state in resonance with the visible input frequency. $M_{\alpha\beta}$ is the Raman transition moment and A_γ is the infrared transition moment which provides the condition that molecules must be both Raman and IR active to produce a SF response.

$$\beta_{\alpha\beta\gamma} = \frac{1}{2\hbar}\frac{M_{\alpha\beta}A_{\gamma}}{(\omega_v - \omega_{\mathrm{IR}} - i\Gamma)} \qquad (1.8)$$

The surface specificity of SFG arises from the nonlinear susceptibility, $\chi^{(2)}$. As a third rank tensor, $\chi^{(2)}$ has 27 components. In a centrosymmetric environment, all directions are equivalent so $\chi^{(2)}_{ijk} = \chi^{(2)}_{-i-j-k}$. For a third rank tensor, a change in the sign of ijk is equivalent to reversing the axis of the system or $\chi^{(2)}_{ijk} = -\chi^{(2)}_{-i-j-k}$. To satisfy both of these conditions $\chi^{(2)}_{ijk}$ must equal 0 which results in SFG being forbidden in centrosymmetric environments such as bulk media. Surfaces and boundaries between two media are non-centrosymmetric and are SF active.

For a planar isotropic surface that is symmetric about the surface normal, $z \neq -z$, but $y \equiv -y$ and $x \equiv -x$. Since the $y \equiv -y$ and $x \equiv -x$, a change in sign of x or y would not change the sign of $\chi^{(2)}_{ijk}$ if this is taken into account with $\chi^{(2)}_{ijk} = -\chi^{(2)}_{-i-j-k}$, the 27 possibilities for $\chi^{(2)}_{ijk}$ reduce to four independent nonzero possibilities for generating a SF signal.

$$\chi^{(2)}_{zxx} \equiv \chi^{(2)}_{zyy} \quad \chi^{(2)}_{xzx} \equiv \chi^{(2)}_{yzy} \quad \chi^{(2)}_{xxz} \equiv \chi^{(2)}_{xxz} \quad \chi^{(2)}_{zzz} \quad (1.9)$$

The electric field of the electromagnetic wave incident on a molecular interface can be resolved into components that are polarized parallel (P) and perpendicular (S) to the plane of incidence.[56, 64] Thus, with P polarized light there are *x* and *z* components and with S polarized light the only component is in the *y* direction. The convention for SFG is to list the polarizations of the electromagnetic waves in order of decreasing wavelength (SF, VIS, IR).[56] The incident polarizations that can produce a SF response are then SSP, SPS, PSS, and PPP.

The SF intensity is proportional to the second order polarization and the second order non-linear susceptibility. The effective second order non-linear susceptibility is composed of the non-resonant ($\chi^{(2)}_{NR,eff}$), effective second order susceptibility strength factor $\left(\chi^{(2)}_{q,eff}\right)$, resonant frequency $\left(\omega_q\right)$, and damping constant of the qth vibrational mode $\left(\Gamma_q\right)$.

$$I_{SF} \propto \left|P^{(2)}\right|^2 \propto \left|\chi^{(2)}_{eff}\right|^2 \qquad (1.10)$$

$$\left|\chi^{(2)}_{eff}\right|^2 = \left|\chi^{(2)}_{NR,eff} + \sum \frac{\chi^{(2)}_{q,eff}}{\omega_{IR}-\omega_q+i\Gamma_q}\right|^2 \qquad (1.11)$$

$$I_{SF} \propto |\chi^{(2)}_{NR,eff} + \sum \frac{\chi^{(2)}_{q,eff}}{\omega_{IR}-\omega_q+i\Gamma_q} + (\chi^{(3)}_1 + i\chi^{(3)}_2)\Phi(0)|^2 \qquad (1.12)$$

When the IR frequency is on resonance with a vibrational mode, the denominator of $\chi^{(2)}_{eff}$ approaches zero, which significantly enhances the SF intensity. Recent studies have shown that at charged interfaces the interfacial potential, $\Phi(0)$, can lead to mixing of the second order and third order nonlinear susceptibilities ($\chi^{(2)}$ and $\chi^{(3)}$).[71-72] This mixing can influence SF lineshapes and intensities (Equation 1.12). The contributions of this $\chi^{(2)}/\chi^{(3)}$ mixing on SF lineshapes and intensities can be calculated using Mathematica workbooks that are available for download.[71] Our analysis on $\chi^{(3)}$ showed slight changes in lineshapes and band positions in the C-H stretching region at low saccharide concentration for the methyl Fermi resonance and the methyl asymmetric stretch, 2940 cm^{-1} and 2960 cm^{-1}, respectively. Our analysis of lipid film organization did not utilize these peaks and instead focused on the methyl and methylene symmetric stretch transitions at 2872 cm^{-1} and 2948 cm^{-1}, respectively. These two symmetric stretch

transitions were not changed systematically outside of experimental uncertainties due to $\chi^{(3)}$ mixing, thus the analysis in this work only includes effects from $\chi^{(2)}$.

For a VSFG response, molecules need to be in a non-centrosymmetric environment. Interfaces differ from bulk in that they are not centrosymmetric, making SFG a valuable surface technique. In addition, for molecules to be SFG active, they must have normal modes that are simultaneously Raman and IR active (Equation 1.8). The polarization of the IR light also limits what vibrational excitations occur—with P polarized incident IR sampling those vibrations having IR transition moments normal to the surface and S polarized IR light probing vibrational moments parallel to the surface. For the lipids studied in this work, monolayer organization was assessed largely on the basis of VSFG spectra acquired under $S_{sum}S_{vis}P_{IR}$ polarization conditions that sampled vibrations aligned normal to the surface. Under these circumstances, vibrational signals from methyl groups dominated the spectra of well-ordered films given that this organization had methyl groups directed along the surface normal and the vibrational moments associated with the methylene groups were both in plane and subject to local inversion symmetry about the middle of the carbon-carbon bonds in the all-*trans* chains The saccharides used are not measurably surface active (in that they do not prefer the surface to the bulk solution). GA does have one methylene group, but vibrational signature from this group was never observed with VSFG, implying that this functional group was either aligned in plane or randomly distributed for cooperatively adsorbed solutes. Trehalose does show a VSFG response that is much smaller in intensity than the response from DPPC.

1.3.2 VSFG Experimental Assemblies

Three VSFG systems were used in this work. Two of the systems are located at PNNL's EMSL facility. The first of these setups was the EKSPLA scanning SFG. This system is a commercially available SFG spectrometer and has been described elsewhere.[62, 73-76] Briefly the EKSPLA has a Nd:YAG laser (EKSPLA PL2251A-50) which is used to produce the fundamental output: a 29 ps pulse at 10 Hz. Part of this fundamental is sent to an optical parametric amplifier (OPA) to produce tunable IR light that can be adjusted from 650 cm to 4300 nm. The other part of the fundamental is converted from the output 1064 nm to a visible beam at 532 nm. This visible beam serves as the upconversion signal for SFG experiments. All O-H vibrational spectra presented in this work were taken on this system.

The second system utilized at the PNNL EMSL facility was the High Resolution Broad Band Sum Frequency Generation Vibrational Spectroscopy system (HR-BB-SFG-VS). This system has been described elsewhere.[77] Briefly, this system uses two Ti:sapphire oscillators/amplifiers: a sub-40 fs Micra-5 (Coherent Inc.) and a 100 ps 76 MHz TIGER (Time-Bandwidth Inc.). These oscillators are electronically synchronized (Synchrolock-AP, Coherent Inc.) and they seed two regenerative amplifiers: the Coherent Legend Elite HE-ps and the Coherent Legend Elite DUO which produce 1.6 W and 7.5 W respectively. The 40 fs pulses are used to pump a Coherent OPerA Solo optical parametric amplifier to produce the IR source. The 100 ps pulse is used to as the 800 nm source. The 800 nm and IR beam are focused onto the sample at 45° and 55°, respectively from surface normal. The SF response is isolated and collected in a

monochromator (Andor Technology, Belfast, Shamrock 750 mm, 1200 lines/mm grating) and CCD (Andor Technology, Newton 971P, back-illuminated).

The VSFG setup at MSU was redesigned as a part of this work. This redesign was intended to both increase the resolution from the previous design (See Figures 1.7 and 1.8) and to add versatility to the system. The versatility improvements included moving the sample stage area to a vertical breadboard to allow for the addition of a mini Langmuir trough as a sample holder and to have easily adjustable angles for the visible and IR light to hit the sample stage.

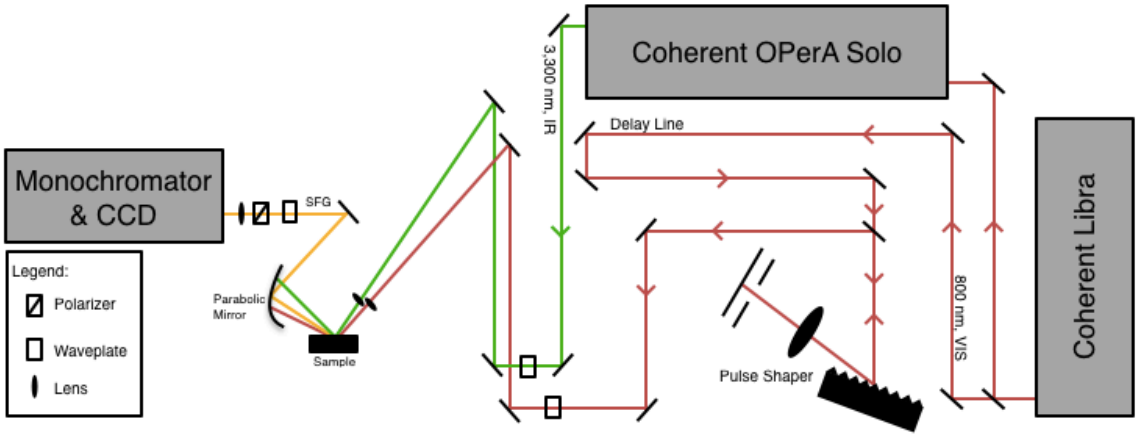

Figure 1.5 Schematic of the redesigned MSU sum frequency generation setup. The major resolution increasing upgrades include the grating (1,400 g/mm) and a long (25 cm) focal length lens in the pulse shaper.

A description of the MSU VSFG apparatus follows. The setup is built around a regeneratively amplified Ti:sapphire laser (Libra, Coherent, 3.4 W, 85 fs pulse duration, 1 kHz repetition rate). The output of this 800 nm laser is split 80/20 with a beam splitter; the 80% portion is directed into a Coherent OPerA Solo OPA. The OPerA Solo is used in

difference frequency mode to produce tunable, broadband IR frequency centered at ~3,300 nm. The remaining output of the Libra is used as the visible upconversion source.

To optimize the SF resolution, the 800 nm pulse is compressed with a 4f pulse shaper. The 4f shaper begins with a diffraction grating (1400 g/mm, blazed at 800, Spectragon) with high efficiency that was salvaged from the Libra Regen cavity. This stretches the beam in the laboratory x-y plane. The expanded beam is collimated with a 25 cm cylindrical lens and a mirror is placed at the focal length (FL) of this lens in a reflective geometry so that the light is reflected back through the same cylindrical lens. The beam on the return path is angled to reflect back at the bottom edge of the input beam so it can be separated after hitting the grating. The diffraction grating collimates the beam. This 4f pulse shaper is optimized using published methods.[78] After the positions of the 4f pulse shaper is optimized, an adjustable slit with a micrometer is placed as close to the reflective mirror as possible. The slit is adjusted to desired power/resolution ratio. After the spectrally narrowed beam goes through the pulse shaper it is steered into a vertical translation stage before going through a waveplate. The light is focused onto the sample with a 10 cm FL lens. To match up timing between the IR and VIS light, the vertical stage is adjusted until signal is found.

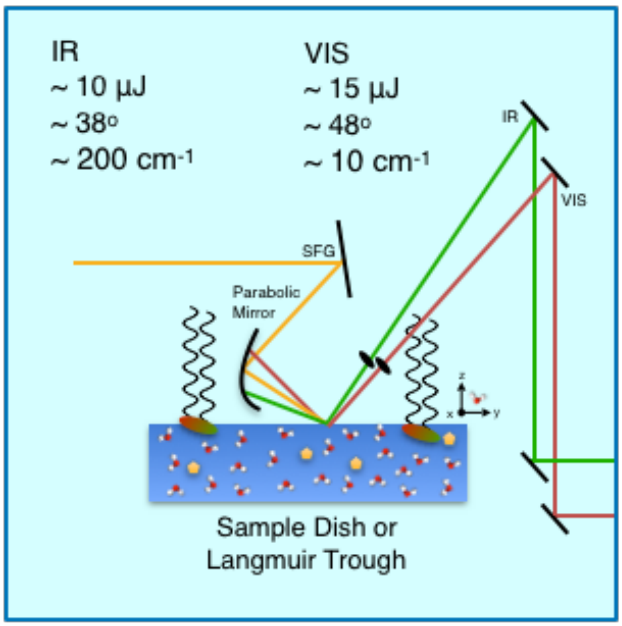

Figure 1.6 Expanded view of SFG sample area. The angle of the 800 nm visible beam is 48° and the 3.3 µm light is angled to the surface at 38°.

The IR light out of the OPerA Solo passes through a waveplate before being directed and focused on the sample area with a 10 cm FL lens (See Figure 1.6). The sample stage has 3 directional adjustment for ease of alignment to different samples. After the sample, the light is collected with a 90° off-axis parabolic mirror with a FL of 10 cm. Following this mirror, the IR and VIS light are blocked with filters and beam stops and SF signal is propagated through a waveplate and polarizer before being focused into the detector. The detector is a SpectraPro-300i by Acton Research Corporation with a 1340 x 100 pixel CCD (PIXIS100B, Princeton Instruments).

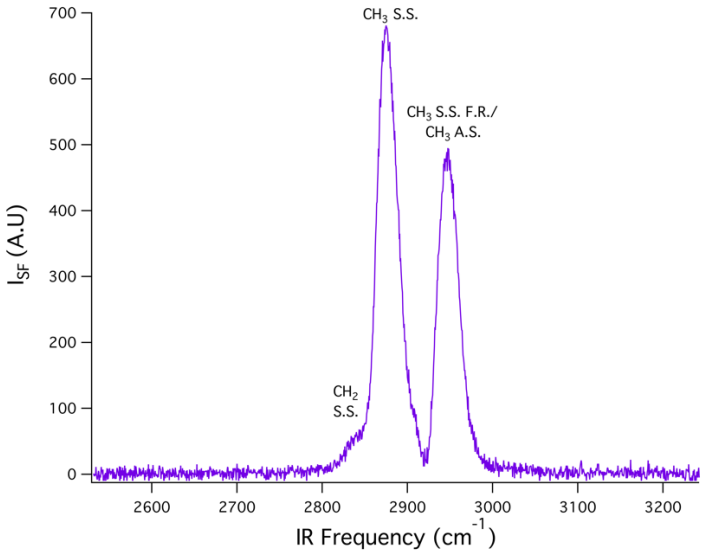

Figure 1.7 SFG spectra of 40 Å^2/molecule DPPC on Millipore water from the MSU SFG system before the system redesign. The CH_2 symmetric stretch (s.s.) at ~2850 cm^{-1} appears as a shoulder on the CH_3 s.s. peak at ~2880 cm^{-1}. The peak at ~2950 cm^{-1} is a convolution of the CH_3 s.s. Fermi resonance (F.R.) and asymmetric methyl stretches.

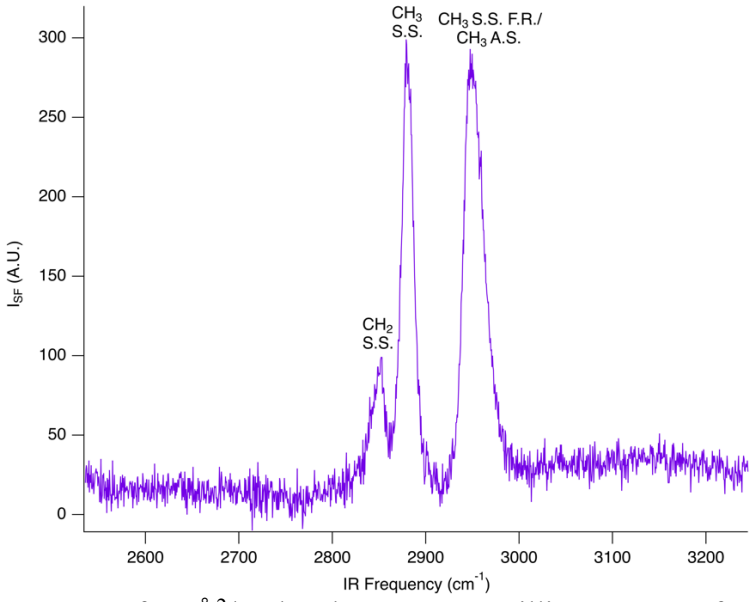

Figure 1.8 SFG spectra of 40 Å^2/molecule DPPC on Millipore water after the SFG system redesign. The resolution has improved and the CH_2 s.s. is clearly distinguished from the CH_3 s.s. peak.

1.4 Additional Methods

In order to acquire additional, complementary information about cooperative adsorption in these lipid/saccharide systems, two additional techniques were used to probe saccharide affinity for lipid monolayers and bilayers. One technique used a Wilhelmy plate/Langmuir trough assembly to measure the surface tension of monolayer systems on saccharide-containing solutions. The other method was differential scanning calorimetry (DSC) where experiments measured the effect(s) of saccharides in solution on lipid bilayer melting temperature.

1.4.1 Surface Tension

Surface tension measurements were done with a NIMA Langmuir trough (Model 302LL) with a NIMA PS4 pressure sensor/Wilhelmy plate and a Micro Processor Interface 104. With this instrument, lipid monolayers were dispersed on the aqueous solution of interest with a Hamilton glass syringe. After equilibration of the lipid constrained to the surface, the barriers were closed to compress the monolayer and surface pressure was recorded.

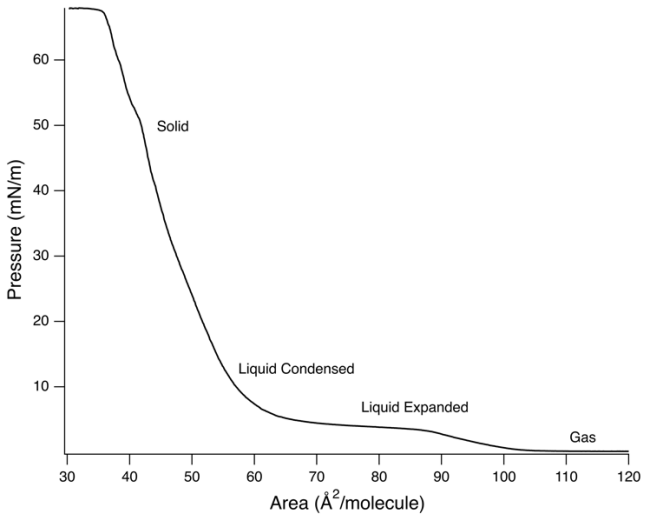

Figure 1.9 Representative π-A isotherm with two-dimensional phases labeled. The monolayer is in a two-dimensional gas phase when it is the most expanded. As the lipid is compressed it goes through a liquid expanded phase, followed by a liquid condensed phase, and then a solid phase before the monolayer eventually collapses.

Surface pressure is inversely related to surface tension via the following relationship.[79]

$$\pi = \gamma_0 - \gamma \quad (1.13)$$

In Equation 1.13, π is the surface tension, γ_0 is the surface pressure of the pure subphase, and γ is the surface pressure of the system of interest. For an ideal monolayer composed of two insoluble surfactants, thermodynamic quantities of such as Gibbs free energy of mixing can be calculated. In Equation 1.14, the Gibbs free energy of mixing is related to the area of the mixed monolayer (A_{12}), the area of a pure monolayer of the first surfactant (A_1), the area of a pure monolayer of the first surfactant (A_2), and the mole fraction of each of these species (χ_1 and χ_2).[80-81]

$$\Delta G^E_{mix} = \int_{\pi_1}^{\pi_2} N_A(A_{12} - x_1A_1 - x_2A_2)d\pi \quad (1.14)$$

In the case of the systems studied in this work, only one species is constrained to the surface, reducing the free energy equation to Equation 1.15.

$$\Delta G_{mix}^{E} = \int_{\pi_1}^{\pi_2} N_A(A_{12} - A_1)d\pi \qquad (1.15)$$

In the ideal case with molecules either constrained to the surface or free to be solvated in bulk solution, a negative Gibbs free energy of mixing is the result of a favorable, stabilizing interaction between the two species. The negative sign is a result of a condensing effect induced by adsorbed solutes or surfactants on the lipid monolayer constrained to the surface. The Gibbs free energy can also be zero, indicating that the subspecies has no net general effect on the lipid film properties. A positive Gibbs free energy of mixing is a result of an expansion of the lipid monolayer relative to the lipid monolayer on a pure aqueous sub-phase. In an ideal case with two species constrained to the surface (Equation 1.14) this behavior is the result of a repulsive interaction. The systems presented in this work are described most accurately by Equation 1.15, and do not account for saccharides being at the surface or for saccharides switching from bulk to surface (and vice versa) as the monolayer is condensed. For these systems, a positive ΔG_{mix}^{E}, requires the lipid molecules to have more space between them while simultaneously reducing the surface tension. These two observables lead to the hypothesis that the larger area per each lipid molecules is a result of the lipid interacting with the saccharide, in what is a favorable lipid-saccharide interaction in support of the proposed cooperative adsorption mechanism.

1.4.2 Differential Scanning Calorimetry

DSC measurements can provide information on lipid/saccharide interactions through changes in the energy required to induce a phase change in the lipid vesicles. These vesicles, when heated, go through a phase change from an ordered gel state to a more fluid liquid crystalline state (Figure 1.10). The peak of the heat flow vs. temperature data required to induce this phase transition is taken to be the system's gel-liquid crystalline transition temperature (T_m) and T_m increases when lipid membranes are dehydrated.[82]

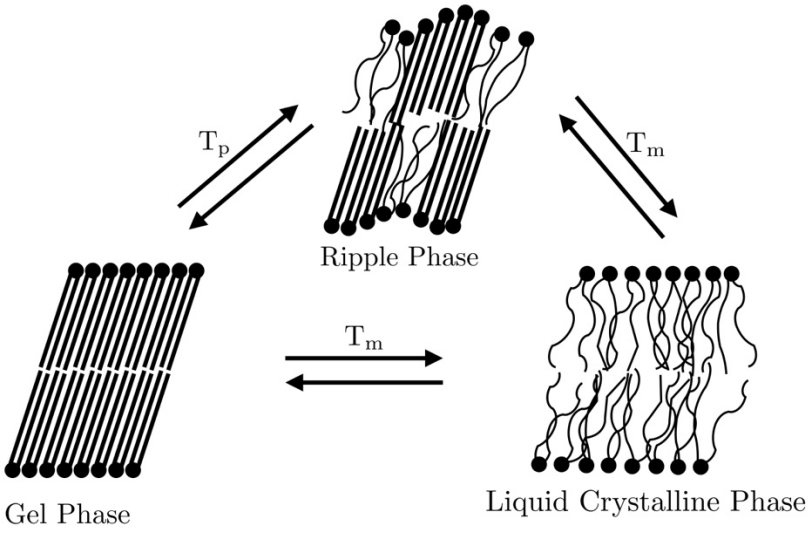

Figure 1.10 Phase transitions of a lipid bilayer. The lipid can go from an ordered, gel state, directly to a disordered, liquid crystalline state or an intermediate transition, called the ripple phase, can occur.

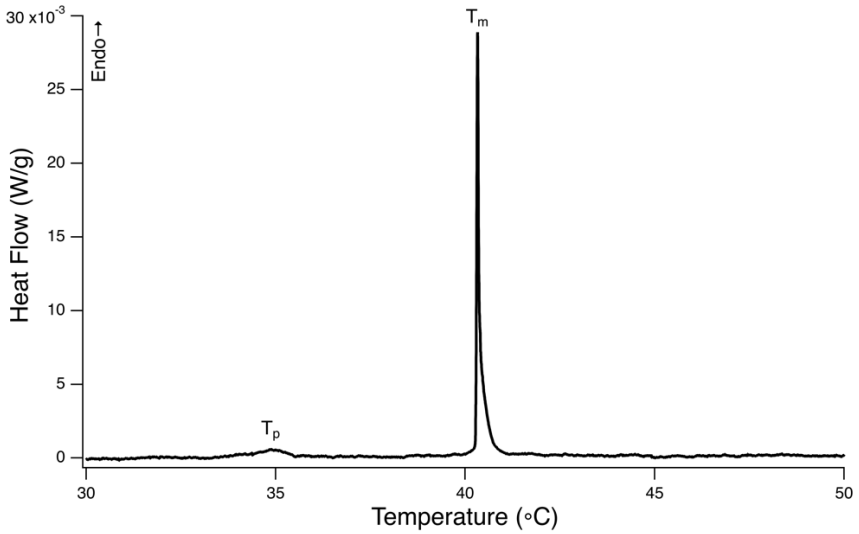

Figure 1.11 DPPC heat flow vs. temperature plot. The labeled peaks correspond to the ripple phase (T_p) and the gel to liquid crystalline phase transition (T_m) at 35°C and 41°C, respectively.

A common way to measure T_m in the case of asymmetric peaks is by using the half height width (HHW).[83-84] The HHW for lipid membrane transitions from gel to liquid crystalline increases in the presence of chaotrops. These chaotrops perturb water structure and are believed to affect membranes through their influence on hydrogen bonding between the membrane and surrounding water structure.[84] Another feature in the DSC curves for some lipid bilayers is termed a pretransition temperature that is a result of portions of the lipid becoming less restricted and forming a ripple phase.[85] Other changes in the main transition peak that can be correlated to interactions between the lipid and saccharides is a broadening of the transition, suggesting a variety of intensity of lipid vesicle interactions with the saccharides which results in a wider range of melting temperatures. The area under the T_m curve corresponds to the enthalpy of the transition.[83]

1.5 Thesis Outline

The overall theme of this research is cooperative adsorption of molecules at interfaces which is investigated through organizational changes in lipid monolayers and bilayers. This section serves to briefly introduce the different systems that will be discussed in each chapter.

Chapter 2. Vibrational Studies of Saccharide-Induced Lipid Film Reorganization at Aqueous/Air Interfaces

Chapter 2 describes investigations that addressed the question "do ocean relevant surfactants and solutes preferentially interact with each other?" To address this question, changes in the organization of the zwitterionic lipid, dipalmitoylphosphatidylcholine (DPPC), due to soluble saccharides including glucosamine (GA) and glucuronic acid (GU) were studied. DPPC was chosen as the surfactant because this lipid is both highly studied[86-88] and prevalent in the ocean through the decomposition of mammalian cells. Monosaccharides were chosen to be the soluble organics of interest, because saccharides, even though highly soluble and not typically surface active, accumulate in great abundance in the sea surface microlayer and in sea spray aerosols.[20, 37-38] In this work, most of the focus was on the monosaccharide, glucosamine, which is the monomer unit of chitin and was chosen because this saccharide is a main component in lobster and crab shells and is environmentally abundant. Elementary studies were performed with glucuronic acid (GU), which was chosen because it is the monomer unit of alginate and a component of some seaweeds.

The ocean is a complex buffer system with a pH of 8.1. To begin to investigate cooperative effects that were ocean relevant, experiments were first done in pure Millipore water, pH 5.8, as a baseline. Glucosamine has a pKa of 7.58,[42] so when additional experiments were done in carbonate buffers, a pH 9 buffer was used to eliminate charge effects from GA. Glucuronic acid has a pKa of 3.20[41] and was a negatively charged anion in the work presented in this chapter.

This work used VSFG measurements in tandem with surface tension and differential scanning calorimetry measurements to show evidence of a condensing effect of DPPC lipids due to the presence of saccharides. VSFG measurements showed similar trends in the lipid ordering at compressed lipid monolayers regardless of the saccharide charge with GA in Millipore water being predominantly positively charged, GU in Millipore water being predominantly negatively charged, and GA in pH 9 buffer being predominantly neutral. Surface tension measurements showed a synergy between GA and buffer ions where surface tension was decreased with both buffer ions and GA molecules, but the change in surface tension was dependent on GA concentration and not buffer pH. DSC measurements showed a consistent trend that both of the soluble saccharides presence in vesicle solutions increased the amount of energy required to change the phase of DPPC from a gel state to a liquid crystalline state. These results taken together, added support to the hypothesis of cooperative adsorption as a mechanism for soluble saccharides to be at the surface as evidenced by organizational and phase change behaviors in the lipid monolayer. This work was published in *Chemical Physics*.

Chapter 3. Organic Enrichment at Aqueous Interfaces: Cooperative Adsorption of Glucuronic Acid to DPPC Monolayers Studied with Vibrational Sum Frequency Generation

Chapter 3 expands on the experiments in Chapter 2 by asking "do anions play a significant role in cooperative adsorption." This chapter goes in more depth on the interaction between DPPC monolayer and biolayers with glucuronic acid. This monosaccharide is relevant to ocean studies as it is the monomer unit of alginate, which is a component of some seaweeds. Much of the interest in glucuronic acid comes from the initial condensing effect GU had on tightly packed DPPC monolayers in Chapter 2. Previous to these experiments, condensing effects of soluble ions on DPPC monolayers had only been attributed to cations, particularly divalent cations.[49-50, 89-92]

VSFG studies of expanded DPPC lipid monolayers show GU concentration dependent ordering of the lipid monolayer. Vibrational studies in the water O-H stretch region add additional information on surface behavior with a GU concentration dependent decrease in the water signal in both expanded and compressed DPPC monolayers. Differential scanning calorimetry measurements feature a second higher melting temperature for the DPPC vesicles. These water SFG measurements coupled with the DSC, imply that GU strengthens lipid-lipid cohesion, which may be a result of GU replacing the water solvating the head groups. Surface tension measurements of these same systems showed the greatest monolayer expansion with larger concentrations of GU in the subphase (> 50 mM).

The same VSFG, DSC, and surface tension measurements for the DPPC/GU system were also done in a pH 9 carbonate buffer to replicate ocean like conditions to

further investigate the cooperative adsorption hypothesis for sea spray aerosol soluble organic accumulation. In the presence of the buffer ions, GU impacts on the lipid monolayer and biolayers are reduced suggesting a competitive aspect to the cooperative adsorption model. With this negative anion, surface tension measurements showed signs of GU outcompeting buffer effects when the GU concentration was at least half of the buffer concentration. In the DSC measurements, GU began to outcompete buffer ions when GU concentration exceeded buffer concentration. These findings place limits on the effects of the cooperative adsorption mechanism in alkaline environmental systems like the ocean. This work has been submitted for publication in *J. Phys. Chem.* and requires minor revisions based on reviewer comments.

Chapter 4. Cooperative Adsorption of Trehalose to DPPC studied with Vibrational Sum Frequency Generation

Chapter 4 looks to answer the questions "how do disaccharides affect lipid structure" and "do uncharged saccharides have a strong affinity for lipids in unbuffered cases?" In this chapter the lipid of interest is still DPPC. Trehalose, a dimer of glucose, was chosen as the soluble saccharide because of its interesting cryoprotective and dehydration protective properties. This disaccharide is found in nature as a component of plants, algae and in shrimp, grasshoppers, locusts, bees, and other insects.[93-95] Thus, from the decay of plant and animal life, it remains a reasonable disaccharide for ocean relevant studies.

Unlike the monosaccharides in the previous chapters, trehalose does have some surface activity and has VSFG signal with a concentration of 100 mM. VSFG

measurements of expanded DPPC monolayers on solutions containing trehalose show an ordering effect when the trehalose concentration in the subphase is greater than 2 mM. The compressed DPPC monolayers show little change with trehalose in the subphase. These observations carry over into surface tension measurements with nearly no changes in surface tension until trehalose reaches 50 mM. DSC measurements show that increasing amounts of trehalose relative to the vesicle concentration results in the growth of a low temperature shoulder in the heat flow vs. temperature curve. This observation correlates with molecular dynamics studies that report the proposed protection mechanisms of trehalose including trehalose hydrogen bonding to the lipid head groups.

Chapter 5. Lipid/saccharide Interface Studies with PE Lipids, Sucrose, and Ocean-like Subphases Followed with Conclusions and Future Directions

Chapter 5 is an insight into investigating effects of changing the lipid head group from a quaternary amine (such as with phosphatidylcholines, PC) to a primary amine (such as phosphoethanolamine PE) with the hypothesis that the less hindered amine on DMPE, a 14:0 PE, would allow result in greater Coulombic interactions with negatively charged saccharides. This hypothesis was tested with VSFG studies of DMPE on Millipore water solutions (pH 5.8) containing either glucosamine (positively charged) or glucuronic acid (negatively charged). Both saccharides have a similar effect on the DMPE monolayer at both condensed and expanded phased. This result does not show a charge-based effect on the monolayer and may indicate that the PE lipid, because it is less hindered self-associates more than PC type lipids, preventing either saccharide from having a large effect on lipid organization.

This chapter includes some work with other saccharides including sucrose and n-acetyl-d-glucosamine, additional ways to analyze and compare SFG and surface tension data, and a look into sea relevant subphases including Instant Ocean, and Baltic sea salt. These experiments provide some insight into future experiments. Following these unpublished experiments are general conclusions for this work as a whole with the most interesting and insightful results compiled together.

1.6 References

1. FitzGibbon, J.; Mensah, K. O., Climate Change as a Wicked Problem: An Evaluation of the Institutional Context for Rural Water Management in Ghana. *SAGE Open* **2012**, *2*, 2158244012448487.

2. Sun, J.; Yang, K., *The Wicked Problem of Climate Change: A New Approach Based on Social Mess and Fragmentation*, 2016; Vol. 8, p 1312.

3. Hansen, J.; Ruedy, R.; Sato, M.; Lo, K., Global Surface Temperature Change. *Reviews of Geophysics* **2010**, *48*.

4. Team, G., Giss Surface Temperature Analysis (Gistemp). NASA Goddard Institute for Space Studies, 2019.

5. Blunden, J., D. S. Arndt, and G. Hartfield , Eds., 2018: State of the Climate in 2017. Bull. Amer. Meteor. Soc., 99 (8), Si–S310, doi:10.1175/2018BAMSStateoftheClimate.1.

6. Derksen, C.; Brown, R., Spring Snow Cover Extent Reductions in the 2008–2012 Period Exceeding Climate Model Projections. *Geophysical Research Letters* **2012**, *39*.

7. Robinson, D. A.; Frei, A., Seasonal Variability of Northern Hemisphere Snow Extent Using Visible Satellite Data. *The Professional Geographer* **2000**, *52*, 307-315.

8. Gardner, A. S., et al., A Reconciled Estimate of Glacier Contributions to Sea Level Rise: 2003 to 2009. *Science* **2013**, *340*, 852-857.

9. Jacob, T.; Wahr, J.; Pfeffer, W. T.; Swenson, S., Recent Contributions of Glaciers and Ice Caps to Sea Level Rise. *Nature* **2012**, *482*, 514.

10. Cavalieri, D. J.; Parkinson, C. L., Arctic Sea Ice Variability and Trends, 1979&Ndash;2010. *The Cryosphere* **2012**, *6*, 881-889.

11. Kwok, R.; Rothrock, D. A., Decline in Arctic Sea Ice Thickness from Submarine and Icesat Records: 1958–2008. *Geophysical Research Letters* **2009**, *36*.

12. Rothrock, D. A.; Yu, Y.; Maykut, G. A., Thinning of the Arctic Sea-Ice Cover. *Geophysical Research Letters* **1999**, *26*, 3469-3472.

13. Laxon, S. W., et al., Cryosat-2 Estimates of Arctic Sea Ice Thickness and Volume. *Geophysical Research Letters* **2013**, *40*, 732-737.

14. Kwok, R.; Cunningham, G. F., Variability of Arctic Sea Ice Thickness and Volume from Cryosat-2. *Philosophical Transactions of the Royal Society A: Mathematical, Physical and Engineering Sciences* **2015**, *373*, 20140157.

15. Nerem, R. S.; Beckley, B. D.; Fasullo, J. T.; Hamlington, B. D.; Masters, D.; Mitchum, G. T., Climate-Change–Driven Accelerated Sea-Level Rise Detected in the Altimeter Era. *Proceedings of the National Academy of Sciences* **2018**, *115*, 2022-2025.

16. Usgcrp *Climate Science Special Report: Fourth National Climate Assessment, Volume I*; U.S. Global Change Research Program: Washington, DC, USA, 2017; p 470.

17. *A National Strategy for Advancing Climate Modeling*; The National Academies Press: Washington, DC, 2012, p 294.

18. Burrows, S. M.; Gobrogge, E.; Fu, L.; Link, K.; Elliott, S. M.; Wang, H.; Walker, R., Oceanfilms-2: Representing Coadsorption of Saccharides in Marine Films and Potential Impacts on Modeled Marine Aerosol Chemistry. *Geophys. Res. Lett.* **2016**, *43*, 8306-8313.

19. Wang, S.; Maltrud, M. E.; Burrows, S. M.; Elliott, S. M.; Cameron-Smith, P., Impacts of Shifts in Phytoplankton Community on Clouds and Climate Via the Sulfur Cycle. *Global Biogeochemical Cycles* **2018**, *32*, 1005-1026.

20. Jayarathne, T., et al., Enrichment of Saccharides and Divalent Cations in Sea Spray Aerosol During Two Phytoplankton Blooms. *Environ. Sci. Technol.* **2016**, *50*, 11511-11520.

21. Meskhidze, N.; Xu, J.; Gantt, B.; Zhang, Y.; Nenes, A.; Ghan, S. J.; Liu, X.; Easter, R.; Zaveri, R., Global Distribution and Climate Forcing of Marine Organic Aerosol: 1. Model Improvements and Evaluation. *Atmos Chem Phys* **2011**, *11*, 11689-11705.

22. Fossum, K. N., et al., Summertime Primary and Secondary Contributions to Southern Ocean Cloud Condensation Nuclei. *Sci. Rep.* **2018**, *8*, 13844.

23. Forestieri, S. D.; Staudt, S. M.; Kuborn, T. M.; Faber, K.; Ruehl, C. R.; Bertram, T. H.; Cappa, C. D., Establishing the Impact of Model Surfactants on Cloud Condensation Nuclei Activity of Sea Spray Aerosol Mimics. **2018**, *18*, 10985-11005.

24. Quinn, P. K.; Coffman, D. J.; Johnson, J. E.; Upchurch, L. M.; Bates, T. S., Small Fraction of Marine Cloud Condensation Nuclei Made up of Sea Spray Aerosol. *Nature Geoscience* **2017**, *10*, 674-679.

25. DeMott, P. J., et al., Sea Spray Aerosol as a Unique Source of Ice Nucleating Particles. *Proceedings of the National Academy of Sciences of the United States of America* **2016**, *113*, 5797-5803.

26. DeMott, P. J., et al., Ice Nucleation by Particles Containing Long-Chain Fatty Acids of Relevance to Freezing by Sea Spray Aerosols. *Environmental science. Processes & impacts* **2018**, *20*, 1559-1569.

27. DeMott, P. J.; Hill, T. C. J. *Marine Ice Nuclei Collections – Magic (Magic-in) Final Campaign Summary*; DOE ARM Climate Research Facility, Pacific Northwest National Laboratory; Richland, Washington: Feb 01, 2016.

28. Wilson, T. W., et al., A Marine Biogenic Source of Atmospheric Ice-Nucleating Particles. *Nature* **2015**, *525*, 234-238.

29. Rosenfeld, D.; Zhu, Y.; Wang, M.; Zheng, Y.; Goren, T.; Yu, S., Aerosol-Driven Droplet Concentrations Dominate Coverage and Water of Oceanic Low-Level Clouds. *Science* **2019**, *363*, eaav0566-11.

30. Han, Z. W.; Li, J. W.; Yao, X. H.; Tan, S. C., A Regional Model Study of the Characteristics and Indirect Effects of Marine Primary Organic Aerosol in Springtime over East Asia. *Atmos Environ* **2019**, *197*, 22-35.

31. McCoy, D. T.; Burrows, S. M.; Wood, R.; Grosvenor, D. P.; Elliott, S. M.; Ma, P. L.; Rasch, P. J.; Hartmann, D. L., Natural Aerosols Explain Seasonal and Spatial Patterns of Southern Ocean Cloud Albedo. *Science Advances* **2015**, *1*, e1500157-e1500157.

32. Carslaw, K. S., et al., Large Contribution of Natural Aerosols to Uncertainty in Indirect Forcing. *Nature* **2013**, *503*, 67-+.

33. Rosenfeld, D.; Lohmann, U.; Raga, G. B.; O'Dowd, C. D.; Kulmala, M.; Fuzzi, S.; Reissell, A.; Andreae, M. O., Flood or Drought: How Do Aerosols Affect Precipitation? *Science* **2008**, *321*, 1309-1313.

34. Fröhlich-Nowoisky, J., et al., Bioaerosols in the Earth System: Climate, Health, and Ecosystem Interactions. *Atmospheric Research* **2016**, *182*, 346-376.

35. Karl, T. R.; Trenberth, K. E., Modern Global Climate Change. *Science* **2003**, *302*, 1719.

36. Russell, L. M.; Hawkins, L. N.; Frossard, A. A.; Quinn, P. K.; Bates, T. S., Carbohydrate-Like Composition of Submicron Atmospheric Particles and Their Production from Ocean Bubble Bursting. *Proc. Natl. Acad. Sci. U. S. A.* **2010**, *107*, 6652-6657.

37. Burrows, S. M.; Ogunro, O.; Frossard, A. A.; Russell, L. M.; Rasch, P. J.; Elliott, S. M., A Physically Based Framework for Modeling the Organic Fractionation of Sea Spray Aerosol from Bubble Film Langmuir Equilibria. *Atmos Chem Phys* **2014**, *14*, 13601-13629.

38. Cunliffe, M.; Engel, A.; Frka, S.; Gašparović, B.; Guitart, C.; Murrell, J. C.; Salter, M.; Stolle, C.; Upstill-Goddard, R.; Wurl, O., Sea Surface Microlayers: A Unified Physicochemical and Biological Perspective of the Air–Ocean Interface. *Progress in Oceanography* **2013**, *109*, 104-116.

39. Grythe, H.; Strom, J.; Krejci, R.; Quinn, P.; Stohl, A., A Review of Sea-Spray Aerosol Source Functions Using a Large Global Set of Sea Salt Aerosol Concentration Measurements. *Atmos Chem Phys* **2014**, *14*, 1277-1297.

40. Hawkins, L. N.; Russell, L., Polysaccharides, Proteins, and Phytoplankton Fragments: Four Chemically Distinct Types of Marine Primary Organic Aerosol Classified by Single Particle Spectromicroscopy. *Adv Meteorol* **2010**, *2010*, 14.

41. Bhattacharyya, L.; Rohrer, J. S., *Applications of Ion Chromatography for Pharmaceutical and Biological Products*; Hoboken, N.J. : John Wiley & Sons, Inc.: Hoboken, N.J., 2012.

42. Bichsel, Y.; von Gunten, U., Formation of Iodo-Trihalomethanes During Disinfection and Oxidation of Iodide-Containing Waters. *Environmental Science & Technology* **2000**, *34*, 2784-2791.

43. Jewison, T., et al., Ymdb: The Yeast Metabolome Database. *Nucleic acids research* **2012**, *40*, D815-20.

44. Ramirez-Gaona, M.; Marcu, A.; Pon, A.; Guo, A. C.; Sajed, T.; Wishart, N. A.; Karu, N.; Djoumbou Feunang, Y.; Arndt, D.; Wishart, D. S., Ymdb 2.0: A Significantly Expanded Version of the Yeast Metabolome Database. *Nucleic acids research* **2017**, *45*, D440-d445.

45. Nakahara, H.; Lee, S.; Shoyama, Y.; Shibata, O., The Role of Palmitic Acid in Pulmonary Surfactant Systems by Langmuir Monolayer Study: Lipid–Peptide Interactions. *Soft Matter* **2011**, *7*, 11351-11359.

46. HUNT, J. H.; GUYOTSIONNEST, P.; Shen, Y. R., Observation of C-H Stretch Vibrations of Monolayers of Molecules Optical Sum-Frequency Generation. *Chemical physics letters* **1987**, *133*, 189-192.

47. Walker, R. A.; Gruetzmacher, J. A.; Richmond, G. L., Phosphatidylcholine Monolayer Structure at a Liquid−Liquid Interface. *Journal of the American Chemical Society* **1998**, *120*, 6991-7003.

48. Ma, G.; Allen, H. C., Dppc Langmuir Monolayer at the Air−Water Interface: Probing the Tail and Head Groups by Vibrational Sum Frequency Generation Spectroscopy. *Langmuir* **2006**, *22*, 5341-5349.

49. Adams, E. M.; Casper, C. B.; Allen, H. C., Effect of Cation Enrichment on Dipalmitoylphosphatidylcholine (Dppc) Monolayers at the Air-Water Interface. *J. Colloid Interface Sci.* **2016**, *478*, 353-364.

50. Adams, E. M.; Verreault, D.; Jayarathne, T.; Cochran, R. E.; Stone, E. A.; Allen, H. C., Surface Organization of a Dppc Monolayer on Concentrated Srcl2 and Zncl2 Solutions. *Phys. Chem. Chem. Phys.* **2016**, *18*, 32345-32357.

51. Link, K. A.; Hsieh, C. Y.; Tuladhar, A.; Chase, Z.; Wang, Z. M.; Wang, H. F.; Walker, R. A., Vibrational Studies of Saccharide-Induced Lipid Film Reorganization at Aqueous/Air Interfaces. *Chem Phys* **2018**, *512*, 104-110.

52. Pan, X.; Yang, F.; Chen, S.; Zhu, X.; Wang, C., Cooperative Effects of Zwitterionic–Ionic Surfactant Mixtures on the Interfacial Water Structure Revealed by Sum Frequency Generation Vibrational Spectroscopy. *Langmuir* **2018**, *34*, 5273-5278.

53. Bulk Contributions Modulate the Sum-Frequency Generation Spectra of Interfacial Water on Model Sea-Spray Aerosols. **2017**, 1-41.

54. Jubb, A. M.; Hua, W.; Allen, H. C., Environmental Chemistry at Vapor/Water Interfaces: Insights from Vibrational Sum Frequency Generation Spectroscopy. *Annual Review of Physical Chemistry* **2012**, *63*, 107-130.

55. Zhang, T.; Brantley, S. L.; Verreault, D.; Dhankani, R.; Corcelli, S. A.; Allen, H. C., Effect of Ph and Salt on Surface-Pka of Phosphatidic Acid Monolayers. *Langmuir* **2017**, acs.langmuir.7b03579-34.

56. Shultz, M. J.; Schnitzer, C.; Simonelli, D.; Baldelli, S., Sum Frequency Generation Spectroscopy of the Aqueous Interface: Ionic and Soluble Molecular Solutions. *Int Rev Phys Chem* **2000**, *19*, 123-153.

57. Velarde, L.; Zhang, X. Y.; Lu, Z.; Joly, A. G.; Wang, Z.; Wang, H. F., Communication: Spectroscopic Phase and Lineshapes in High-Resolution Broadband Sum Frequency Vibrational Spectroscopy: Resolving Interfacial Inhomogeneities of “Identical" Molecular Groups. *J. Chem. Phys.* **2011**, *135*, 241102.

58. Wang, H.-F., Sum Frequency Generation Vibrational Spectroscopy (Sfg-Vs) for Complex Molecular Surfaces and Interfaces: Spectral Lineshape Measurement and Analysis Plus Some Controversial Issues. *Progress in Surface Science* **2016**, *91*, 155-182.

59. Wang, H.-F.; Gan, W.; Lu, R.; Rao, Y.; Wu, B.-h., Quantitative Spectral and Orientational Analysis in Surface Sum Frequency Generation Vibrational Spectroscopy (Sfg-Vs). *International Reviews in Physical Chemistry* **2005**, *24*, 191-256.

60. Wang, H.-F.; Velarde, L.; Gan, W.; Fu, L., Quantitative Sum-Frequency Generation Vibrational Spectroscopy of Molecular Surfaces and Interfaces: Lineshape, Polarization, and Orientation. **2015**, *66*, 189-216.

61. Wang, H. F.; Gan, W.; Lu, R.; Rao, Y.; Wu, B. H., Quantitative Spectral and Orientational Analysis in Surface Sum Frequency Generation Vibrational Spectroscopy (Sfg-Vs). **2005**, *24*, 191-256.

62. Zhang, Z.; Guo, Y.; Lu, Z.; Velarde, L.; Wang, H. F., Resolving Two Closely Overlapping -Cn Vibrations and Structure in the Langmuir Mono Layer of the Long-Chain Nonadecanenitrile by Polarization Sum Frequency Generation Vibrational Spectroscopy. *J. Phys. Chem. C* **2012**, *116*, 2976-2987.

63. Zhang, D.; Gutow, J.; Physical, K. E. T. J. o.; 1994, Vibrational Spectra, Orientations, and Phase Transitions in Long-Chain Amphiphiles at the Air/Water Interface: Probing the Head and Tail Groups by Sum Frequency …. *ACS Publications*.

64. Lambert, A. G.; Davies, P. B.; Neivandt, D. J., Implementing the Theory of Sum Frequency Generation Vibrational Spectroscopy: A Tutorial Review. *Applied Spectroscopy Reviews* **2005**, *40*, 103-145.

65. Hung, K.-K.; Stege, U.; Hore, D. K., Ir Absorption, Raman Scattering, and Ir-Vis Sum-Frequency Generation Spectroscopy as Quantitative Probes of Surface Structure. *Applied Spectroscopy Reviews* **2014**, *50*, 351-376.

66. Shen, Y. R., Surface-Properties Probed by 2nd-Harmonic and Sum-Frequency Generation. **1989**, *337*, 519-525.

67. Shen, Y. R., Basic Theory of Surface Sum-Frequency Generation. *Journal of Physical Chemistry C* **2012**, *116*, 15505-15509.

68. Ye, S.; Noda, H.; Morita, S.; Kohei Uosaki, a.; Osawa, M., Surface Molecular Structures of Langmuir−Blodgett Films of Stearic Acid on Solid Substrates Studied by Sum Frequency Generation Spectroscopy. *Langmuir* **2003**, *19*, 2238-2242.

69. Ye, S.; Osawa, M., Molecular Structures on Solid Substrates Probed by Sum Frequency Generation (Sfg) Vibration Spectroscopy. *Chemistry Letters* **2009**, *38*, 386-391.

70. Bain, C. D., Sum-Frequency Vibrational Spectroscopy of the Solid/Liquid Interface. *Journal of the Chemical Society, Faraday Transactions* **1995**, *91*, 1281-16.

71. Ohno, P. E.; Wang, H. F.; Geiger, F. M., Second-Order Spectral Lineshapes from Charged Interfaces. *Nat. Commun.* **2017**, *8*, 1032.

72. Ohno, P. E.; Wang, H. F.; Paesani, F.; Skinner, J. L.; Geiger, F. M., Second-Order Vibrational Lineshapes from the Air/Water Interface. *J. Phys. Chem. A* **2018**, *122*, 4457-4464.

73. Liu, W.; Fu, L.; Wang, Z.; Sohrabpour, Z.; Li, X.; Liu, Y.; Wang, H. F.; Yan, E. C. Y., Two Dimensional Crowding Effects on Protein Folding at Interfaces Observed by Chiral Vibrational Sum Frequency Generation Spectroscopy. *Phys. Chem. Chem. Phys.* **2018**, *20*, 22421-22426.

74. Lu, Z.; Karakoti, A.; Velarde, L.; Wang, W. N.; Yang, P.; Thevuthasan, S.; Wang, H. F., Dissociative Binding of Carboxylic Acid Ligand on Nanoceria Surface in Aqueous Solution: A Joint in Situ Spectroscopic Characterization and First-Principles Study. *J. Phys. Chem. C* **2013**, *117*, 24329-24338.

75. Mifflin, A. L., et al., Accurate Line Shapes from Sub-1 Cm(-1) Resolution Sum Frequency Generation Vibrational Spectroscopy of Alpha-Pinene at Room Temperature. *J. Phys. Chem. A* **2015**, *119*, 1292-1302.

76. Olenick, L. L.; Chase, H. M.; Fu, L.; Zhang, Y.; McGeachy, A. C.; Dogangun, M.; Walter, S. R.; Wang, H. F.; Geiger, F. M., Single-Component Supported Lipid Bilayers Probed Using Broadband Nonlinear Optics. *Phys. Chem. Chem. Phys.* **2018**, *20*, 3063-3072.

77. Velarde, L.; Wang, H.-F., Capturing Inhomogeneous Broadening of the –Cn Stretch Vibration in a Langmuir Monolayer with High-Resolution Spectra and Ultrafast Vibrational Dynamics in Sum-Frequency Generation Vibrational Spectroscopy (Sfg-Vs). *Journal of Chemical Physics* **2013**, *139*, 084204.

78. Vaughn, J., Ultrafast Pulse Shaping. In *Ultrafast Optics Textbook*, Trebino, R., Ed. Internet, 2015.

79. Aston, M. S., The Study of Surfactant Monolayers by Surface Pressure?Area Measurement. *Chemical Society Reviews* **1993**, *22*, 67-5.

80. Blume, A., Lipids at the Air–Water Interface. *ChemTexts* **2018**, *4*, 1-25.

81. Gzyl-Malcher, B.; Paluch, M., Studies of Lipid Interactions in Mixed Langmuir Monolayers. *Thin Solid Films* **2008**, *516*, 8865-8872.

82. Kodama, M.; Kuwabara, M.; Seki, S., Sucessive Phase-Transition Phenomena and Phase Diagram of the Phosphatidylcholine-Water System as Revealed by Differential Scanning Calorimetry. *Biochim. Biophys. Acta, Biomembr.* **2002**, 567-570.

83. McElhaney, R. N., The Use of Differential Scanning Calorimetry and Differential Thermal-Analysis in Studies of Model and Biological-Membranes. *Chem Phys Lipids* **1982**, *30*, 229-259.

84. Jain, M. K.; Wu, N. M., Effect of Small Molecules on the Dipalmitoyl Lecithin Liposomal Bilayer: Iii. Phase Transition in Lipid Bilayer. *J. Membr. Biol.* **1977**, *34*, 157-201.

85. Riske, K. A.; Barroso, R. P.; Vequi-Suplicy, C. C.; Germano, R.; Henriques, V. B.; Lamy, M. T., Lipid Bilayer Pre-Transition as the Beginning of the Melting Process. *Biochim. Biophys. Acta* **2009**, *1788*, 954-963.

86. Cutro, A. C.; Disalvo, E. A.; Frías, M. A., Effects of Phenylalanine on the Liquid-Expanded and Liquid-Condensed States of Phosphatidylcholine Monolayers. *Lipid Insights* **2019**, *12*, 117863531882092-9.

87. Adamczewski, P.; Tsoukanova, V., Phenylalanine Intercalation Parameters for Liquid-Disordered Phase Domains – a Membrane Model Study. **2018**, 1-8.

88. Feng, R.-J.; Li, X.; Zhang, Z.; Lu, Z.; Guo, Y., Spectral Assignment and Orientational Analysis in a Vibrational Sum Frequency Generation Study of Dppc Monolayers at the Air/Water Interface. *Journal of Chemical Physics* **2016**, *145*, 244707-12.

89. Casper, C. B.; Verreault, D.; Adams, E. M.; Hua, W.; Allen, H. C., Surface Potential of Dppc Monolayers on Concentrated Aqueous Salt Solutions. *J. Phys. Chem. B* **2016**, *120*, 2043-52.

90. Casillas-Ituarte, N. N.; Chen, X.; Castada, H.; Allen, H. C., Na(+) and Ca(2+) Effect on the Hydration and Orientation of the Phosphate Group of Dppc at Air-Water and Air-Hydrated Silica Interfaces. *J. Phys. Chem. B* **2010**, *114*, 9485-9495.

91. LIS, L. J.; LIS, W. T.; PARSEGIAN, V. A.; RAND, R. P., Adsorption of Divalent Cations to a Variety of Phosphatidylcholine Bilayers. *Biochemistry* **1981**, *20*, 1771-1777.

92. LIS, L. J.; PARSEGIAN, V. A.; RAND, R. P., Binding of Divalent Cations to Dipalmitoylphosphatidylcholine Bilayers and Its Effect on Bilayer Interaction. *Biochemistry* **2002**, *20*, 1761-1770.

93. Gil, A. M.; Belton, P. S.; and, V. F. S. A. P. A. M.; 1996, Spectroscopic Studies of Solid A-A Trehalose. *Elsevier*.

94. Becker, A.; Schloder, P.; Steele, J. E.; Wegener, G., The Regulation of Trehalose Metabolism in Insects. *Experientia* **1996**, *52*, 433-9.

95. Elbein, A. D.; Carroll, D.; Pastuszak, I.; Pan, Y. T., New Insights on Trehalose: A Multifunctional Molecule. *Glycobiology* **2003**, *13*, 17R-27R.

CHAPTER TWO

VIBRATIONAL STUDIES OF SACCHARIDE-INDUCED LIPID FILM REORGANIZATION AT AQUEOUS/VAPOR INTERFACES

Contribution of Authors and Co-Authors

Manuscript in Chapter 2

Author: Katie A. Link

Contributions: Collected and analyzed experimental data. Assisted in writing and editing manuscript.

Co-Author: Chia-Yun Hsieh

Contributions: Collected Langmuir trough data.

Co-Author: Aashish Tuladhar

Contributions: Assisted with vibrational sum frequency data collection and edited the manuscript.

Co-Author: Zizwe Chase

Contributions: Assisted with vibrational sum frequency data collection and edited the manuscript.

Co-Author: Zheming Wang

Contributions: Edited the manuscript.

Co-Author: Hongfei Wang

Contributions: Edited the manuscript.

Co-Author: Robert A. Walker

Contributions: Assisted with data analysis, writing the manuscript, and editing the manuscript.

Manuscript Information

Katie A. Link, Chia-Yun Hsieh, Aashish Tuladhar, Zizwe Chase, Zheming Wang, Hongfei Wang, and Robert A. Walker

Chemical Physics

Status of Manuscript:
____ Prepared for submission to a peer-reviewed journal
____ Officially submitted to a peer-reviewed journal
____ Accepted by a peer-reviewed journal
__x_ Published in a peer-reviewed journal

Published by Elsevier
Volume 512, 104-110
DOI: 10.1016/j.chemphys.2018.02.011

CHAPTER TWO

VIBRATIONAL STUDIES OF SACCHARIDE-INDUCED LIPID FILM REORGANIZATION AT AQUEOUS/VAPOR INTERFACES

2.1 Introduction

Lipid monolayers fulfill important biological and technological roles as they promote respiration in lung surfactant,[96-98] inhibit ocular tear evaporation,[99-100] and serve as the simplest models for understanding fluidity, permeability, and miscibility in more complex biological membranes.[48, 101-102] Additionally, lipid monolayers have been used as media to support sensor technologies.[103-104] In each application, lipid film function depends sensitively on structure and organization within the monolayer.

Organization in lipid monolayers adsorbed to water/air interfaces depends sensitively on conditions of the aqueous sub-phase. Divalent cations such as Ca^{2+} and Zn^{2+} are known to induce lipid monolayer condensation,[49-50, 105] whereas small antimicrobial peptides and simple surfactants intercalate into lipid films and induce structural disorder.[106-107] Recent studies have reported that simple, soluble biomolecules also show an affinity for lipid films. Solutes such as phenylalanine[108-109] and trehalose[110] associate with lipid membranes, altering membrane permeability and phase behavior.

Recent studies have raised the prospect that solute interactions with insoluble lipid monolayers may even have meteorological consequences.[111] Sea spray aerosols (SSA) nucleate ice cloud condensation with an efficacy that depends directly on SSA organic content.[112] Current descriptions of SSA composition present a paradox: data from

field studies suggest that SSAs contain significantly more organic material than predicted based on the relative abundance of surface active, biogenic organic matter. In fact, the organic content of sub-micron SSA particles can reach up to 80% by mass.[113-116] To put this figure in context, a 500 nm diameter water droplet covered with a tightly packed insoluble lipid or fatty acid (e.g. stearic acid) monolayer would have an organic content of < 5% by mass. The origin of observed organic enrichment in SSAs remains speculative and presents a challenge to emerging models of aerosol effects on atmospheric chemistry and climate science.

One mechanism that can account for organic enrichment in SSAs is cooperative adsorption. Cooperative adsorption describes a synergy that enhances the surface concentration of one (or more) organic species relative to expectations based on models that assume no interactions between adsorbates. This mechanism was proposed to explain SSA organic enrichment by Burrows and coworkers.[111] In that work, the authors used a Langmuir model to parameterize marine organic species partitioning into SSAs across bubble surfaces. Motivating this model was the assumption that ocean surfaces are covered (in whole or in part) with biogenic films consisting of lipids, proteins, and polysaccharides. A subsequent study used surface specific vibrational spectroscopy to determine if glucosamine (GA), a simple, soluble monosaccharide and the monomer unit of the biopolymer chitin, cooperatively adsorbs to tightly packed dipalmitoylphosphatidylcholine (DPPC) monolayers adsorbed to an aqueous/vapor interface.[117] Experimental data were used to infer cooperative glucosamine adsorption to the lipid monolayer through a change in solvating water structure. Fitting results to a

modified Langmuir isotherm, the authors reported an effective saccharide adsorption energy of -41 kJ/mole. The authors also noted that in the absence of a lipid film, glucosamine did not show any surface affinity as evidenced by surface water structure that did not change with increasing GA concentrations up to 20 mM.

The effects of GA cooperative adsorption on DPPC monolayer organization was not addressed directly in the report by Burrows, *et al*.[117] In the tightly packed monolayers studied, DPPC surface coverage was reported to be 2.5 lipids/nm^2 or 40 Å^2/molecule with DPPC acyl chains expected to adopt highly ordered, all-*trans* conformations. Changes that result from cooperative adsorption to the headgroup region would not be expected to change individual chain conformation but the literature provides some evidence that solute-headgroup interactions will affect the overall tilt of chains within insoluble lipid monolayers.[118-122] To further examine the viability of cooperative adsorption as a mechanism for interfacial organic enrichment, experiments described below consider cooperative adsorption of two simple monosaccharides, GA and glucuronic acid (GU), with tightly packed DPPC monolayers (40 Å^2/molecule). The effects of lipid surface coverage are also examined briefly using DPPC monolayers in their liquid condensed state (55 Å^2/molecule).

In this study, structure and organization in the DPPC films are monitored using vibrational sum frequency generation (VSFG) while thermodynamic changes resulting from cooperative adsorption are observed via surface tension measured with a Langmuir Trough and melting temperature measured with differential scanning calorimetry (DSC). Experiments in the tightly packed limit with GA were performed with two different

aqueous phase pH conditions – 5.8 and 9.0 – with the latter pH being much closer to natural oceanic conditions (pH = 8.1). Differences in pH affect saccharide charge: GA, with a pKa of 7.58, is > 98% positively charged at pH 5.8 and > 96% neutral at pH 9.0, while GU, with a pKa of 3.20, is > 99.6% negatively charged at pH 5.8.[123-124]

All three families of experiments – Langmuir trough, VSFG, and DSC – show evidence that glucosamine and glucuronic acid spontaneously associate with lipid films, even though the saccharides themselves are not surface active. GA and GU both induce a higher degree of order in tightly packed DPPC films on pH 5.8 solutions and, in the case of GA, this effect is more pronounced in solutions buffered to pH 9. GA also induces marked changes in VSFG intensities from DPPC films in their liquid condensed state (55Å^2/molecule) that suggest a lipid monolayer condensing effect. While this effect has been reported for divalent metal cations,[105, 118, 125] spectra reported below are, to our knowledge, the first evidence that organic solutes can induce similar effects. DSC data show that both GA and GU raise the DPPC gel to liquid crystalline transition temperature, also implying saccharide-lipid association, although the effect seems much more pronounced for GU than for GA. Taken together, our data indicate that GA and GU coordinate between lipids within the film and that these interactions are driven primarily through dipolar and hydrogen bonding associations rather than Coulomb attractions.

2.2 Experimental

2.2.1 Materials

1,2-dipalmitoyl-*sn*-glycero-3-phosphocholine (DPPC, powder, > 99%) was

purchased from Avanti Polar Lipids Inc. (Alabaster, Alabama). D-(+)-Glucosamine hydrochloride (GA, crystalline, ≥ 99%), D- Glucuronic acid (GU, powder, ≥ 98%), sodium carbonate (≥ 99.5%), sodium bicarbonate (≥ 99.7%), potassium phosphate monobasic (≥ 99%), and potassium phosphate dibasic (≥ 98%) were purchased from Sigma-Aldrich (St. Louis, MO). HPLC grade chloroform (99.9%) was purchased from Fisher Scientific. All chemicals were used without further purification. Millipore water (resistivity of 18.2 MΩ) was used for all aqueous sample preparation.

2.2.2 Preparation of Samples

DPPC stock solutions (1 mM) were prepared in HPLC grade chloroform and sonicated for 30 minutes. Solutions of glucosamine (GA) and glucuronic acid (GU) were prepared in Millipore water and sonicated for 30 minutes. Millipore solutions had a pH of 5.8. Buffer solutions at pH 9.0 (100 mM) were made with sodium carbonate and sodium bicarbonate. Buffer solutions of 6.5 and 8.5 (10 mM) were made with potassium phosphate monobasic and dibasic. Glucosamine or glucuronic acid was added to the buffer solutions before testing the pH. Solution pH plays an important role in determining speciation of the two saccharides. GA has a pK_a of 7.58, meaning that in both Millipore and in the pH 6.5 buffer, the majority of GA in solution is positively charged whereas at pH 8.5, the neutral amine is the dominant species. GU, with its pKa of 3.20, is predominately negatively charged in all experiments.

To prepare samples for VSFG, the aqueous solution of interest was poured into a clean Teflon petri dish. Petri dishes were cleaned with copious amounts of methanol and Millipore water and then treated with UV/Ozone. The DPPC stock solution was spread

on the surface of the aqueous solution with a glass microsyringe. After placing DPPC on the surface the sample was allowed to sit for 10 minutes so that the chloroform could evaporate and the DPPC monolayer could equilibrate.

2.2.3 Langmuir Trough Experiments

The NIMA Langmuir trough used in these experiments is a Model 302LL equipped with a PS4 pressure sensor and a Micro Processor Interface 104. The PTFE trough and barriers were wiped with chloroform on Kimwipes. Afterwards the trough and barriers were rinsed with Millipore. The surface tension of Millipore water is then measured against the standard value (72.8 mN/M at 20°C).

The solution of interest was then added to the trough until both barriers were wetted. A paper Wilhelmy plate (Brown Waite Engineering) is then lowered into the solution. Once saturated with the bulk phase, the Wilhelmy plate is lifted out of the solution and slowly lowered until it comes into contact with the surface at which point the pressure sensor is zeroed. The barriers of the trough are then closed, and the surface tension is monitored. Any deviations in the surface tension are considered an impurity and the trough is then emptied, cleaned and reset. If the surface tension remains constant, the barriers are opened and a glass microsyringe is used to spread the DPPC monolayer evenly across the surface. The trough is then left to equilibrate for 10 min.[126]

To collect a pressure-area isotherm, the barriers of the Langmuir trough are closed at a speed of 10 cm^2/min and the surface pressure (Π) is recorded as a function of surface area. The surface pressure is related to the surface tension of the neat bulk phase (γ_0) and the surfactant monolayer (γ) with Equation 2.1.

$$\Pi=\gamma_0-\gamma \qquad (2.1)$$

Pressure-area isotherms for DPPC are well reported in the literature. On Millipore water and buffered aqueous solutions, the DPPC isotherm is characterized by a liftoff pressure at 100 Å^2/molecule and a liquid expanded/liquid condensed coexistence plateau between 80 Å^2/molecule and 55 Å^2/molecule. At higher surface coverages, the DPPC isotherm rises steeply before collapsing at 38 Å^2/molecule. Representative isotherms are shown in Figure 2.1.

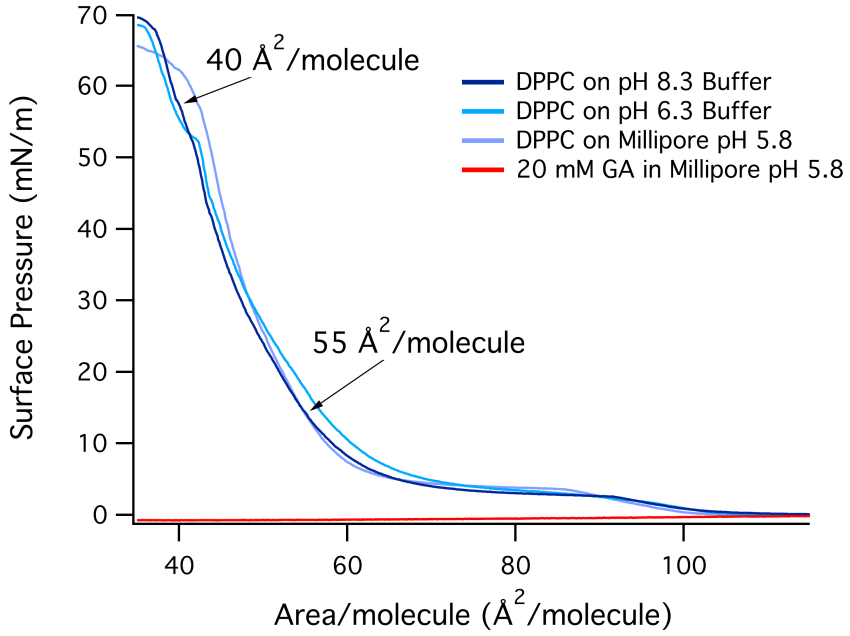

Figure 2.1 DPPC isotherms on aqueous solutions of varying pH with no dissolved saccharide. The red/bottom trace is an 'isotherm' recorded for a 20 mM GA solution with no DPPC present.

Two notable observations in these isotherms are that i) the distinguishing features of the DPPC 2D phase transitions are insensitive to solution pH, and ii) buffering conditions and GA, without DPPC, has no discernible effect on the surface pressure which is consistent with its high aqueous phase solubility of ~1 g/ml at room temperature

(~4.5 M). Prior spectroscopic studies showed that at concentrations up to 20 mM GA, water's surface vibrational structure was unchanged.[117]

2.2.4 VSFG Experiments

Sum frequency generation experiments were done at Pacific Northwest National Lab's (PNNL) EMSL facility. The details of this facility have been described in detail elsewhere.[127] Briefly, the high resolution broadband sum frequency generation vibrational spectroscopy (HR-BB-SFG-VS) utilizes two Ti:sapphire oscillators/amplifiers. The two oscillators, ~100 ps 76 MHz TIGER (Time- Bandwidth Inc.) and sub-40 fs Micra-5 (Coherent Inc.) are electronically synchronized (Synchrolock-AP, Coherent Inc., Palo Alto, CA). The oscillators seed the two regenerative amplifiers: the Coherent Legend Elite HE-ps and the Coherent Legend Elite DUO, which produces ~1.6 W and ~ 7.5 W respectively. The 40 fs pulses are used to pump an optical parametric amplifier (OPerA-Solo, Coherent Inc.) to produce the IR pulse; the 100 ps pulse is used as the 800 nm source. The 800 nm visible beam and the IR beam are focused at the interface at 45° and 55°, respectively from surface normal. The sum frequency response is then isolated from the visible and IR input and collected in a monochromator (Andor Technology, Belfast, Shamrock 750 mm, 1200 lines/mm grating) and CCD (Andor Technology, Newton 971P, back-illuminated).

For surface areas of 40 $Å^2$/molecule, a series of 4-5 scans, each acquired over 5 minutes, was averaged. For lower surface coverage (55 $Å^2$/molecule), two 10-minute scans were averaged. Averaged scans were background corrected with a spectrum taken with unsynchronized pulses. Spectral intensity was normalized from an averaged

background subtracted SF response from a thick z-cut quartz crystal.

We note that prior measurements of the aqueous vapor interface where the aqueous phase consisted of 20 mM GA showed a distinct free –OH band at 3715 cm^{-1} implying that GA is not surface active.[117]

2.2.5 DPPC Vesicle Preparation and DSC Measurements

Small unilamellar vesicles (SUV) were made using standard protocols.[128-130] A ~1 mg/mL lipid/chloroform solution was mixed in a round bottom flask. The chloroform was then removed with a rotary evaporator (> 60°C), which left behind a lipid film. The film was rehydrated with Millipore water to make a 20 mM DPPC vesicle solution. The solution was sonicated for 30 minutes above the melting temperature of DPPC (41°C) to produce SUVs. Glucosamine and glucuronic acid were introduced after vesicle formation with a final DPPC concentration of 10 mM and a saccharide concentration of 50 mM. The DPPC/saccharide solutions were left to equilibrate for ≥ 8 hours before doing DSC measurements.

DSC measurements were performed on a TA Instruments Discovery DSC (New Castle, DE). Tzero pans and Tzero hermetic lids, purchased from TA instruments, were used the reaction vessel. First, sealed pans were equilibrated to 20°C. Then the temperature was ramped up by 0.5°C/min until 55°C (T_m DPPC = 41°C). The difference between the heat flow into the sample and the reference was recorded at each temperature interval. DSC measurements were done a minimum of 3 times with at least 2 different vesicle solutions and the reported data were the average. DSC measurements were analyzed to evaluate how saccharides affected DPPC's gel to liquid crystalline phase

transition temperature (T_m).

2.3 Results and Discussion

2.3.1 Pressure Area Isotherms

This research is focused on the effects of monosaccharides on DPPC lipid monolayer structure for monolayers with two distinct surface coverages. The first coverage is 40 $Å^2$/molecule. At this coverage, the DPPC monolayer is a 2-dimensional solid. The second coverage corresponds to 55 $Å^2$/molecule where DPPC is in its liquid condensed phase (coverages are marked on Figure 2.1).

Figure 2.2 shows Langmuir isotherms for DPPC on glucosamine-containing solutions with and without a buffer. The top portion of this figure reports DPPC isotherms on unbuffered solutions with 4 GA concentrations in Millipore water. These data show little dependence on glucosamine concentration over the range sampled. The one regime where small, reproducible changes are observed occurs at high surface coverages where DPPC monolayers are more condensed with GA present. Such results are consistent with observations reported by Gobrogge, *et al.* where increasing concentration of GA (in Millipore water) disrupted interfacial aqueous structure—a result that was interpreted in terms of cooperative GA adsorption displacing surface water.[117]

The bottom panel of Figure 2.2 shows the surface pressure isotherms acquired with DPPC films adsorbed to the aqueous/vapor interface where the aqueous phase consists of a *buffered* solution containing GA. Increasing the pH with a 10 mM phosphate buffer to either 6.5 or 8.5 results in noticeable expansion of the lipid monolayer when GA

is present in solution. The synergy between the buffer and 0.5 mM GA shifts the liquid expanded-liquid condensed coexistence plateau by ~20-25 $Å^2$/molecule to larger surface areas relative to DPPC on solutions containing only buffer or only GA. Such behavior is consistent with soluble solutes associated with the insoluble lipids increasing each lipid's 'effective' area per molecule. At 55 $Å^2$/molecule, the lipid monolayer has expanded by ~9 $Å^2$/DPPC molecule with the addition of 0.5 mM GA and an additional ~18 $Å^2$/DPPC molecule with 2 mM GA. At the highest surface coverages (approaching 40 $Å^2$/DPPC molecule), the isotherms converge with a common slope and collapse pressure.

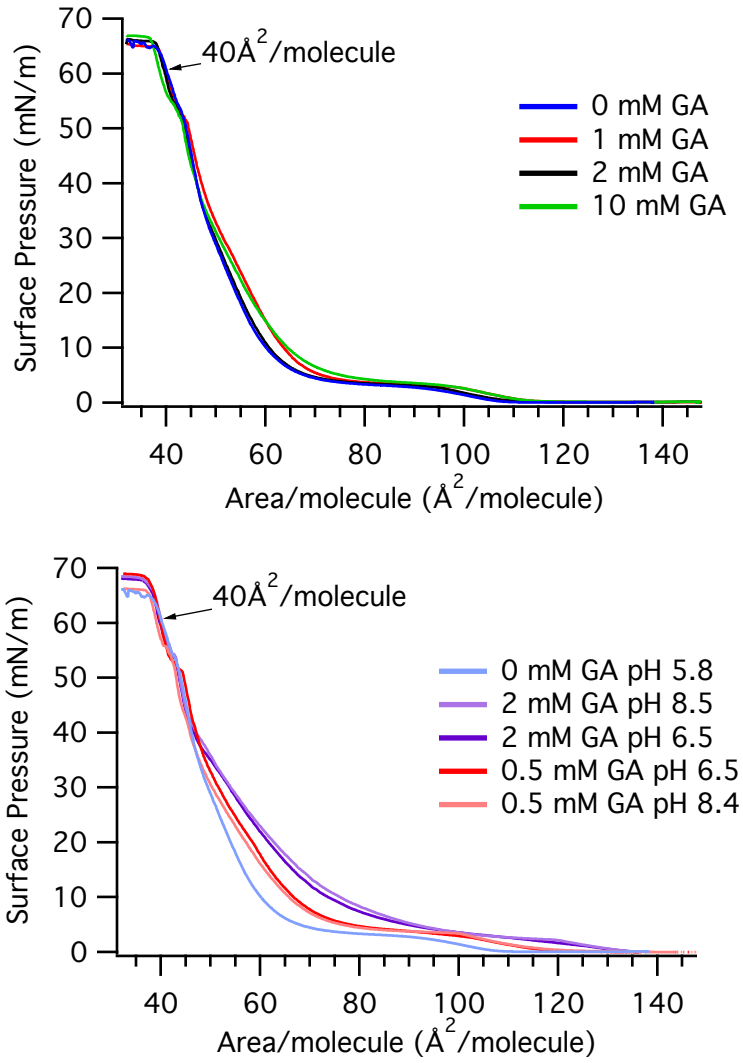

Figure 2.2 Isotherms of DPPC monolayers on varying aqueous surfaces. Top: DPPC isotherms on solutions containing 0.0 mM to 10.0 mM GA dissolved in Millipore (pH 5.8). Bottom: DPPC isotherms on aqueous solutions (having different pH) with 0, 0.50 and 2.0 mM GA.

The fact that such behavior is apparent only with buffer *and* saccharide present implies a degree of interfacial complexity and a heterogeneous distribution of species present in the interfacial region. Similar effects have been noted before (although never explored systematically) in studies examining lipid spreading across aqueous/vapor

interfaces.[131-134] Clarifying and refining questions of surface composition and structure will be critical for any effort seeking to model the chemistry occurring at environmentally relevant interfaces.

2.3.2 VSFG 40 Å^2/molecule

DPPC on GA solutions at pH 5.8

In the two-dimensional solid phase, DPPC acyl chain organization is only modestly sensitive to changes in the underlying subphase GA concentration as evidenced by the $-CH_3$ symmetric stretch (~2870 cm^{-1}, r^+)[135-136] peak intensity remaining unchanged to within experimental uncertainty as the glucosamine concentration varies between 0.0 to 10 mM and only small, systematic changes observed in the intensity of the CH_2 (~2846 cm^{-1}, d^+) symmetric stretch intensity as a function of GA concentration (Figure 2.3). Nevertheless, this small change in d^+ intensity strongly affects the r^+ to d^+ ratio that is used frequently to infer order and organization within alkyl monolayers adsorbed to aqueous interfaces.[69, 137-138] Under SSP polarization conditions, an increasing r^+/d^+ ratio indicates an increase in acyl chain ordering within the DPPC monolayer. For the spectra shown in Figure 2.3, r^+/d^+ ranges from 6.0 ([GA] = 0) to 17 ([GA] = 10 mM).

Given that the acyl chains are already tightly packed in the 2-dimensional solid phase at surface coverages of 40 Å^2/molecule, we propose that changes in this r^+/d^+ ordering parameter may result from small changes in monolayer tilt, similar to phenomena reported in grazing incidence X-ray diffraction studies of divalent cation association with phosphocholine monolayers.[120] This hypothesis deserves further examination with alternately polarized VSFG experiments. Other symmetry allowed

VSFG combinations including $S_{Sum}P_{Vis}S_{IR}$ and $P_{Sum}P_{Vis}P_{IR}$ probe C-H stretches having their IR transition moment aligned in the plane of the surface and can be used to determine functional group orientation. Results of these additional experiments will be the reported in future work.

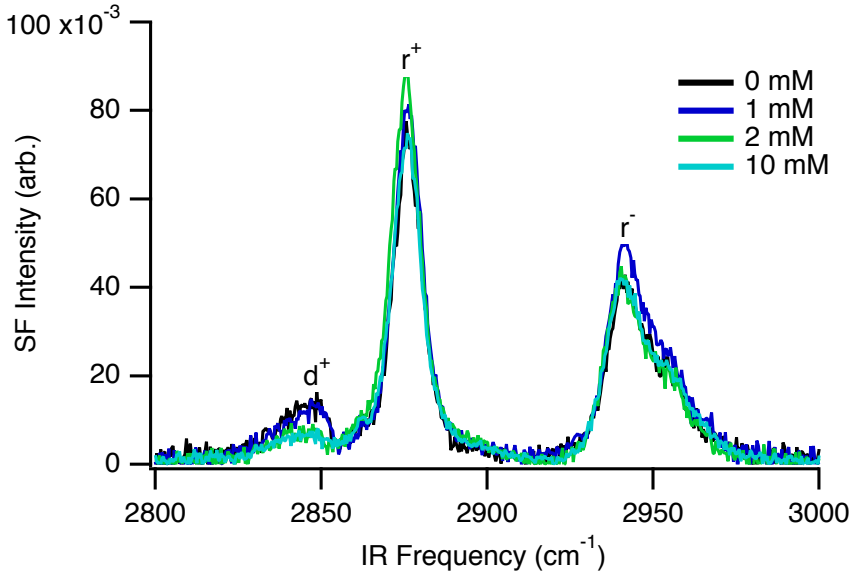

Figure 2.3 VSF spectra (*SSP* polarization) of 40 Å^2/molecule DPPC at the liquid/vapor interface as a function of glucosamine concentration in the subphase. Labeling conventions include a + for a symmetric stretch and a – for an antisymmetric stretch. The d refers to a CH_2 stretch and the r to a CH_3 stretch. The r^- peak intensity is compounded with signal from the r^-_{FR} (~2930 cm^{-1}) and the r^- in and out of plane antisymmetric stretches (~2962 cm^{-1} and ~2952 cm^{-1} respectively [135]) and are not discussed in the following analysis.

2.3.3 VSFG 40 Å^2/molecule
DPPC on GA solutions at pH 9.0

Despite similarities in DPPC monolayer isotherms at low and high pH (Figure 2.1), DPPC monolayer organization changes considerably as a function of subphase pH when GA is also present. Figure 2.4 shows VSFG spectra for tightly packed DPPC monolayers (40 Å^2/molecule) adsorbed to an aqueous-vapor interface with the subphase

buffered to a pH of 9. In the absence of GA, the r^+ intensity is significantly weaker and the d^+ intensity is noticeably stronger than in spectra from tightly packed monolayers at pH 5.8. The DPPC r^+/d^+ ratio under these conditions is approximately 2.

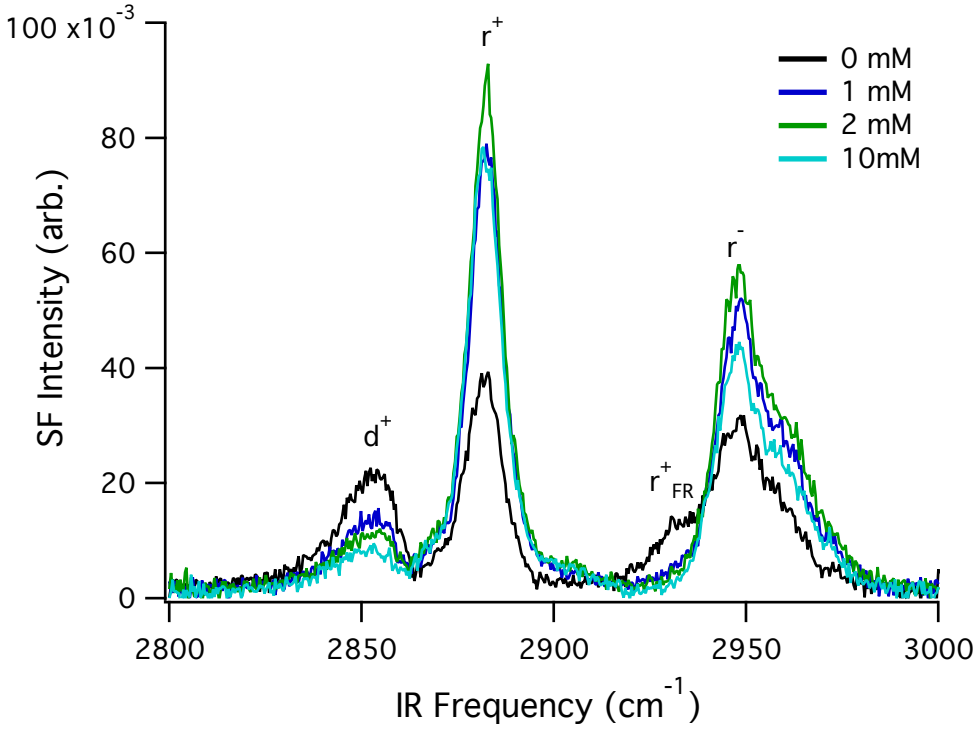

Figure 2.4 VSF spectra (*SSP* polarization) of 40 Å^2/molecule DPPC at a pH 9.0 liquid/vapor interface as a function of glucosamine concentration in the subphase.

On pH 9 solutions containing increasing amounts of GA, r^+ intensity rises sharply, d^+ intensity diminishes, and intensity grows in the band structure centered at 2950 cm^{-1}, a region generally associated with both a r^+ Fermi resonance coupling and the methyl antisymmetric stretch (r^-). The r^+/d^+ ratio reaches an asymptotic limit of ~15, similar to values observed for DPPC on the pH 5.8 solutions. This behavior is captured in Figure 2.5 showing r^+/d^+ ratios for all of the lipid/saccharide systems reported here.

With a pK_a of 7.58, GA is > 96% neutral in pH 9 aqueous solutions making the

results shown in Figure 2.4 surprising. If the small effects of GA on DPPC monolayer organization at pH 5.8 were due to cooperative adsorption, one might reasonably expect these interactions to be due to Coulomb attractions between the positively charged GAH^+ and the negatively charged lipid phosphate headgroup. At the higher pH, the relative amount of neutral amine (GA) and its protonated conjugate acid (GAH^+) has changed by a factor of ~10^3, yet the effect of GA on the DPPC monolayer organization is just as pronounced.

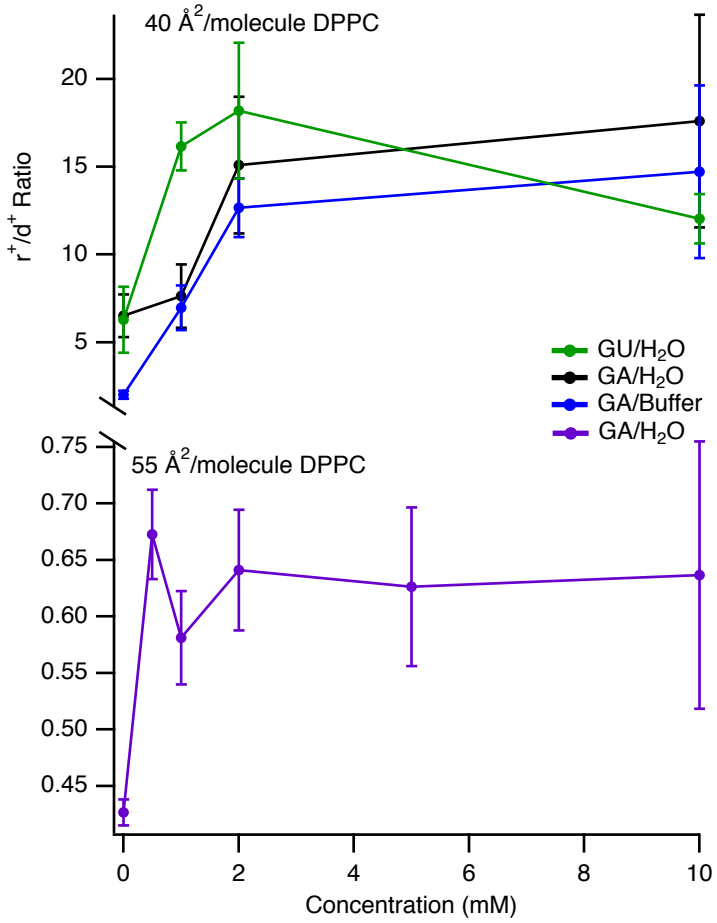

Figure 2.5 Ratios of DPPC's CH_3 symmetric stretch (r^+) to CH_2 symmetric stretch (d^+) band intensities as a function of saccharide concentration. The top trace shows results for tightly packed (40Å^2/molecule) DPPC monolayers. The bottom trace shows data for a DPPC monolayer in its liquid condensed state (55Å^2/molecule).

2.3.4 VSFG 55 Å^2/molecule

<u>DPPC on GA solutions at pH 5.8</u>

One common denominator between VSFG spectra from tightly packed DPPC monolayers on pH 5.8 and pH 9 solutions containing GA is that the r^+ band is always stronger than the d^+ band. Such behavior is expected given that the lipid acyl chains should already be well ordered with few gauche defects. To explore this relationship

further, we carried out a series of VSFG experiments on monolayers having DPPC surface coverages of 55Å^2/molecule as a function of GA concentration.

Figure 2.6 shows spectra from DPPC monolayers with a surface coverage of 55Å^2/molecule on solutions having different amounts of GA. Not surprisingly, monolayers with this more expanded surface coverage show considerably more acyl chain disorder than those monolayers that are tightly packed. In the absence of GA, the monolayer's r^+/d^+ ratio is less than 0.45.

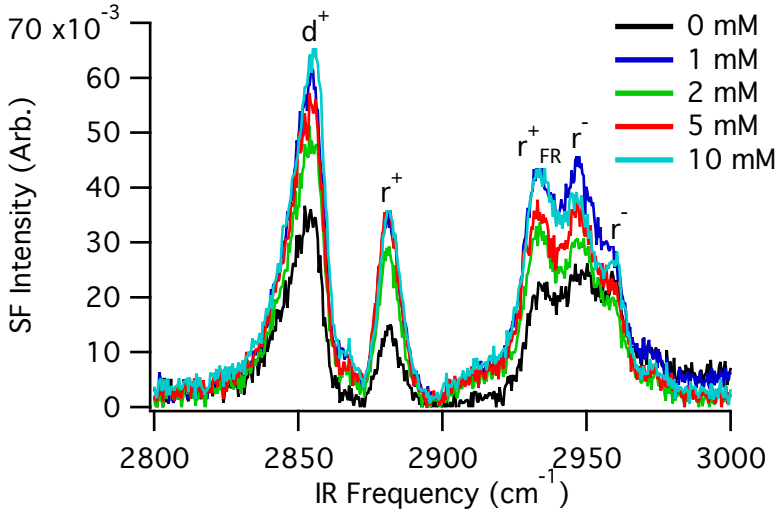

Figure 2.6 VSF spectra (*SSP* polarization) of 55 Å^2/molecule DPPC at the liquid/vapor interface as a function of glucosamine concentration in the subphase.

The d^+ feature consistently remains stronger than r^+ with increasing GA concentration, but addition of the saccharide more strongly influences the methyl symmetric stretch intensity, as evidenced by a 3-fold rise in r^+ intensity and a 50% rise in the r^+/d^+ ratio to 0.65 as GA concentration increases to 20 mM. (Figure 2.5) This behavior is consistent with GA cooperatively adsorbing to the DPPC monolayer and inducing a condensation effect as has been reported for lipid monolayers in the presence of charged,

soluble alkyl surfactants.[139]

2.3.5 VSFG 40 Å^2/molecule
DPPC on GU solutions at pH 5.8

To begin examining the generality of observations made with GA, preliminary experiments were performed with a second monosaccharide, glucuronic acid (GU). Like GA, GU is a simple monosaccharide but with a carboxylic acid in the 2-position and a pK_a of 3.20. In aqueous solutions having a pH of 5.8, > 95% of all GU in solution is negatively charged.

Figure 2.7 shows VSFG spectra of tightly packed DPPC monolayers adsorbed to a pH 5.8 aqueous-vapor interface as a function of GU bulk concentration. Similar to the data reported for GA-containing solutions, increasing GU suppresses d^+.

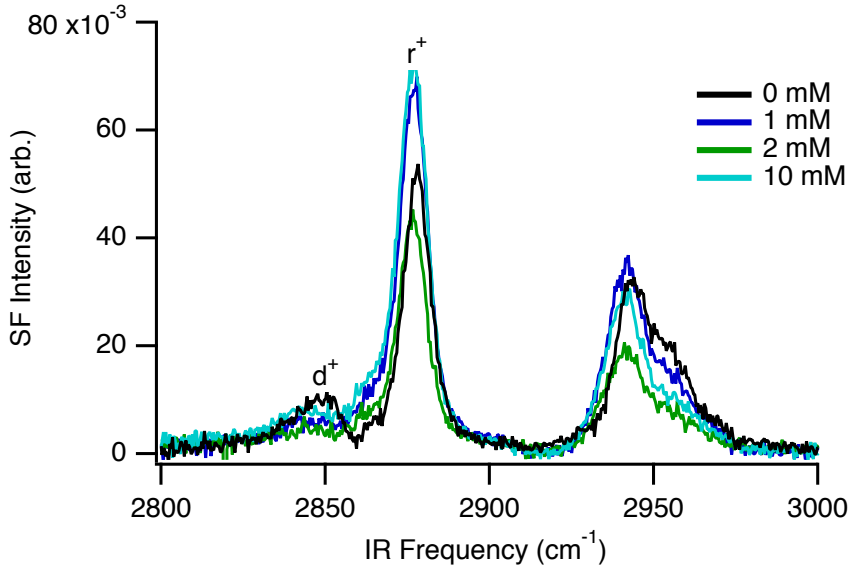

Figure 2.7 VSF spectra (*SSP* polarization) of 40 Å^2/molecule DPPC at a pH 5.8 liquid/vapor interface as a function of glucuronic acid concentration in the subphase.

The r^+/d^+ ratios shown in Figure 2.5 for the DPPC/GU system behave similarly to

those observed for the DPPC/GA systems. Between GU concentrations of 2 mM and 10 mM, r^+/d^+ falls from a value of 18 to 12, but given how sensitive this ratio is to small changes in the small d^+ intensity, additional studies are necessary to determine whether or not this effect is real.

2.3.6 DSC: Saccharide induced effect on DPPC Vesicles

A final means of testing whether or not soluble monosaccharides associate with lipid films is to examine what effects these saccharides have on lipid membrane phase behavior. DSC traces of vesicles containing DPPC are shown in Figure 2.8. The black trace is DPPC vesicles in Millipore with a T_m of 40.58 ± 0.02. With the addition of GA to the vesicle solution after rehydration, the T_m of DPPC is shifted to a higher temperature by 0.25°C. With GU present, the DPPC has 2 distinct transition temperatures. The first is shifted by 1.9°C higher, the second by 1.02°C from the pure DPPC.

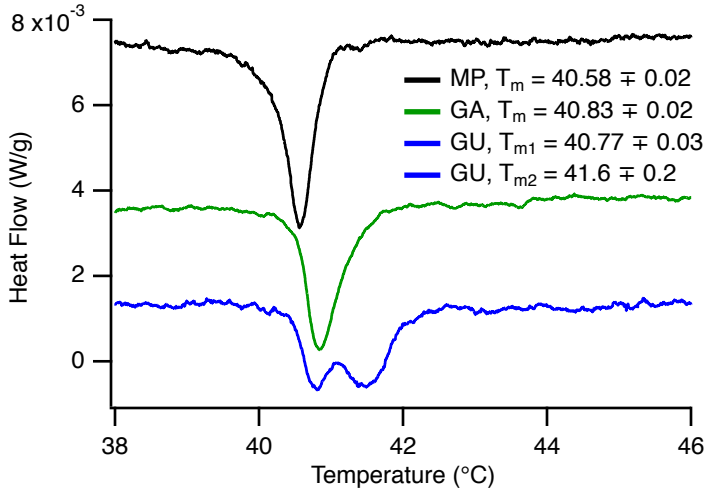

Figure 2.8 Calorimetric traces of DPPC vesicles in saccharide containing solutions.

The increase in the T_m with the addition of either GA or GU indicates saccharide

association with the lipid vesicles. The two- endotherm behavior in the DPPC/GU trace is consistent with previous reports of dehydration of a DPPC bilayer. Kodama *et. al.* reported that a decrease in water content from 80 wt% to 47 wt% resulted in another endotherm appearing as a shoulder of the original isotherm, but shifted to a higher temperature.[140] This behavior mirrors the effects that GU has on DPPC membrane behavior in vesicles. Specifically, the second transition temperature suggests that negative GU ions are displacing solvating water surrounding the DPPC headgroups. If true, this behavior is interesting in that the dehydration of DPPC monolayers and vesicles is normally attributed to cation, not anion, effects on charged ions.[141]

The incorporation of GU into the vesicle structure as replacement for water lends evidence to a cooperatively between GU and the positively charged 3' amine group. The association of GAH^+(causing the shift to higher T_m) to the negatively charged phosphate group of the DPPC has less of a dehydration effect than the presumed GU^- association with the positively charged quaternary ammonium headgroup, suggesting that negatively charged associations to lipid structures may be more impactful than previous studies have assumed.

2.4. Conclusions

Experimental studies described in this work broadly surveyed the effects of soluble monosaccharides on the organization and phase behavior of DPPC films. Specifically, surface tension isotherms showed that while saccharides modestly alter DPPC monolayer formation, saccharides *and* buffer constituents expand the monolayer

and induce significant reorganization that is apparent in changes of vibrational band intensities. For the conditions sampled in these experiments, synergy between the soluble saccharide and the lipid film effect does not correlate with pH but rather the amount of saccharide present. DSC data also suggest measurable association between monosaccharides in solution and the DPPC membranes in vesicle bilayers. Together, these results add plausibility to the hypothesis that cooperative adsorption can enhance the organic content of aqueous/vapor interfaces in environmentally relevant systems.

2.5 References

48. Ma, G.; Allen, H. C., Dppc Langmuir Monolayer at the Air−Water Interface: Probing the Tail and Head Groups by Vibrational Sum Frequency Generation Spectroscopy. *Langmuir* **2006**, *22*, 5341-5349.

49. Adams, E. M.; Casper, C. B.; Allen, H. C., Effect of Cation Enrichment on Dipalmitoylphosphatidylcholine (Dppc) Monolayers at the Air-Water Interface. *J. Colloid Interface Sci.* **2016**, *478*, 353-364.

50. Adams, E. M.; Verreault, D.; Jayarathne, T.; Cochran, R. E.; Stone, E. A.; Allen, H. C., Surface Organization of a Dppc Monolayer on Concentrated Srcl2 and Zncl2 Solutions. *Phys. Chem. Chem. Phys.* **2016**, *18*, 32345-32357.

69. Ye, S.; Osawa, M., Molecular Structures on Solid Substrates Probed by Sum Frequency Generation (Sfg) Vibration Spectroscopy. *Chemistry Letters* **2009**, *38*, 386-391.

96. Zhang, H.; Fan, Q.; Wang, Y. E.; Neal, C. R.; Zuo, Y. Y., Comparative Study of Clinical Pulmonary Surfactants Using Atomic Force Microscopy. *Biochim Biophys Acta* **2011**, *1808*, 1832-42.

97. Ma, G.; Allen, H. C., New Insights into Lung Surfactant Monolayers Using Vibrational Sum Frequency Generation Spectroscopy. *Photochemistry and Photobiology* **2006**, *82*, 1517-1529.

98. Nag, K.; Perez-Gil, J.; Ruano, M. L.; Worthman, L. A.; Stewart, J.; Casals, C.; Keough, K. M., Phase Transitions in Films of Lung Surfactant at the Air-Water Interface. *Biophysical journal* **1998**, *74*, 2983-2995.

99. Kulovesi, P.; Telenius, J.; Koivuniemi, A.; Brezesinski, G.; Vattulainen, I.; Holopainen, J. M., The Impact of Lipid Composition on the Stability of the Tear Fluid Lipid Layer. *Soft Matter* **2012**, *8*, 5826-5834.

100. Mathers, W., Evaporation from the Ocular Surface. *Experimental Eye Research* **2004**, *78*, 389-394.

101. Plant, A. L., Supported Hybrid Bilayer Membranes as Rugged Cell Membrane Mimics. *Langmuir* **1999**, *15*, 5128-5135.

102. Sackmann, E., Supported Membranes: Scientific and Practical Applications. *Science* **1996**, *271*, 43-48.

103. Borden, M. A.; Longo, M. L., Oxygen Permeability of Fully Condensed Lipid Monolayers. *Journal of Physical Chemistry B* **2004**, *108*, 6009-6016.

104. Scholl, F. A.; Morais, P. V.; Gabriel, R. C.; Schoning, M. J.; Siqueira, J. R.; Caseli, L., Carbon Nanotubes Arranged as Smart Interfaces in Lipid Langmuir-Blodgett Films Enhancing the Enzymatic Properties of Penicillinase for Biosensing Applications. *Acs Applied Materials & Interfaces* **2017**, *9*, 31054-31066.

105. Kucerka, N.; Dushanov, E.; Kholmurodov, K. T.; Katsaras, J.; Uhrikova, D., Calcium and Zinc Differentially Affect the Structure of Lipid Membranes. *Langmuir* **2017**, *33*, 3134-3141.

106. Ciumac, D.; Campbell, R. A.; Xu, H.; Clifton, L. A.; Hughes, A. V.; Webster, J. R. P.; Lu, J. R., Implications of Lipid Monolayer Charge Characteristics on Their Selective Interactions with a Short Antimicrobial Peptide. *Colloids and Surfaces B-Biointerfaces* **2017**, *150*, 308-316.

107. Joondan, N.; Jhaumeer-Laulloo, S.; Caumul, P., Effect of Chain Length on the Micellization, Antibacterial, Dppc Interaction and Antioxidant Activities of L-3,4-Dihydroxyphenylalanine (L-Dopa) Esters. *Journal of Surfactants and Detergents* **2015**, *18*, 1095-1104.

108. Griffith, E. C.; Perkins, R. J.; Telesford, D. M.; Adams, E. M.; Cwiklik, L.; Allen, H. C.; Roeseova, M.; Vaida, V., Interaction of L-Phenylalanine with a Phospholipid Monolayer at the Water-Air Interface. *Journal of Physical Chemistry B* **2015**, *119*, 9038-9048.

109. Perkins, R.; Vaida, V., Phenylalanine Increases Membrane Permeability. *Journal of the American Chemical Society* **2017**, *139*, 14388-14391.

110. Doxastakis, M.; Sum, A. K.; de Pablo, J. J., Modulating Membrane Properties: The Effect of Trehalose and Cholesterol on a Phospholipid Bilayer. *Journal of Physical Chemistry B* **2005**, *109*, 24173-24181.

111. Burrows, S. M.; Ogunro, O.; Frossard, A. A.; Russell, L. M.; Rasch, P. J.; Elliott, S. M., A Physically Based Framework for Modeling the Organic Fractionation of Sea Spray Aerosol from Bubble Film Langmuir Equilibria. *Atmospheric Chemistry and Physics* **2014**, *14*, 13601-13629.

112. Wilson, T. W., et al., A Marine Biogenic Source of Atmospheric Ice-Nucleating Particles. *Nature* **2015**, *525*, 234-+.

113. Aller, J. Y.; Radway, J. C.; Kilthau, W. P.; Bothe, D. W.; Wilson, T. W.; Vaillancourt, R. D.; Quinn, P. K.; Coffman, D. J.; Murray, B. J.; Knopf, D. A., Size-Resolved Characterization of the Polysaccharidic and Proteinaceous Components of Sea Spray Aerosol. *Atmospheric Environment* **2017**, *154*, 331-347.

114. Ault, A. P., et al., Size-Dependent Changes in Sea Spray Aerosol Composition and Properties with Different Seawater Conditions. *Environmental Science & Technology* **2013**, *47*, 5603-5612.

115. O'Dowd, C. D.; De Leeuw, G., Marine Aerosol Production: A Review of the Current Knowledge. *Philosophical Transactions of the Royal Society a-Mathematical Physical and Engineering Sciences* **2007**, *365*, 1753-1774.

116. Quinn, P. K.; Bates, T. S.; Schulz, K. S.; Coffman, D. J.; Frossard, A. A.; Russell, L. M.; Keene, W. C.; Kieber, D. J., Contribution of Sea Surface Carbon Pool to Organic Matter Enrichment in Sea Spray Aerosol. *Nature Geoscience* **2014**, *7*, 228-232.

117. Burrows, S. M.; Gobrogge, E.; Fu, L.; Link, K.; Elliott, S. M.; Wang, H. F.; Walker, R., Oceanfilms-2: Representing Coadsorption of Saccharides in Marine Films and Potential Impacts on Modeled Marine Aerosol Chemistry. *Geophysical Research Letters* **2016**, *43*, 8306-8313.

118. Adams, E. M.; Casper, C. B.; Allen, H. C., Effect of Cation Enrichment on Dipalmitoylphosphatidylcholine (Dppc) Monolayers at the Air-Water Interface. *Journal of Colloid and Interface Science* **2016**, *478*, 353-364.

119. Ferber, U. M.; Kaggwa, G.; Jarvis, S. P., Direct Imaging of Salt Effects on Lipid Bilayer Ordering at Sub-Molecular Resolution. *European Biophysics Journal with Biophysics Letters* **2011**, *40*, 329-338.

120. Ghosh, S. K.; Castorph, S.; Konovalov, O.; Salditt, T.; Jahn, R.; Holt, M., Measuring Ca2+ Induced Structural Changes in Lipid Monolayers: Implications for Synaptic Vesicle Exocytosis. *Biophysical Journal* **2012**, *102*, 1394-1402.

121. Kewalramani, S.; Hlaing, H.; Ocko, B. M.; Kuzmenko, I.; Fukoto, M., Effects of Divalent Cations on Phase Behavior and Structure of a Zwitterionic Phosphlipid (Dmpc) Monolayer at the Air-Water Interface. *Journal of Physical Chemistry Letters* **2010**, *1*, 489-495.

122. Lin, W.; Clark, A. J.; Paesani, F., Effects of Surface Pressure on the Properties of Langmuir Monolayers and Interfacial Water at Model Sea Spray Aerosol Surfaces. *Langmuir* **2015**, *31*, 2147-2156.

123. Bichsel, Y.; vonGunten, U., Formation of Iodo-Trihalomethanes During Disinfection and Oxidation of Iodide Containing Waters. *Environmental Science and Technology* **2000**, *34*, 2784-2791.

124. Rohrer, J. S., *Applications of Ion Chromatography for Parmaceutical and Biological Products*, 1st ed.; John Wiley and Sons, Inc., 2012, p 457.

125. Adams, E. M.; Verreault, D.; Jayarathne, T.; Cochran, R. E.; Stone, E. A.; Allen, H. C., Surface Organization of a Dppc Monolayer on Concentrated Srcl2 and Zncl2 Solutions. *Physical Chemistry Chemical Physics* **2016**, *18*, 32345-32357.

126. Aston, M. S., The Study of Surfactant Monolayers by Surface Pressure Area Measurement. *Chemical Society Reviews* **1993**, *22*, 67-71.

127. Velarde, L.; Wang, H. F., Capturing Inhomogeneous Broadening of the -Cn Stretch Vibration in a Langmuir Monolayer with High-Resolution Spectra and Ultrafast Vibrational Dynamics in Sum-Frequency Generation Vibrational Spectroscopy (Sfg-Vs). *Journal of Chemical Physics* **2013**, *139*.

128. Gobrogge, C. A.; Blanchard, H. S.; Walker, R. A., Temperature-Dependent Partitioning of Coumarin 152 in Phosphatidylcholine Lipid Bilayers. *Journal of Physical Chemistry B* **2017**, *121*, 4061-4070.

129. Gobrogge, C. A.; Walker, R. A., Quantifying Solute Partitioning in Phosphatidylcholine Membranes. *Analytical Chemistry* **2017**, *89*, 12587-12595.

130. Avanti_Polar_Lipids Liposome Preparation. https://avantilipids.com/tech-support/liposome-preparation/

131. Kozak, M.; Domka, L.; Jurga, S., Interactions of Cationic Surfactantswith Dppc. *Journal of Thermal Analysis and Calorimetry* **2007**, *88*, 395-399.

132. Mansour, H. M.; Zografi, G., Relationships between Equilibrium Spreading Pressure and Phase Equilibria of Phospholipid Bilayers and Monolayers at the Air-Water Interface. *Langmuir* **2007**, *23*, 3809-3819.

133. McConlogue, C. W.; Malamud, D.; Vanderlick, T. K., Interaction of Dppc Monolayers with Soluble Surfactants: Electrostatic Effects of Membrane Perturbants. *Biochimica Et Biophysica Acta-Biomembranes* **1998**, *1372*, 124-134.

134. Clark, G. A.; Henderson, J. M.; Heffern, C.; Akgün, B.; Majewski, J.; Lee, K. Y. C., Synergistic Interactions of Sugars/Polyols and Monovalent Salts with Phospholipids Depend Upon Sugar/Polyol Complexity and Anion Identity. *Langmuir* **2015**, *31*, 12688-12698.

135. Macphail, R. A.; Strauss, H. L.; Snyder, R. G.; Elliger, C. A., C-H Stretching Modes and the Structure of Normal Alkyl Chains .2. Long, All-Trans Chains *Journal of Physical Chemistry* **1984**, *88*, 334-341.

136. Snyder, R. G.; Strauss, H. L.; Elliger, C. A., C-H Stretching Modes and the Structure of Normal Alkyl Chains . 1. Long Disordered Chains *Journal of Physical Chemistry* **1982**, *86*, 5145-5150.

137. Can, S. Z.; Mago, D. D.; Walker, R. A., Structure and Organization of Hexadecanol Isomers Adsorbed to the Air/Water Interface. *Langmuir* **2006**, *22*, 8043-8049.

138. Walker, R. A.; Gruetzmacher, J. A.; Richmond, G. L., Phosphatidylcholine Monolayer Structure at a Liquid-Liquid Interface. *Journal of the American Chemical Society* **1998**, *120*, 6991-7003.

139. Can, S. Z.; Chang, C. F.; Walker, R. A., Spontaneous Formation of Dppc Monolayers at Aqueous/Vapor Interfaces and the Impact of Charged Surfactants. *Biochimica Et Biophysica Acta-Biomembranes* **2008**, *1778*, 2368-2377.

140. Kodama, M.; Kuwabara, M.; Seki, S., Successive Phase-Transition Phenomena and Phase Diagram of the Phosphatidylcholine-Water System as Revealed by Differential Scanning Calorimetry. *Biochimica et Biophysica Acta (BBA) - Biomembranes* **1982**, *689*, 567-570.

141. Minami, H.; Inoue, T., Dehydration of Hydrated Bilayer of Dipalmitoylphosphatidylcholine Caused by Beryllium Ion: Evidence from a Differential Scanning Calorimetry of Bilayer Phase Transition. *Journal of Colloid and Interface Science* **1998**, *206*, 338-341.

CHAPTER THREE

ORGANIC ENRICHMENT AT AQUEOUS INTERFACES: COOPERATIVE ADSORPTION OF GLUCURONIC ACID TO DPPC MONOLAYERS STUDIED WITH VIBRATIONAL SUM FREQUENCY GENERATION

Contribution of Authors and Co-Authors

Manuscript in Chapter 3

Author: Katie A. Link

Contributions: Collected and analyzed experimental data. Assisted in writing and editing manuscript.

Co-Author: Gabrielle N. Spurzem

Contributions: Collected differential scanning calorimetry data and Langmuir trough data.

Co-Author: Aashish Tuladhar

Contributions: Assisted with vibrational sum frequency data collection and edited the manuscript.

Co-Author: Zizwe Chase

Contributions: Assisted with vibrational sum frequency data collection and edited the manuscript.

Co-Author: Zheming Wang

Contributions: Edited the manuscript.

Co-Author: Hongfei Wang

Contributions: Edited the manuscript.

Co-Author: Robert A. Walker

Contributions: Assisted with data analysis and editing manuscript.

Manuscript Information Page

Katie A. Link, Gabrielle N. Spurzem, Aashish Tuladhar, Zizwe Chase, Zheming Wang, Hongfei Wang, and Robert A. Walker
Journal of Physical Chemistry B

Status of the Manuscript
____Prepared for submission to peer-reviewed journal
_X_Officially submitted to a peer-reviewed journal
____Accepted by a peer-reviewed journal
____Published in a peer-reviewed journal

Publisher: American Chemical Society
Date of Submission: March 2019

CHAPTER THREE

ORGANIC ENRICHMENT AT AQUEOUS INTERFACES: COOPERATIVE ADSORPTION OF GLUCURONIC ACID TO DPPC MONOLAYERS STUDIED WITH VIBRATIONAL SUM FREQUENCY GENERATION

3.1. Introduction

Correlating molecular behavior to global phenomena is a tenuous exercise, but sea spray aerosols (SSAs) can provide such a link. Globally, SSAs serve as cloud condensation nuclei[22, 36] and ice condensation nuclei,[28] both of which affect cloud lifetime and radiative properties.[21, 28] Cloud formation and cloud dynamics are critical variables in models used to determine global albedo and the impact of solar energy retention on global climate change. The efficacy of SSA to form clouds is significantly enhanced by SSA organic content,[37, 40] and recent field studies have reported surprisingly high organic content in freshly formed SSAs prompting the question of how this organic matter was incorporated into the aerosol droplets.[36] SSAs can be produced in several different ways. One source of SSA production occurs when bubbles burst at the ocean surface creating film drops (typically < 1 μm in diameter) from the bubble remnants. The void at the surface left by the bubble bursting results in a jet that produces larger bubbles (2-20 μm in diameter). Aerosols can also be produced from larger drops that are formed when spume is pulled off of waves, usually due to high winds. Large splash drops can contribute to SSAs, but these are typically too large to remain suspended and mostly propagate smaller aerosol formation through the other mechanisms.[20, 39]

SSAs are complex and chemically heterogeneous systems. Primary aerosol emissions at the ocean surface are responsible for ~50% of all aerosol mass,[142] and SSA organic content is often enriched in comparison to the dissolved oceanic organic content. Saccharide concentration at the sea surface microlayer (SSML) is 1-10x the concentration of salt (0.4 - 0.5 mM), and the concentration ratio of saccharide to salt is even greater in SSA with an enrichment of more than 10^3 having been observed in fine SSA particles.[20] SSAs can contain a collection of additional organic and biological molecules acquired from the sea-surface microlayer. These organic and biological molecules include protein fragments, phytoplankton, lipids, among other species. SSA organic content is important given the link between SSAs and cloud nucleation.[28] These empirical observations, however, cannot account for the fact that SSAs often show organic enrichment – up to 77% by mass[143] – beyond what one would predict based simply on insoluble surfactant films adsorbed to the water-air interface when the aerosols form.

One proposed mechanism developed to account for organic enrichment in SSAs is a cooperative adsorption model.[18] Cooperative adsorption describes interactions between an insoluble Langmuir film adsorbed to the aqueous/vapor interface and soluble organics that would not normally be enriched at the surface. This cooperative interaction arises from noncovalent interactions and drives soluble organics to the surface to associate with the headgroups of insoluble monomers comprising the Langmuir film. A previous study of saccharide adsorption to a DPPC interface showed Langmuir adsorption behavior with a $C_{1/2,gluc,2} = 1.25 \pm 0.45$ mM glucosamine.[18] This work and other reports proposed that cooperative adsorption arose from Coulombic interactions between zwitterionic lipid

headgroups and positively charged monosaccharides.[18, 51] These studies have not examined how *negatively* charged species would interact with the zwitterionic lipid films in chemically complex systems (such as buffered solutions and/or high ionic strengths). These considerations have recently been integrated into the OCEANFILMS modeling program designed to improve simulations of primary aerosol mass.[144] Another recent climate model on marine primary organic aerosols found that reducing surface tension (i.e. by increasing interfacial organic content) resulted in more marine primary organic aerosols being activated to form cloud droplets leading to smaller cloud droplet effective radii and a stronger indirect radiative effect.[30]

Work described in this manuscript expands this examination of cooperative adsorption in model environmental systems. Specifically, a combination of vibrational sum frequency generation (VSFG) experiments, differential scanning calorimetry measurements and Langmuir surface pressure isotherms are used to test the ability of lipid films adsorbed to aqueous/vapor interfaces to draw anionic soluble saccharides to the aqueous/vapor interface. The lipid films consist of dipalmitoylphosphatidylcholine (DPPC) at different surface coverages on solutions containing the monosaccharide glucuronic acid (GU). The GU bulk concentration is varied between 1 and 100 mM in aqueous solutions having different ionic strengths and pH. DPPC is a zwitterionic phosphocholine molecule that was chosen, in part, because of its prevalence in biological membranes and widespread use as a surrogate in studies that examine lipid membrane structure and dynamics.[101-102, 145] Glucuronic acid is the monomer unit of alginate and has a pKa of 3.20.[41] In ambient Millipore water (pH of 5.8) and in more alkaline solutions

such as blood plasma (pH 7.4) and the ocean (8.1), glucuronic acid is deprotonated.[101-102, 145] GU is not surface active as evidenced by both surface tension and spectroscopic data (Vide infra).

Results reported in this work show that negatively charged glucuronic acid can cause a moderately packed DPPC monolayer to become more organized and that this organization depends on GU concentration in the subphase. This reorganization induced by glucuronic acid is minimized when the DPPC monolayer is already tightly packed into a two-dimensional solid or when other aqueous ions compete with glucuronic acid for access to the zwitterionic DPPC headgroups. Most studies that examine solute ion effects on lipid monolayer organization have focused on divalent cations.[49-50, 89-91] For example, in cation/DPPC systems the negatively charged phosphate group on the lipid head interacts strongly with the cation, especially if the cation is divalent such as Ca^{2+}, Mg^{2+}, or Zn^{2+}. The result of this interaction is monolayer condensation. DPPC, however, also has a positively charged tertiary amine. Interactions between solution phase anions and DPPC's positive but shielded charge are not often thought to be responsible for monolayer condensation. Nevertheless, the DPPC-GU systems studied in this work show strong evidence of anionic solutes interacting strongly with DPPC headgroups provided that the solution does not contain other charged species that will compete with the GU. Organic enrichment through this cooperative adsorption mechanism has yet to be addressed in models describing SSA formation.[146]

3.2. Experimental

3.2.1 Materials

1,2-dipalmitoyl-*sn*-*glycero*-3-phosphocholine (DPPC, powder, >99%) was purchased from Avanti Polar Lipids Inc. (Alabaster, Alabama). D-Glucuronic acid (GU, powder, ≥98%), sodium carbonate monobasic (powder, ≥99%), sodium carbonate dibasic (powder, ≥98%), and sodium hydroxide (pellets, ≥98%) were purchased from Sigma-Aldrich (St. Louis, MO). HPLC grade chloroform (99.9%) was purchased from Fisher Scientific. All chemicals were used without further purification. Millipore water (resistivity of 18.2 MΩ) was used for all aqueous sample preparation.

3.2.2 Preparation of Samples

Lipid stock solutions (0.7 mg/mL) were prepared in chloroform and sonicated for 20 minutes. Buffer solutions of pH 9.0 (100 mM) were made with sodium carbonate and sodium bicarbonate. Glucuronic acid (pKa 3.20) was added to buffer solutions before adjusting the pH of the solution to 9.0 with sodium hydroxide.

For VSFG experiments, aqueous samples were prepared in either a Teflon Petri dish or a Pyrex borosilicate Petri dish bottom. Teflon Petri dishes were cleaned with Liquinox (Alconox Inc.) and then rinsed with Millipore water before being treated with UV/ozone (Novascan PSD Pro Series Digital UV Ozone System). Borosilicate Petri dishes were acid washed (50/50 vol. nitric/sulfuric) and then rinsed multiple times with Millipore water before use. The DPPC-containing spreading solvent was deposited on the surface of the aqueous solution with a Hamilton glass microsyringe.

3.2.3 Vibrational Sum Frequency Generation

Vibrational sum frequency generation (VSFG) is a second order nonlinear spectroscopy technique that only probes molecular vibrations that are non-centrosymmetric. This capability allows study of molecules at surfaces without contributions from the bulk phase. To produce VSFG signal, two incident laser sources—a fixed 800 nm visible laser and a tunable IR source are combined spatially and temporally at a surface. If the IR source is resonant with a vibrational mode of surface species, the sum frequency signal becomes resonantly enhanced.

The sum frequency intensity, $I(\omega)$, (Equation 3.1) is proportional to the square of the second-order nonlinear susceptibilities $\chi^{(2)}$. The effective second-order nonlinear susceptibility is made up of a non-resonant part, $\chi^{(2)}_{NR,eff}$ and a resonantly enhanced term, , $\chi^{(2)}_{q,eff}$, that depends on the resonant frequency, ω_q, and the damping constant of the qth vibrational mode, Γ_q, (Equation 3.2).[56] Recent studies have shown that at charged aqueous interfaces, the potential of the interface, $\Phi(0)$ can lead to mixing of the second and third order nonlinear susceptibilities, $\chi^{(3)}$;[71-72] this mixing can also affect SF intensities and lineshapes, sometimes in non-intuitive ways (Equation 3.3).

$$I(\omega) \propto |\chi^{(2)}_{eff}|^2 \qquad (3.1)$$

$$\left|\chi^{(2)}_{eff}\right|^2 = \left|\chi^{(2)}_{NR,eff} + \sum \frac{\chi^{(2)}_{q,eff}}{\omega_{IR}-\omega_q+i\Gamma_q}\right|^2 \qquad (3.2)$$

$$I(\omega) \propto |\chi^{(2)}_{NR} + \sum \frac{\chi^{(2)}_{q,eff}}{\omega_{IR}-\omega_q+i\Gamma_q} + (\chi^{(3)}_1 + i\chi^{(3)}_2)\Phi(0)|^2 \qquad (3.3)$$

The role of $\chi^{(3)}$ and $\chi^{(2)}$ mixing and its impact on SFG data has been examined extensively by Geiger and coworkers.[71] Procedures for assessing χ^3's effect(s) on features observed in SFG spectra are available for download.[71]

In the experiments described below, we considered contributions from a simple $\chi^{(2)}$ response as well as the role played by the static, electric field induced $\chi^{(3)}$ effect. Careful analysis showed that including $\chi^{(3)}$ led to very little change in intensities, line shapes and band positions in the C-H stretching region (2800-3000 cm^{-1}). Slight differences were observed at the lowest GU concentrations but only for the methyl Fermi resonance (2940 cm^{-1}) and the methyl asymmetric stretch (2960 cm^{-1}) features. Our analysis of lipid monolayer structure and organization did not include these features and instead focused on methyl and methylene symmetric stretch transitions at 2872 and 2948 cm^{-1}, respectively. For these spectral bands, changes induced by $\chi^{(3)}$ were indistinguishable from day-to-day experimental uncertainties, thus the data presented below including intensity ratios reflect only a $\chi^{(2)}$ contribution.

The experiments in this work were acquired under three polarization conditions (SF, VIS, IR): SSP, PPP, and SPS. PPP polarization samples all nonzero $\chi^{(2)}$ elements and SPS and SSP only sample a single $\chi^{(2)}$ element. In this analysis, the SSP polarization combination is used to measure film organization.

We note that VSFG has been used previously to perform ex situ measurements of SSA surface composition. Specifically, Geiger and coworkers collected aerosol particles from the Scripps wave flume and then tested the surface for the presence of organic species. They found clear evidence of organic accumulation at these surfaces, but broad lineshapes

and a lack of distinctly assigned features led the authors to conclude that natural SSA have heterogeneous alkyl coating on their surfaces.[147-148]

Vibrational Sum Frequency System at Montana State University: Two different assemblies were used to acquire VSF spectra. At Montana State University, the VSFG assembly is built around a Coherent Libra Ti:Sapphire laser with a 85 fs pulse width and a 1 kHz repetition rate. This amplified system produces 3.3 W of 800 nm light. A beam splitter reflects 80% of this light into a Coherent OPerA Solo optical parametric amplifier that generates the IR light centered at 3.4 μm used in the VSFG measurements. The remaining 20% of the 800 nm output is shaped with a 4-f pulse shaper using a grating (1400 grooves/mm^{-1}) blazed at 800 nm (Spectrogon), a 25 cm FL cylindrical lens and an adjustable slit. This pulse shaper results in resolution that is sub-10 cm^{-1}. Both the IR and visible light polarizations are controlled with waveplates before being focused onto the sample with 10 cm FL lenses. The laser beams must be overlapped spatially and temporally to create the sum frequency signal. This SF signal is reflected using a 10 cm FL off-axis parabolic mirror to collimate the light before focusing the SF signal into a monochromator (SpectraPro-300i, Acton Research Corporation) and then dispersing onto a 1340 x 100 pixel CCD (PIXIS100B, Princeton Instruments). SFG spectra were normalized using the SFG response off of a gold wafer and corrected for background contributions. The 2918 cm^{-1} peak of DMSO[57] was used to calibrate the IR frequency of the SFG signal. Spectral features in the different regions were normalized to the instrument response from a gold substrate so that relative intensities could be compared quantitatively.[149-150]

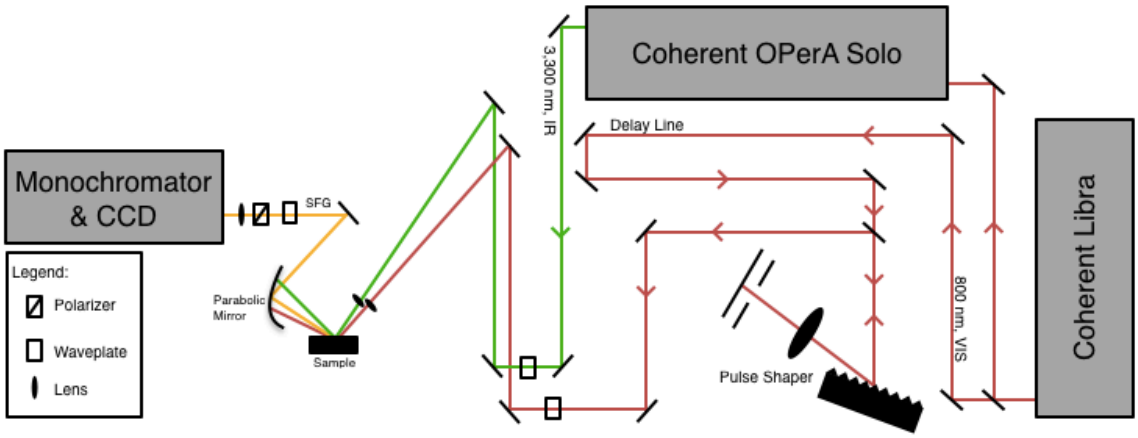

Figure 3.1 Layout of the MSU SFG system. The pulse shaper is made up of a grating, a 25 cm cylindrical lens, a variable slit, and a mirror.

Scanning Sum Frequency Generation: The SFG spectrometer used to probe O-H vibrations presented in this work has been described elsewhere.[62, 73-76] Briefly, this spectrometer (EKSPLA) utilizes a Nd:YAG laser (EKSPLA PL2251A-50) with a 29 ps pulse at 10 Hz. Part of this fundamental output is converted from 1064 nm to a visible (532 nm) beam. The remaining fundamental is sent to an OPA to produce IR light that is tunable from 650 cm^{-1} to 4300 cm^{-1}. One point to note is that data acquired with the scanning SFG system were not referenced to any external standard so band intensities, especially at the extreme edges of the spectral range covered, were subject to greater uncertainties in their relative concentrations.

3.2.4 Surface Tension

Surface tension measurements were made with a NIMA Langmuir trough (Model 302LL) with a NIMA PS4 pressure sensor and a Micro Processor Interface 104. The Langmuir trough was cleaned with chloroform and Millipore water before use. Paper Wilhelmy plates (Brown Waite Engineering) were used to measure surface tension. This

assembly consistently showed an accuracy of (0.4 mN/m) and precision of (0.2 mN/m) using Millipore water (18.2 MΩ-cm) as a standard.

For pressure-area isotherms, the Langmuir trough barriers were closed at a speed of 10 cm^2/min. The surface pressure (π) was measured as a function of surface area. This surface pressure is related to the surface tension of the underlying neat liquid phase (γ_0) and the surface tension of the subphase and a surfactant monolayer (γ).

$$\pi = \gamma_0 - \gamma \quad (3.4)$$

For ideal mixed monolayers containing two species that are restricted to the surface, intermolecular interactions can be quantified by calculating the excess free energy of mixing, ΔG^E_{mix}. This free energy, shown in Equation 3.5, is dependent on A_{12}, which is the measured area per molecule of a mixed monolayer, A_1 and A_2, which are the area per molecule of a pure monolayer of one of the species in the mixed monolayer, and x_1 and x_2 which are the mole fractions of each of the species in the mixed monolayer.[80-81]

$$\Delta G^E_{mix} = \int_{\pi_1}^{\pi_2} N_A(A_{12} - x_1A_1 - x_2A_2)d\pi \quad (3.5)$$

While the surface films examined in these studies consisted of an insoluble lipid and a highly soluble saccharide, treating these systems as mixed monolayers afforded us the opportunity to assess how cooperative adsorption affected surface free energy.

3.2.5 Differential Scanning Calorimetry

Differential scanning calorimetry (DSC) measurements were made using a TA Instruments Discovery (New Castle, DE). For these experiments, sealed Tzero pans and Tzero hermetic lids (TA Instruments) were equilibrated at 20°C. Following equilibration,

the pans were heated by 0.5°C/min until 55°C to capture the transition temperature T_m of DPPC at approximately 41°C.

Vesicle solutions were made using standard protocols.[151] Briefly, a ~1 mg/ml solution of DPPC in chloroform was prepared in a round bottom flask. The chloroform was removed with a rotary evaporator with a bath temperature that was ~10°C greater than T_m of DPPC. The remaining lipid film was rehydrated with either Millipore water or 100 mM pH 9.0 carbonate buffer and then sonicated for 30 minutes in a bath that was ~10°C greater than the T_m. The vesicle solutions were then mixed into GU solutions in the appropriate solvent (Millipore water or 100 mM pH 9.0 carbonate buffer) producing a vesicle solution that was 10 mM DPPC. These solutions were left to equilibrate for ≥ 8 hours before use.

3.3. Results and Discussion

3.3.1 High Concentration Glucosamine

Surface Tension and Free Energy Measurements: Figure 3.2 shows pressure-area isotherms for DPPC on solutions having different concentrations of glucuronic acid. We note here that GU itself is not surface active. The surface tension of GU containing aqueous solutions showed no dependence on GU concentration (the measured surface tension of a 50 mM GU solution was 73.2 ± 0.4 mN/m at 21˚C). The pH of these bulk solutions containing GU is 3.3. The most notable isotherm is from DPPC on a 50 mM GU solution. This isotherm characteristically has higher surface pressures (π) at all surface coverages of DPPC compared to the other isotherms shown. At a given area, a

higher π requires the system's surface tension to be lower than the reference, consistent with the hypothesis that the DPPC film is drawing additional material to the interface from bulk solution.

Another feature of the DPPC-on-50-mM-GU isotherm in Figure 3.2 is the change in slope at 41 mN/m. Similar behavior has been observed previously in DPPC/fibrinogen[152] and in DPPC/DPPG mixtures mixed with recombinant surfactant-associated protein C (SP-C);[153] this result has been interpreted as the solute being 'squeezed' out of the insoluble Langmuir film leading to a higher isothermal compressibility. This slope-change is evident, but much less pronounced in the sub-50 mM isotherms. By forcing GU out of the monolayer, the 50 mM isotherm at high pressures approaches behavior similar to that of other isotherms from solutions having lower GU concentrations. With the DPPC molecules approaching the collapse pressure of the monolayer one expects little impetus for the (deprotonated) glucuronic acid to remain coordinated with insoluble DPPC monomers.

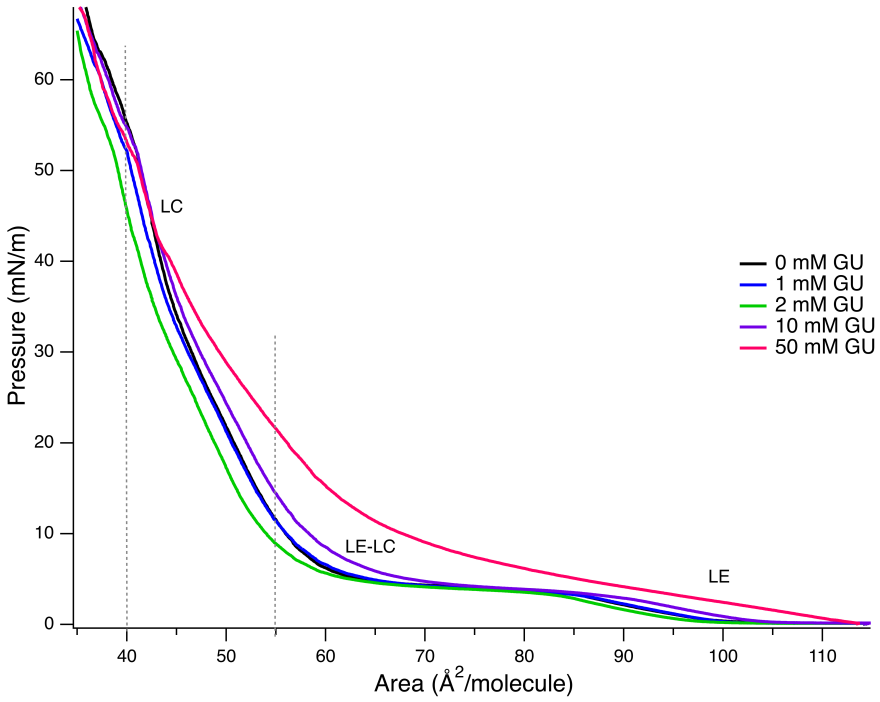

Figure 3.2 π-A isotherms of DPPC on various concentrations of GU at room temperature (21 °C). Vertical dotted lines correspond to 40 and 55 Å^2/mol DPPC surface coverage which is the surface coverage VSFG measurements were taken.

Isotherm data in Figure 3.2 can be used to quantify the effects of cooperative adsorption on surface thermodynamics. For excess free energy of mixing calculations, Equation 3.5 is simplified with the following approximations: first, DPPC is assumed to be the only species constrained to the aqueous/vapor interface. Species 2, GU, is not surface active by itself given the invariance of the surface tension to GU bulk concentration. With these assumptions, Equation 3.5 becomes:

$$\Delta G^E_{mix} = \int_{\pi_1}^{\pi_2} N_A(A_{12} - A_1)d\pi \qquad (3.6)$$

The excess of free energy of mixing is plotted against surface pressure in Figure 3.3. In an ideal mixed monolayer, a negative ΔG^E_{mix} indicates attractive interactions between the components of the monolayer and signifies a more stable monolayer.[81] In

this limit, DPPC on 1 and 2 mM solutions of GU are more condensed and are stabilized. For higher GU concentrations, because the mixing is not ideal, stability criteria need to change to account for the sign change in the excess free energy. The positive ΔG_{mix}^{E} for the 10 and 50 mM GU sub-phases is a result of the DPPC molecules being more 'expanded' than the ideal pure DPPC phase. For 'expanded' monolayers, at any given surface area, the surface pressure is greater and thus the surface tension of the mixed solution is lower. One possible mechanism for this lower surface tension is that GU, at higher concentrations, replaces the water at the surface because of Coulomb interactions with the DPPC head group (further evidence for water replacement by GU is shown in the DSC results). This surface tension lowering at higher saccharide concentrations (≥10 mM) is a possible source of soluble organics in SSA given that lower surface tensions have been correlated to a greater activation of primary marine aerosols.[30]

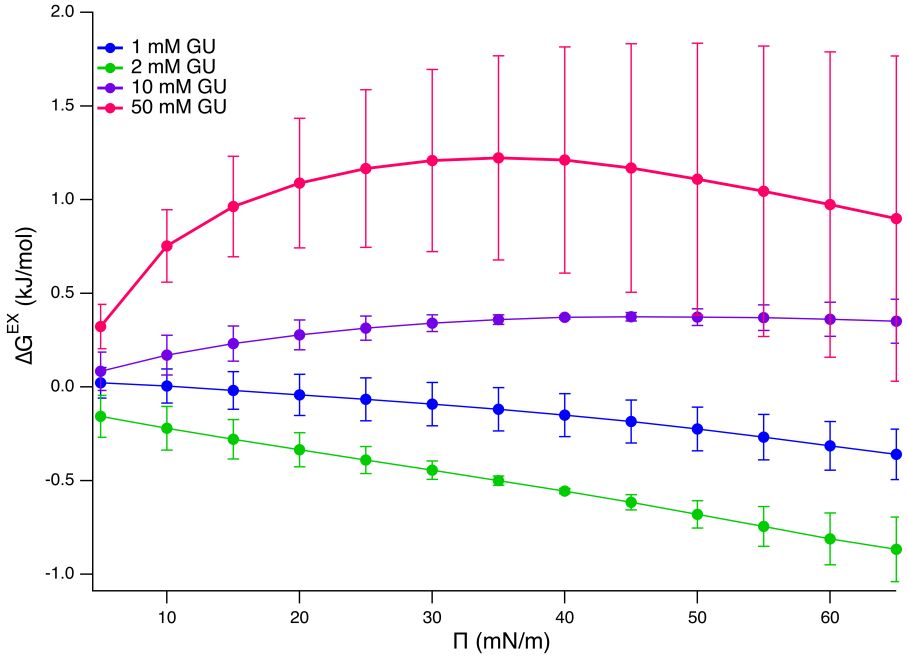

Figure 3.3 Excess free energy of mixing for DPPC on aqueous GU solutions. The reported errors correspond to the standard deviation of 2-3 independent π-A isotherms.

C-H VSFG: Figure 3.4 shows VSFG spectra acquired from DPPC films on a pure Millipore water solution (top) and on a 50 mM GU solution (bottom). The left and right columns correspond to DPPC surface coverage of 55 $Å^2$/molecule and 40 $Å^2$/molecule, respectively. Each panel of Figure 3.4 contains VSFG spectra acquired under symmetry allowed VSFG polarization combinations (SSP, SPS and PPP; PSS data not included). Of note in all spectra is the relative intensities of the methyl symmetric stretch at 2870 cm^{-1} (r^+) and the methylene symmetric stretch at 2840 cm^{-1} (d^+).[154-155] Frequently, the intensity ratio, r^+/d^+, is used as a measure of relative order within organic monolayers studied with VSFG in an SSP polarization configuration.[50, 156-158] P-polarized infrared light probes those vibrations having their IR transition moment aligned primarily along the surface normal. Consequently, a tightly packed monolayer with upright alkyl chains will show a

large r^+ response from the methyl groups directed away from the subphase and a weak or nonexistent d^+ response due in part to the d^+ transition moment being aligned in the surface plane and also because of local inversion symmetry found in all-*trans* chains. A consequence of this monolayer organization is a large r^+/d^+ ratio that can be ≥ 20.[156] At lower surface coverages, alkyl chains become more disordered with *gauche* defects that diminish the r^+ signal and give rise to a larger d^+ response. While the r^+/d^+ ratio has never been correlated quantitatively with any sort of order/disorder parameter, it nevertheless serves as a useful tool for qualitatively assessing monolayer organization.

Looking first at the more expanded DPPC monolayer (55 $Å^2$/molecule, first column), one observes that the d^+ band is relatively large implying a high degree of chain disorder as evidenced by an r^+/d^+ ratio of less than unity. These results are consistent with similar findings reported by Allen, *et al*.[50] Addition of GU to the aqueous subphase causes changes in the spectra, most notably by enhancing r^+ intensity so that when aqueous GU concentrations exceed 10 mM (lower left panel, Figure 3.4), the r^+/d^+ ratio has risen from 0.5 (at 0.0 mM GU) to > 1, showing that chains have adopted a more upright orientation. Interestingly, the origin of this change appears to be growth of the r^+ intensity rather than a decrease in d^+ intensity

A second change in the 55 $Å^2$/molecule DPPC spectra occurs with the SPS polarization. On a water subphase, the peak at 2960 cm^{-1} assigned to a CH_3 asymmetric stretch (r^-) is almost non-existent (top left panel, Figure 3.4). On an aqueous subphase containing 50 mM, however, the r^- vibrational band is quite strong. The presence of this vibrational signal in the plane of the surface can result from structural and/or dynamic

changes in the DPPC monolayer. Certainly, a larger r^+ feature observed in the SSP spectra implies a more upright lipid chain orientation leading one to also expect a larger r^- response in the SPS spectrum. However, the literature also contains numerous examples where a large r^+ response *does not* always correlate with large r^- signal for reasons related to molecular dynamics. Rapid internal rotation of a methyl group about its C_3 axis will preferentially suppress VSFG signal from r^- relative to r^+.[159] We propose that the strong r^- response observed in expanded DPPC monolayers on a 50 mM GU solution is due to condensation of DPPC monomers induced by GU solutes that have cooperatively adsorbed to the aqueous/vapor interface. Such condensation would restrict methyl rotation and allow the r^- transition to acquire appreciable intensity in the SPS VSFG spectrum.

In tightly packed DPPC monolayers (40 $Å^2$/molecule, right column in Figure 3.4), changes in monolayer organization as a function of aqueous GU concentration are more subtle. At higher GU concentrations, d^+ intensity increases compared to the d^+ intensity of tightly packed DPPC on pure water. Figure 3.5 shows the r^+/d^+ ratios for both the expanded 55 $Å^2$/molecule and the tightly packed 40 $Å^2$/molecule. In the 55 $Å^2$/molecule data, an increase in the ratio as the GU concentration increases supports the idea that GU is changing the DPPC organization at the surface. In the 40 $Å^2$/molecule data, where the data show an initial drop in this ordering, changes in organization are attributed to a change in overall molecular tilt, given that the DPPC acyl chains themselves should already be in all-trans configurations with very little free area available to reorganize conformational structure. This ratio then increases with additional GU and with 100 mM

GU in the subphase, the ratio returns to a value close to that of DPPC on pure water. In both cases – expanded and tightly packed – changes in the VSFG spectrum resulting from GU in the aqueous subphase support a cooperative adsorption mechanism.

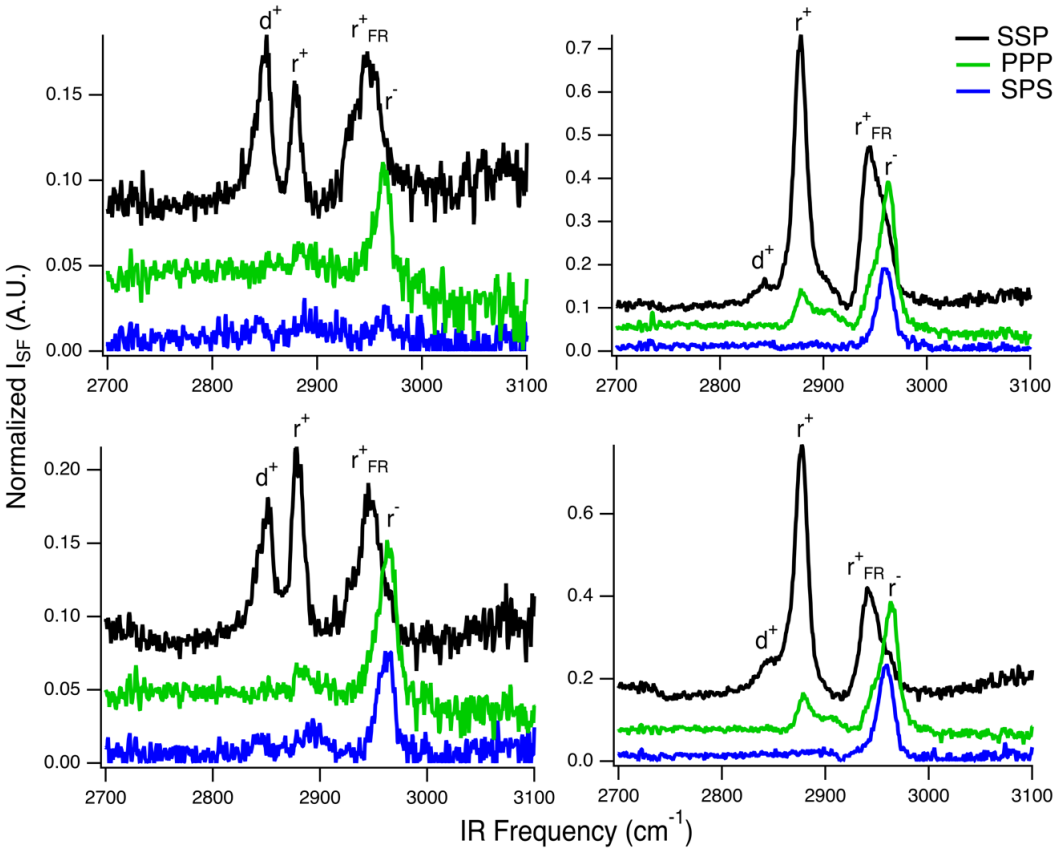

Figure 3.4. SF spectra of DPPC. The top row is DPPC on water and the bottom row is on a 50 mM GU solution. The left column has a surface coverage of 55 $Å^2$/molecule DPPC and the right 40 $Å^2$/molecule DPPC.

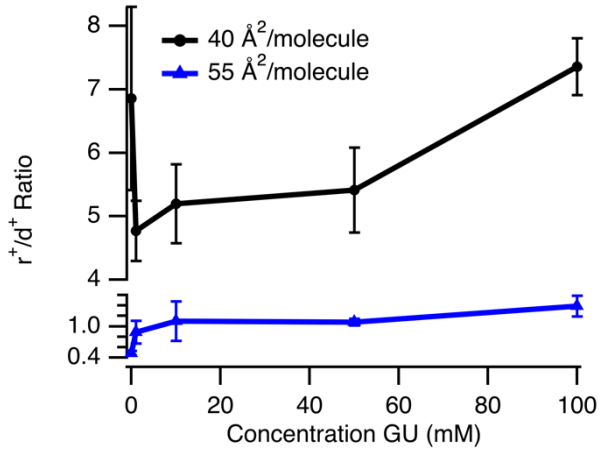

Figure 3.5 Ratio of the CH_3 symmetric stretch (r^+) to the CH_2 symmetric stretch (d^+). For each GU concentration, data was averaged over four data acquisitions on a single day. The reported error is the standard deviation of this averaged data from 2-4 different independent experiments.

O-H Vibrational Region: To further examine GU induced changes to DPPC monolayer organization, spectra were acquired in the O-H stretching region. Figure 3.6 shows VSFG spectra covering an expanded IR frequency range and acquired from expanded DPPC monolayers (55 $Å^2$/molecule) as a function of GU concentration. The IR frequency range now covers the 3000 – 3700 cm^{-1} and is dominated by broad vibrational resonances. The feature at 3250 cm^{-1} has been attributed to tetrahedrally hydrogen bound water molecules or coupled hydrogen bond donors. The feature at 3400 cm^{-1} is typically assigned to asymmetrically hydrogen bound water molecules or loosely coordinated water molecules such as those found in liquid water. The first observation from data in Figure 3.6 is that addition of GU to the aqueous subphase changes the structure of interfacial water. There is a shift in the maximum water intensity from the 3400 cm^{-1} peak to the 3250 cm^{-1} peak in the spectrum of DPPC on 1 mM GU compared to the spectra of DPPC on pure water. This shift in intensity from 3400 cm^{-1} to 3250 cm^{-1}

indicates an increase in the *relative* amount tetrahedrally hydrogen bound water molecules. Second, the *total* intensity in the –OH stretching region diminishes as GU concentration increases. This reduced intensity can be a result of fewer water molecules in the anisotropic interfacial region or from a more randomly organized surface. Given that the interface has a significant amount of formal charge (from the DPPC headgroups and any negatively charged GU) *and* given the observed shift in vibrational intensity from disordered water (at 3400 cm^{-1}) to ordered water (at 3250 cm^{-1}), a more randomized surface structure is unlikely. Instead, we propose that the observed reduction in overall water intensity is due to GU cooperatively adsorbing to the lipid surface, diminishing the width of the double layer and, by extension, reducing the width of the anisotropic region containing water molecules that contribute to a VSFG spectrum. Similar results are observed for the 40 $Å^2$/molecule DPPC film as well, although the magnitude of these changes is much less pronounced.

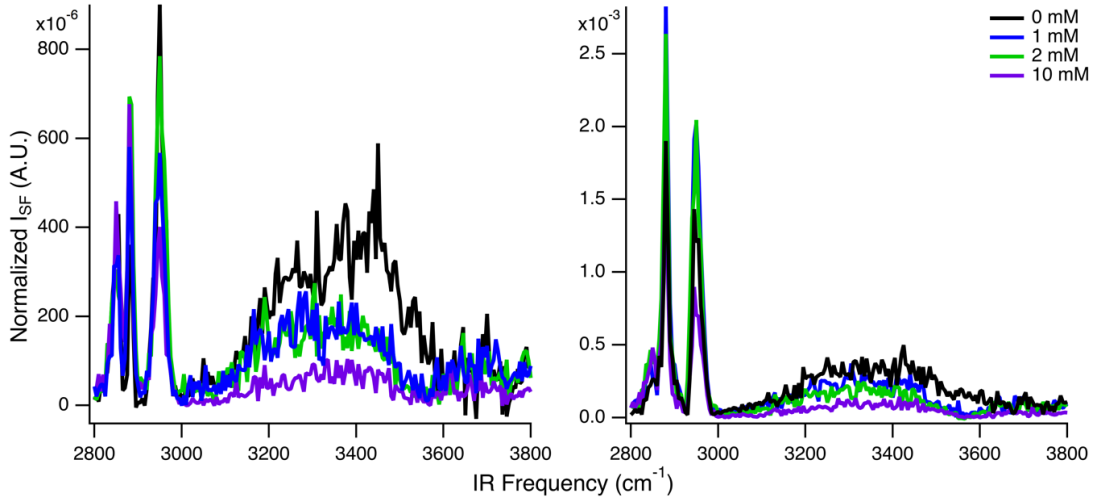

Figure 3.6 O-H vibrational region for 55 $Å^2$/molecule DPPC (left) and 40 $Å^2$/molecule DPPC (right) on various concentrations of GU/Millipore solutions.

Consequences of GU Association with DPPC Bilayers: Glucuronic molecules adsorb cooperatively to lipid monolayers at the aqueous/air interface likely displacing water molecules and – we believe – shrinking the double layer that contains water structured by the lipid headgroups. To search further for signs of this saccharide-lipid association, DPPC vesicles were prepared in a buffered aqueous solution. After vesicle formation, GU was introduced to solution and the effects of GU addition on bilayer structure were tested with differential scanning calorimetry. The main transition of the DPPC bilayers is the phase change from a gel to a liquid crystalline state at 40.4 ˚C. There is an additional phase transition below the main transition, forming a "ripple phase", in which a flat membrane in the gel phase becomes a periodically undulated bilayer.[85] The presence of GU in the lipid vesicle solution results in three significant changes to the DPPC vesicle endotherm. First, the data show a linear increase in the T_m as the concentration of GU added to the vesicle solution is increased. This linear trend is reminiscent of colligative properties that change with increasing solute concentration. In bulk solution, colligative properties result from a reduction of a liquid's chemical potential because of the presence of a solute.

The second significant change to the DSC endotherms is that the DPPC phase transition from gel to liquid crystalline phase splits into two distinct melting temperatures with a weaker peak appearing in the endotherm at temperatures 1-2°C higher than the main transition. The introduction of a second peak in lipid endotherms has been reported previously and attributed to dehydration of the vesicles' lipid head groups.[82] This dehydration mirrors the trend in the DPPC isotherm on 50 mM of glucuronic acid where

there is evidence that GU may be replacing water molecules at the surface and creating a lower surface tension. Additional evidence of this dehydration appears in the VSFG spectra where contributions from water in the OH stretching region diminish with increasing GU concentration. This second T_m, labeled T_{m2}, also increases linearly in temperature with glucuronic acid concentration. Other instances of a second, distinct peak in PC lipids, have occurred with divalent and trivalent cations. These ions are expected to be located at the bilayer surface—interacting with the headgroup's negatively charged phosphate[83] and are expected to have significant effects on the lipid packing due to rearrangement of the zwitterionic headgroup region, resulting in a more condensed monolayer.[160] To our knowledge, data shown in Figure 3.7 are the first to show this effect with cooperatively adsorbed *anions*. With the growth of the second peak at the expense of the first peak, ΔH_{cal} has not significantly changed between the original and new peak.[83, 160]

GU, in concentrations >50 mM, results in a loss of the ripple phase transition, labeled T_p (pretransition temperature). Prior studies have shown that T_p for phosphatidylcholines (PCs) is scarcely affected by moderate concentrations (1 M) of monovalent cations K^+ and Na^+. With divalent cations (1 M Mg^{2+} and Ca^{2+} (> 10 mM)), T_p increases. Additionally, Ca^{2+} concentrations above 1 mM have reduced ΔH_{cal} of the pretransition, but the ΔH_{cal} increases with Ca^{2+} concentrations above 10 mM. Data in Figure 3.7 show an entirely different result compared to divalent cation-induced condensing effects on T_m.

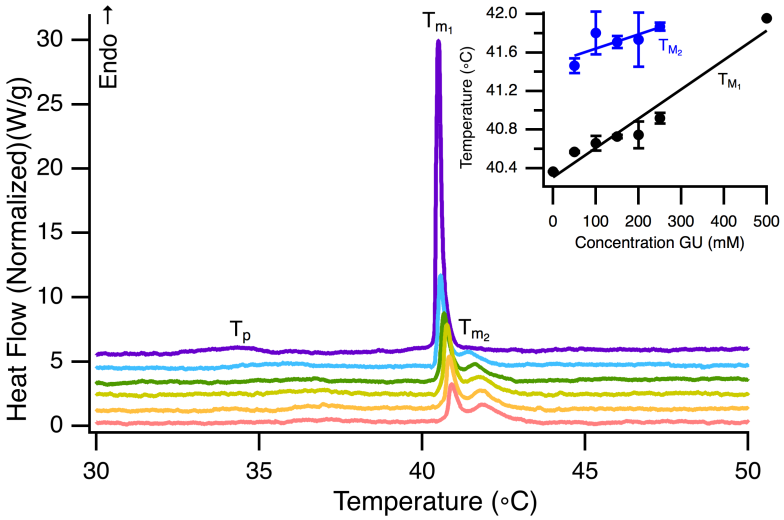

Figure 3.7 DSC measurements for DPPC vesicles in Millipore solutions with GU. All transitions are endothermic. The concentration of GU increases by 50 mM successively from top (0 mM) to bottom (250 mM) trace. Peak temperatures for both the T_{m1} and T_{m2} transitions are plotted in the inset. Error bars are calculated from the standard deviation from three measurement.

3.3.2 Buffers

VSFG, Langmuir trough and DSC measurements described in Section 3.2 all support a cooperative adsorption mechanism between DPPC and glucuronic acid solutes in solutions made from Millipore water (pH = 5.8). Data presented in the previous sections show that GU condenses expanded DPPC films and forces a reorganization of the lipid acyl chains. While the mechanism responsible for DPPC-GU association remains unconfirmed, the most probable explanation is Coulomb attraction between the negatively charged GU and DPPC's positively charged quaternary ammonium group. This Coulomb attraction appears to partially dehydrate the lipid headgroup, a result that is consistent with DSC data shown in Figure 3.7 (for DPPC vesicles in GU-containing aqueous solution) and VSFG data shown in Figure 3.6. Whether such interactions remain

important under environmentally relevant conditions is a question that must be addressed before cooperative adsorption can be considered as a strong driving force responsible for organic enrichment in the sea-surface microlayer. Specifically, oceans are buffered to a pH of 8.1 due primarily to dissolved carbonate/bicarbonate species. Furthermore, ocean water generally has high ionic strength (~0.7M) comprised primarily of monovalent and divalent cations as well as Cl^-, and SO_4^{2-}. Experiments described in the following section examine the impact of a carbonate buffer (pH = 9.0) on GU's cooperative adsorption to DPPC monolayers. Data suggest that sufficiently high ionic strengths will impede DPPC-GU association and limit cooperative adsorption.

Surface Tension and Excess Free Energy of Mixing: Isotherm data from DPPC monolayers on buffer solutions do not differ significantly with GU concentrations ≤ 10 mM (Figure 3.8). Unlike the unbuffered case (Figure 3.2) where the addition of GU led to measurable changes in surface pressure at given DPPC surface coverages, surface pressure data from DPPC on buffer solutions at the same coverages (40 $Å^2$/DPPC and 55 $Å^2$/DPPC) are virtually identical. Only when GU concentration is increased to 50 mM does isotherm behavior change significantly, again becoming more expanded similar to the observed behavior for DPPC monolayers on unbuffered solutions containing GU. If Coulomb attractions were responsible for cooperative GU adsorption to DPPC monolayers from unbuffered aqueous solutions, then one might reasonably expect the excess carbonate/bicarbonate ions in the buffered solutions to fulfill the same function. Such interactions would make the monolayer's structure and organization largely insensitive to GU concentration. When GU concentration reaches half of the buffer

concentration, GU causes an expansion of the DPPC monolayer and a corresponding reduction in the surface tension in the system—paralleling the effects of GU at 10 and 50 mM in the unbuffered cases.

The pressure-area isotherms in Figure 3.8 show two slope changes in the liquid condensed phase at ~45 mN/m and ~55 mM/m. The presence of these slope changes with no GU present in the subphase indicates that any 'squeeze-out' effects would be from buffer ions being squeezed out of the DPPC monolayer in the 0 mM GU case. For the GU containing subphases, attributing any 'squeeze-out' effects to either the buffer or GU is difficult. With the 50 mM GU subphase, these slope changes are the more pronounced than in the other π-Area isotherms and these changes occur at lower surface pressure. The lower surface pressure of these 'squeeze-out' effects is reminiscent of the proposed 'solute expulsion' observed in the 50 mM GU/Millipore samples and this may indicate GU being preferentially removed from the monolayer relative to carbonate.

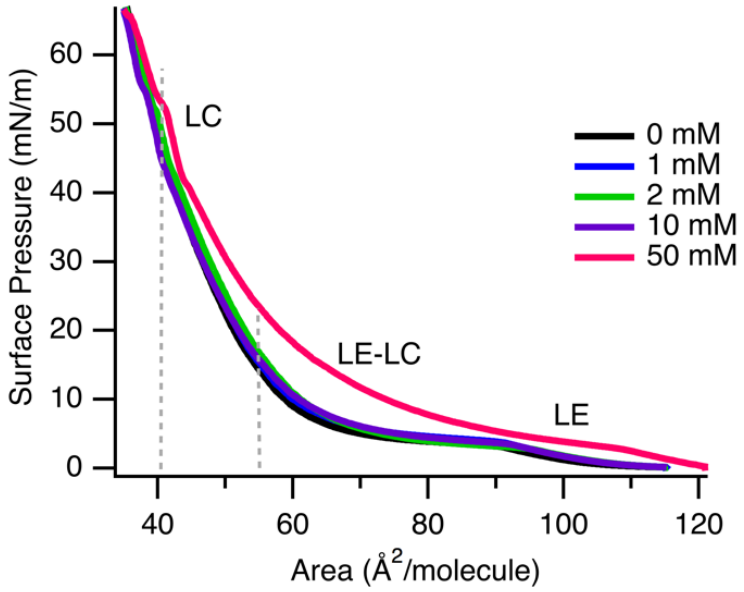

Figure 3.8. π-A isotherms of DPPC on various concentrations of GU in pH 9.0 buffer (sodium carbonate and sodium bicarbonate) at room temperature (21 °C). Vertical dotted lines correspond to 40 and 55 $Å^2$/mol DPPC surface coverage which is the surface coverage VSFG measurements were taken.

For the excess free energy of mixing calculations, the same approximations as in the water solution were made. For the three lower concentrations of GU used (1, 2, 10 mM) the excess free energy of mixing is negative. This indicates that adding GU to the subphase results in a more stable monolayer. In the case of the 50 mM GU/buffer solution, the area/molecule is expanded, and the system's surface tension is lowered. This surface tension lowering again indicates the GU is in sufficiently high concentration relative to the buffer to competitively associate with the lipid monolayer and disrupt lipid headgroup solvation. Field studies of the sea surface microlayer (SSML) have shown saccharide concentrations is in considerable excess relative to bulk,[20] so the cooperative adsorption mechanism may still be a relevant pathway for soluble organic accumulation in SSA.

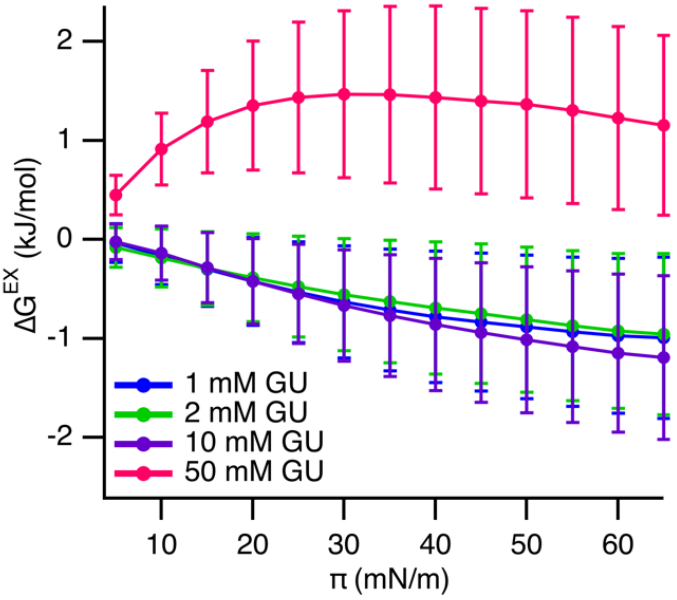

Figure 3.9. Free energy of mixing for DPPC on Buffers. The reported errors correspond to the standard deviation of 2-3 independent π-A isotherms.

C-H VSFG: Isothermal data in Figures 3.8 and 3.9 support observations from VSFG experiments performed on the same systems. Similar to Figure 3.4, Figure 3.10 shows VSFG spectra from DPPC films on a pure buffered subphase (top) and on a buffered subphase containing 10 mM GU solution (bottom). The left and right columns correspond to DPPC surface coverages of 55 Å^2/molecule and 40 Å^2/molecule, respectively. Each panel of Figure 3.10 contains VSFG spectra acquired under symmetry allowed VSFG polarization combinations (SSP, SPS and PPP; PSS data not included). Again, the relative intensities of the methyl symmetric stretch at 2870 cm^{-1} (r^+) and the methylene symmetric stretch at 2840 cm^{-1} (d^+) are the relevant quantities used to assess lipid film structure and organization.

Lipid organization in 40 Å^2/molecule films shows very little dependence on GU concentration from 0 mM to 10 mM GU in pH 9 buffered solutions. In contrast to

changes observed on unbuffered solutions where the r^+/d^+ ratio diminishes from 7.0 to 4.8 with small additions of GU, adding GU to buffered solutions results in the tightly packed DPPC r^+/d^+ ratio changing from 5.6 to 7.0 (Figure 3.11). We surmise that if Coulomb attractions were the driving force behind GU cooperative adsorption in unbuffered solutions, then these interactions will be suppressed by the higher ionic strength buffer. Reduced Coulomb attraction between GU and DPPC means that DPPC monolayer organization should be insensitive to GU bulk concentration and the r^+/d^+ ratio should not change significantly.

In the 55 $Å^2$/molecule data, the ratio for the solutions containing GU is slightly but measurably higher than the solutions that do not contain GU. More importantly, organization in these expanded monolayers on buffered solutions is significantly enhanced (with and without GU) compared to similar DPPC coverages on Millipore water. Together, these results imply that GU may cooperatively adsorb weakly to more expanded DPPC monolayers on alkaline solutions but most of the lipid monolayer organization is controlled by the inorganic carbonate/bicarbonate species.

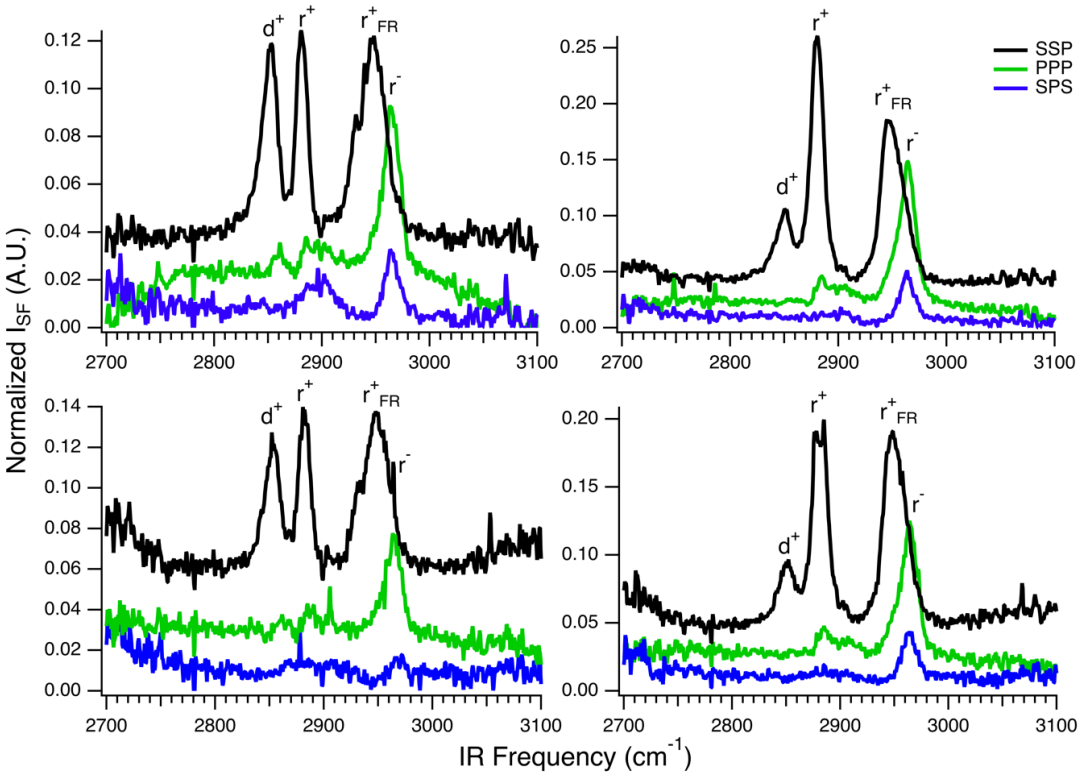

Figure 3.10 SF spectra of DPPC with a pH 9.0 buffer subphase. The top row is DPPC on a 100 mM carbonate buffer with no glucuronic acid and the bottom row is on a 100 mM carbonate buffer with 10 mM GU. The left column has a surface coverage of 55 $Å^2$/molecule DPPC and the right 40 $Å^2$/molecule DPPC.

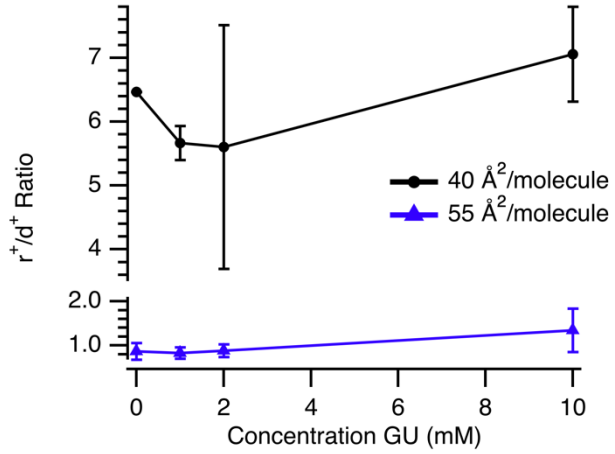

Figure 3.11. r^+/d^+ ratios for DPPC on buffers. For each GU concentration, data was averaged over four data acquisitions on a single day. The reported error is the standard deviation of this averaged data from three different independent measurements.

O-H Stretch: The OH vibrational spectra on buffer solutions show similar intensities for the OH stretching region regardless of GU concentration (Figure 3.12). In all instances including solutions that do not contain GU, the free OH peak is nonexistent and the spectral intensity in the hydrogen bonded region is significantly diminished compared to similar spectra acquired from DPPC monolayers on Millipore water. Again, these findings support a picture where carbonate/bicarbonate ions strongly associate with the DPPC headgroups leaving GU with little opportunity to cooperatively adsorb to the aqueous interface. The peaks at 3200 and 3400 cm^{-1} are all similar in intensity showing that changes in GU concentration is not causing significant changes to the surface water structure because the much higher concentration of buffer ions mitigates any affect from the GU ions.

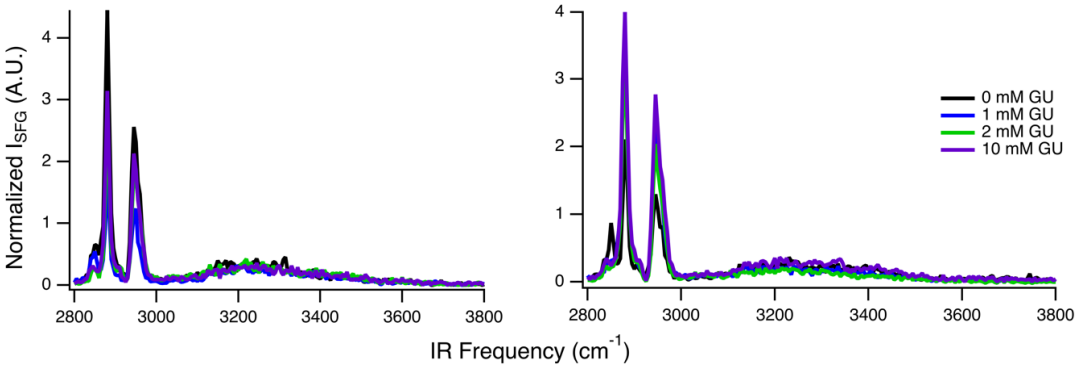

Figure 3.12. O-H vibrational region for 55 $Å^2$/molecule DPPC (left) and 40 $Å^2$/molecule DPPC (right) on various concentrations of GU in pH 9.0 carbonate buffer.

Lipid Bilayers in Buffered Solution: For the lipid vesicles in buffer solution, the first two concentrations, 0 mM and 50 mM GU, fall within the solution's buffering capacity. By 100 mM GU, the pH of the vesicle solution is reduced to 7 and for 250 mM GU, the vesicle-containing solution pH is again 3.3. Once the GU concentration is greater than the buffer, the second phase transition reappears (T_{m2}), the pretransition temperature disappears, and the T_m increases linearly with GU concentration. These same effects were observed in the DSC results from vesicles in unbuffered Millipore water, leading us to propose that competition between the buffer ions and the GU ions is responsible for changing phase transition behavior in the bilayers.

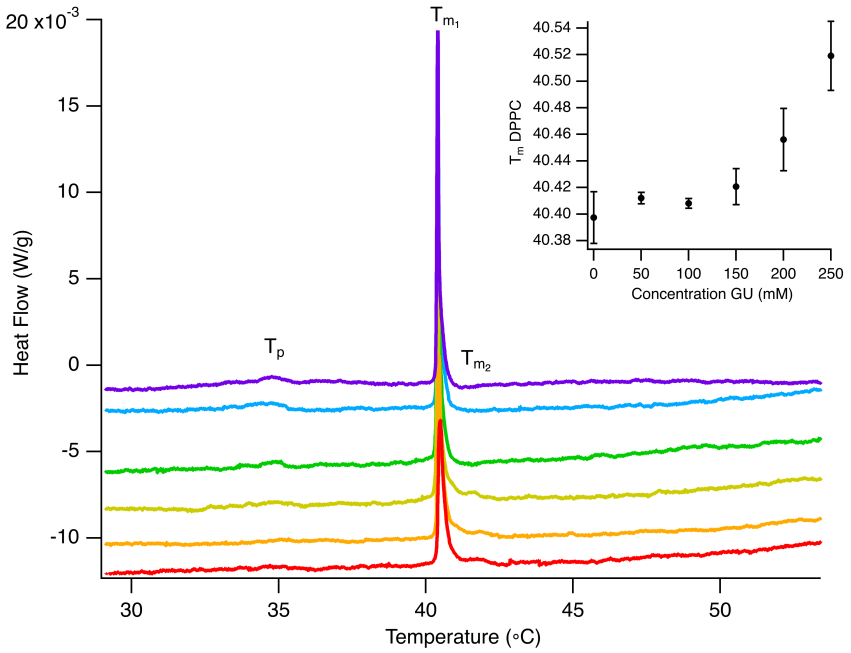

Figure 3.13. DSC measurements for DPPC vesicles in buffer solutions with GU. All transitions are endothermic. The concentration of GU increases by 50 mM successively from top (0 mM) to bottom (250 mM) trace. Peak temperature for T_{m1} transition is plotted in the inset. Error bars are from the standard deviation of three measurements.

3.4. Conclusions

Experimental studies described in this work show that the negatively charged monosaccharide, glucuronic acid, causes structural changes to moderately packed DPPC films and alters phase behaviors of these films. Specifically, larger concentrations of GU, 50 mM, show a larger footprint (area/molecule) in surface tension measurements which we believe is due to cooperatively adsorbed solutes to the lipid monolayer. Differential scanning calorimetry results also show a dehydration effect resulting in a second transition in the DPPC monolayer. This cooperative adsorption of GU to the DPPC film is competitive when there are buffer ions present in greater abundance than the GU solutes. As shown in the SFG and surface tension data, when the concentration of buffer

is 10x greater than the concentration of GU, few changes are seen to DPPC organization. When GU concentration reaches 50% of buffer concentration, we see an expansion of the DPPC footprint in surface tension measurements that is similar to the data in the pure water measurements. In the DSC measurements, we see GU associated phase changes when the GU concentration is equal to the buffer concentration. These results show that anions can have a significant effect on film organization even though there is a competition for available charge sites at the interface. The changes in surface tension, even with competition from buffer ions, add support to cooperative adsorption being a mechanism for increased organic content at the surface.

3.5 References

18. Burrows, S. M.; Gobrogge, E.; Fu, L.; Link, K.; Elliott, S. M.; Wang, H.; Walker, R., Oceanfilms-2: Representing Coadsorption of Saccharides in Marine Films and Potential Impacts on Modeled Marine Aerosol Chemistry. *Geophys. Res. Lett.* **2016**, *43*, 8306-8313.

20. Jayarathne, T., et al., Enrichment of Saccharides and Divalent Cations in Sea Spray Aerosol During Two Phytoplankton Blooms. *Environ. Sci. Technol.* **2016**, *50*, 11511-11520.

21. Meskhidze, N.; Xu, J.; Gantt, B.; Zhang, Y.; Nenes, A.; Ghan, S. J.; Liu, X.; Easter, R.; Zaveri, R., Global Distribution and Climate Forcing of Marine Organic Aerosol: 1. Model Improvements and Evaluation. *Atmos Chem Phys* **2011**, *11*, 11689-11705.

22. Fossum, K. N., et al., Summertime Primary and Secondary Contributions to Southern Ocean Cloud Condensation Nuclei. *Sci. Rep.* **2018**, *8*, 13844.

28. Wilson, T. W., et al., A Marine Biogenic Source of Atmospheric Ice-Nucleating Particles. *Nature* **2015**, *525*, 234-238.

30. Han, Z. W.; Li, J. W.; Yao, X. H.; Tan, S. C., A Regional Model Study of the Characteristics and Indirect Effects of Marine Primary Organic Aerosol in Springtime over East Asia. *Atmos Environ* **2019**, *197*, 22-35.

36. Russell, L. M.; Hawkins, L. N.; Frossard, A. A.; Quinn, P. K.; Bates, T. S., Carbohydrate-Like Composition of Submicron Atmospheric Particles and Their Production from Ocean Bubble Bursting. *Proc. Natl. Acad. Sci. U. S. A.* **2010**, *107*, 6652-6657.

37. Burrows, S. M.; Ogunro, O.; Frossard, A. A.; Russell, L. M.; Rasch, P. J.; Elliott, S. M., A Physically Based Framework for Modeling the Organic Fractionation of Sea Spray Aerosol from Bubble Film Langmuir Equilibria. *Atmos Chem Phys* **2014**, *14*, 13601-13629.

39. Grythe, H.; Strom, J.; Krejci, R.; Quinn, P.; Stohl, A., A Review of Sea-Spray Aerosol Source Functions Using a Large Global Set of Sea Salt Aerosol Concentration Measurements. *Atmos Chem Phys* **2014**, *14*, 1277-1297.

40. Hawkins, L. N.; Russell, L., Polysaccharides, Proteins, and Phytoplankton Fragments: Four Chemically Distinct Types of Marine Primary Organic Aerosol Classified by Single Particle Spectromicroscopy. *Adv Meteorol* **2010**, *2010*, 14.

41. Bhattacharyya, L.; Rohrer, J. S., *Applications of Ion Chromatography for Pharmaceutical and Biological Products*; Hoboken, N.J. : John Wiley & Sons, Inc.: Hoboken, N.J., 2012.

49. Adams, E. M.; Casper, C. B.; Allen, H. C., Effect of Cation Enrichment on Dipalmitoylphosphatidylcholine (Dppc) Monolayers at the Air-Water Interface. *J. Colloid Interface Sci.* **2016**, *478*, 353-364.

50. Adams, E. M.; Verreault, D.; Jayarathne, T.; Cochran, R. E.; Stone, E. A.; Allen, H. C., Surface Organization of a Dppc Monolayer on Concentrated Srcl2 and Zncl2 Solutions. *Phys. Chem. Chem. Phys.* **2016**, *18*, 32345-32357.

51. Link, K. A.; Hsieh, C. Y.; Tuladhar, A.; Chase, Z.; Wang, Z. M.; Wang, H. F.; Walker, R. A., Vibrational Studies of Saccharide-Induced Lipid Film Reorganization at Aqueous/Air Interfaces. *Chem Phys* **2018**, *512*, 104-110.

56. Shultz, M. J.; Schnitzer, C.; Simonelli, D.; Baldelli, S., Sum Frequency Generation Spectroscopy of the Aqueous Interface: Ionic and Soluble Molecular Solutions. *Int Rev Phys Chem* **2000**, *19*, 123-153.

57. Velarde, L.; Zhang, X. Y.; Lu, Z.; Joly, A. G.; Wang, Z.; Wang, H. F., Communication: Spectroscopic Phase and Lineshapes in High-Resolution Broadband Sum Frequency Vibrational Spectroscopy: Resolving Interfacial Inhomogeneities of “Identical" Molecular Groups. *J. Chem. Phys.* **2011**, *135*, 241102.

62. Zhang, Z.; Guo, Y.; Lu, Z.; Velarde, L.; Wang, H. F., Resolving Two Closely Overlapping -Cn Vibrations and Structure in the Langmuir Mono Layer of the Long-Chain Nonadecanenitrile by Polarization Sum Frequency Generation Vibrational Spectroscopy. *J. Phys. Chem. C* **2012**, *116*, 2976-2987.

71. Ohno, P. E.; Wang, H. F.; Geiger, F. M., Second-Order Spectral Lineshapes from Charged Interfaces. *Nat. Commun.* **2017**, *8*, 1032.

72. Ohno, P. E.; Wang, H. F.; Paesani, F.; Skinner, J. L.; Geiger, F. M., Second-Order Vibrational Lineshapes from the Air/Water Interface. *J. Phys. Chem. A* **2018**, *122*, 4457-4464.

73. Liu, W.; Fu, L.; Wang, Z.; Sohrabpour, Z.; Li, X.; Liu, Y.; Wang, H. F.; Yan, E. C. Y., Two Dimensional Crowding Effects on Protein Folding at Interfaces Observed by Chiral Vibrational Sum Frequency Generation Spectroscopy. *Phys. Chem. Chem. Phys.* **2018**, *20*, 22421-22426.

74. Lu, Z.; Karakoti, A.; Velarde, L.; Wang, W. N.; Yang, P.; Thevuthasan, S.; Wang, H. F., Dissociative Binding of Carboxylic Acid Ligand on Nanoceria Surface in Aqueous Solution: A Joint in Situ Spectroscopic Characterization and First-Principles Study. *J. Phys. Chem. C* **2013**, *117*, 24329-24338.

75. Mifflin, A. L., et al., Accurate Line Shapes from Sub-1 Cm(-1) Resolution Sum Frequency Generation Vibrational Spectroscopy of Alpha-Pinene at Room Temperature. *J. Phys. Chem. A* **2015**, *119*, 1292-1302.

76. Olenick, L. L.; Chase, H. M.; Fu, L.; Zhang, Y.; McGeachy, A. C.; Dogangun, M.; Walter, S. R.; Wang, H. F.; Geiger, F. M., Single-Component Supported Lipid Bilayers Probed Using Broadband Nonlinear Optics. *Phys. Chem. Chem. Phys.* **2018**, *20*, 3063-3072.

80. Blume, A., Lipids at the Air–Water Interface. *ChemTexts* **2018**, *4*, 1-25.

81. Gzyl-Malcher, B.; Paluch, M., Studies of Lipid Interactions in Mixed Langmuir Monolayers. *Thin Solid Films* **2008**, *516*, 8865-8872.

82. Kodama, M.; Kuwabara, M.; Seki, S., Sucessive Phase-Transition Phenomena and Phase Diagram of the Phosphatidylcholine-Water System as Revealed by Differential Scanning Calorimetry. *Biochim. Biophys. Acta, Biomembr.* **2002**, 567-570.

83. McElhaney, R. N., The Use of Differential Scanning Calorimetry and Differential Thermal-Analysis in Studies of Model and Biological-Membranes. *Chem Phys Lipids* **1982**, *30*, 229-259.

85. Riske, K. A.; Barroso, R. P.; Vequi-Suplicy, C. C.; Germano, R.; Henriques, V. B.; Lamy, M. T., Lipid Bilayer Pre-Transition as the Beginning of the Melting Process. *Biochim. Biophys. Acta* **2009**, *1788*, 954-963.

89. Casper, C. B.; Verreault, D.; Adams, E. M.; Hua, W.; Allen, H. C., Surface Potential of Dppc Monolayers on Concentrated Aqueous Salt Solutions. *J. Phys. Chem. B* **2016**, *120*, 2043-52.

90. Casillas-Ituarte, N. N.; Chen, X.; Castada, H.; Allen, H. C., Na(+) and Ca(2+) Effect on the Hydration and Orientation of the Phosphate Group of Dppc at Air-Water and Air-Hydrated Silica Interfaces. *J. Phys. Chem. B* **2010**, *114*, 9485-9495.

91. LIS, L. J.; LIS, W. T.; PARSEGIAN, V. A.; RAND, R. P., Adsorption of Divalent Cations to a Variety of Phosphatidylcholine Bilayers. *Biochemistry* **1981**, *20*, 1771-1777.

101. Plant, A. L., Supported Hybrid Bilayer Membranes as Rugged Cell Membrane Mimics. *Langmuir* **1999**, *15*, 5128-5135.

102. Sackmann, E., Supported Membranes: Scientific and Practical Applications. *Science* **1996**, *271*, 43-48.

142. Pham, D. Q., et al., Biological Impacts on Carbon Speciation and Morphology of Sea Spray Aerosol. *ACS Earth Space Chem.* **2017**, *1*, 551-561.

143. Facchini, M. C., et al., Primary Submicron Marine Aerosol Dominated by Insoluble Organic Colloids and Aggregates. *Geophys. Res. Lett.* **2008**, *35*.

144. Elliott, S., et al., Does Marine Surface Tension Have Global Biogeography? Addition for the Oceanfilms Package. *Atmosphere* **2018**, *9*, 216-232.

145. Ahmed, S. N.; Brown, D. A.; London, E., On the Origin of Sphingolipid/Cholesterol-Rich Detergent-Insoluble Cell Membranes: Physiological Concentrations of Cholesterol and Sphingolipid Induce Formation of a Detergent-Insoluble, Liquid-Ordered Lipid Phase in Model Membranes. *Biochemistry* **1997**, *36*, 10944-10953.

146. Schill, S. R.; Burrows, S. M.; Hasenecz, E. S.; Stone, E. A.; Bertram, T. H., The Impact of Divalent Cations on the Enrichment of Soluble Saccharides in Primary Sea Spray Aerosol. *Atmosphere* **2018**, *9*, 476-417.

147. Reddy, S. K.; Thiraux, R.; Wellen Rudd, B. A.; Lin, L.; Adel, T.; Joutsuka, T.; Geiger, F. M.; Allen, H. C.; Morita, A.; Paesani, F., Bulk Contributions Modulate the Sum-Frequency Generation Spectra of Water on Model Sea-Spray Aerosols. *Chem* **2018**, *4*, 1629-1644.

148. Ebben, C. J.; Ault, A. P.; Ruppel, M. J.; Ryder, O. S.; Bertram, T. H.; Grassian, V. H.; Prather, K. A.; Geiger, F. M., Size-Resolved Sea Spray Aerosol Particles Studied by Vibrational Sum Frequency Generation. *The Journal of Physical Chemistry A* **2013**, *117*, 6589-6601.

149. Can, S. Z.; Mago, D. D.; Esenturk, O.; Walker, R. A., Balancing Hydrophobic and Hydrophilic Forces at the Water/Vapor Interface: Surface Structure of Soluble Alcohol Monolayers. *The Journal of Physical Chemistry C* **2007**, *111*, 8739-8748.

150. Esenturk, O.; Walker, R. A., Surface Vibrational Structure at Alkane Liquid/Vapor Interfaces. *J Chem Phys* **2006**, *125*, 174701.

151. Gobrogge, C. A.; Kong, V. A.; Walker, R. A., Temperature-Dependent Partitioning of C152 in Binary Phosphatidylcholine Membranes and Mixed Phosphatidylcholine/Phosphatidylethanolamine Membranes. *J. Phys. Chem. B* **2017**, *121*, 7889-7898.

152. Kuo, R. R.; Chang, C. H.; Yang, Y. M.; Maa, J. R., Induced Removal of Dipalmitoyl Phosphatidylcholine by the Exclusion of Fibrinogen from Compressed Monolayers at Air/Liquid Interfaces. *J. Colloid Interface Sci.* **2003**, *257*, 108-115.

153. Amrein, M.; von Nahmen, A.; Sieber, M., A Scanning Force- and Fluorescence Light Microscopy Study of the Structure and Function of a Model Pulmonary Surfactant. *Eur. Biophys. J.* **1997**, *26*, 349-357.

154. Snyder, R. G.; Strauss, H. L.; Elliger, C. A., Carbon-Hydrogen Stretching Modes and the Structure of N-Alkyl Chains. 1. Long, Disordered Chains. *J. Phys. Chem.* **1982**, *86*, 5145-5150.

155. MacPhail, R. A.; Strauss, H. L.; Snyder, R. G.; Elliger, C. A., Carbon-Hydrogen Stretching Modes and the Structure of *N*-Alkyl Chains. 2. Long, All-Trans Chains. *J. Phys. Chem.* **1984**, *88*, 334-341.

156. Can, S. Z.; Mago, D. D.; Walker, R. A., Structure and Organization of Hexadecanol Isomers Adsorbed to the Air/Water Interface. In *Langmuir*, 2006; Vol. 22, pp 8043-8049.

157. Walker, R. A.; Gruetzmacher, J. A.; Richmond, G. L., Phosphatidylcholine Monolayer Structure at a Liquid−Liquid Interface. In *J. Am. Chem. Soc.*, 1998; Vol. 120, pp 6991-7003.

158. Conboy, J. C.; Messmer, M. C.; Richmond, G. L., Dependence of Alkyl Chain Conformation of Simple Ionic Surfactants on Head Group Functionality as Studied by Vibrational Sum-Frequency Spectroscopy. *J. Phys. Chem. B* **1997**, *101*, 6724-6733.

159. Fourkas, J. T.; Walker, R. A.; Can, S. Z.; Gershgoren, E., Effects of Reorientation in Vibrational Sum-Frequency Spectroscopy. *J. Phys. Chem. C* **2007**, *111*, 8902-8915.

160. Jain, M. K.; Wu, N. M., Effect of Small Molecules on the Dipalmitoyl Lecithin Liposomal Bilayer: Iii. Phase Transition in Lipid Bilayer. *The Journal of Membrane Biology*, *34*, 157-201.

CHAPTER FOUR

COOPERATIVE ADSORPTION OF TREHALOSE TO DPPC STUDIED WITH VIBRATIONAL SUM FREQUENCY GENERATION

Contribution of Authors and Co-Authors

Manuscript in Chapter 4

Author: Katie A. Link

Contributions: Collected and analyzed experimental data. Assisted in writing and editing manuscript.

Co-Author: Gabrielle N. Spurzem

Contributions: Collected differential scanning calorimetry data and Langmuir trough data.

Co-Author: Aashish Tuladhar

Contributions: Assisted with vibrational sum frequency data collection and edited the manuscript.

Co-Author: Zizwe Chase

Contributions: Assisted with vibrational sum frequency data collection and edited the manuscript.

Co-Author: Zheming Wang

Contributions: Edited the manuscript.

Co-Author: Hongfei Wang

Contributions: Edited the manuscript.

Co-Author: Robert A. Walker

Contributions: Assisted with data analysis and editing manuscript.

Manuscript Information

Katie A. Link, Gabrielle N. Spurzem, Aashish Tuladhar, Zizwe Chase, Zheming Wang, Hongfei Wang, and Robert A. Walker

Status of Manuscript:
__x_ Prepared for submission to a peer-reviewed journal
____ Officially submitted to a peer-reviewed journal
____ Accepted by a peer-reviewed journal
____ Published in a peer-reviewed journal

CHAPTER FOUR

COOPERATIVE ADSORPTION OF TREHALOSE TO DPPC STUDIED WITH VIBRATIONAL SUM FREQUENCY GENERATION

4.1 Introduction

Lipid film interactions with small molecules, such as carbohydrates and synthetic organics continue to attract attention due to the link between these associations and biological and environmental processes.[161-164] Lipid monolayers and bilayers have been used as model systems to examine processes as diverse as drug/membrane interactions and organic enrichment in sea spray aerosols.[51, 161] Of the many lipid systems used to study these phenomena, dipalmitoylphosphatidylcholine (DPPC), a diacyl C_{16} zwtterionic lipid, is one of the most commonly studied systems in part because of its prevalence in mammalian cell membranes and its importance as the primary component of lung surfactant.[165]

Saccharides associating with lipid membranes are particularly important given their ability to protect membrane structure and integrity from environmentally hostile conditions. Specifically, organisms have been able to survive dehydration by accumulating large concentrations of saccharides in the cell membrane.[163] For example, trehalose (Tre), a di-saccharide composed of two glucose molecules, has been reported to be an effective cryoprotectant.[166-167] Trehalose, with concentrations as low as 0.1 g Tre/g lipid prevents membranes from fusing together when dehydrated.[166] At higher Tre

concentrations, 1 g Tre/g lipid, the water soluble contents of vesicles are prevented from leaking out during rehydration.[166] While the effects of Tre on membrane integrity are clear, the mechanism responsible for the Tre's protective effects remains under debate.

Experimental studies of Tre with membranes have focused on elucidating Tre's bioprotective mechanisms using techniques including NMR,[93] DSC,[168-170] and FTIR.[171-172] While some methods have not identified one specific mechanism,[163] IR experiments have suggested that Tre replaces water molecules and binds to the carbonyl and/or phosphate groups on phosphocholines.[171, 173] Several hypotheses have been advanced to explain the experimental and computational results of how Tre interacts with lipids and the water around the lipid membranes. For example, the water replacement hypothesis suggests that the saccharides replace water molecules near the lipid by forming H-bonds with the charged groups at the surface.[163, 174] Alternatively, the water entrapment hypothesis suggests that the saccharides concentrate water near the membrane and preserve the hydration shell.[163, 174] The vitrification hypothesis suggests that the sugars form amorphous glasses that reduce mechanical disruption in membranes.[163, 174] The hydration forces hypothesis suggests that sugar molecules are excluded from the surface which indirectly reduces the compressive stress in the membrane during dehydration. The head group-bridging hypothesis is an extension of the water replacement hypothesis in which the sugars H-bonds with multiple lipid headgroups forming a scaffold.[163] Many researchers have acknowledged that a combination of these mechanisms likely work in tandem to keep the membrane hydrated.[163, 174] Of these mechanisms, MD simulations typically point to the water replacement and H-bond bridging as being most important,[164,

[174-175] but characteristics of all the above mechanisms can occur in simulations,[163] leaving considerable ambiguity about this process.

An important point to note is that very little work has considered Tre-lipid interactions under conditions that are likely to be found in nature, namely with fully hydrated lipid monolayers/bilayers in a solution of relatively dilute Tre. Under these circumstances, the lipid film will have to attract Tre from solution, enriching Tre content at the film surface through some sort of cooperative adsorption mechanism. In this context, cooperative adsorption has been used to describe interactions between insoluble Langmuir films at aqueous/vapor interfaces and soluble organic molecules. The soluble organics are adsorbed to the interface through noncovalent interactions with the lipid headgroups. Earlier work has shown that cooperative adsorption can significantly enhance soluble saccharide content at aqueous vapor interfaces covered with DPPC monolayers.[18, 51] A previous study on a monosaccharide/DPPC system showed Langmuir adsorption behavior with a $C_{1/2,gluc,2}$= 1.25±0.45 mM glucosamine.[18] Other studies of DPPC/sugar adsorptions have indicated a cooperative adsorption behavior in the limiting cases of a moderately packed DPPC monolayer in situations where the saccharide did not compete with other ions in solution. [51, 176]

Studies described below tested whether or not cooperative adsorption will draw Tre from aqueous solutions to a DPPC monolayer adsorbed to the aqueous-vapor interface. Unlike the charged monosaccharides glucosamine and glucuronic acid used in the cooperative adsorption studies in Chapters 2 and 3, Tre is uncharged and larger (a disaccharide). Studies described below include both surface tension measurements and

surface specific, nonlinear optical vibrational experiments. Together, results show that cooperative adsorption *does* enhance interfacial Tre concentrations and that adsorbed Tre promotes organization within the DPPC film. These effects become less pronounced with DPPC monolayers that are already tightly packed. To explore these interactions further, DSC measurements were performed to discover what effect(s) Tre had on the thermodynamic properties of lipid vesicle bilayers. Results showed Tre does interact with the lipid membranes when the Tre concentration is ~50 mM; this corresponds to about 0.8 g Tre to 4 μg lipid. Langmuir isotherms show little change in surface tension with Tre below this concentration. DSC measurements were not done below this 50 mM threshold, but the higher the Tre concentration, the more the DSC data showed the growth of a low temperature shoulder. VSFG measurements show more sensitivity to lower Tre concentrations with a strong increase in methyl signatures with 10 mM Tre in the subphase. These results support a cooperative adsorption mechanism that suggests the Tre interacts noncovalently with the monolayer. Based on literature reports the noncovalent interaction is likely hydrogen bonding, but measurements in this work do not decisively identify whether this H-bonding occurs with headgroups or the lipid's 3-carbon glycero backbone. In addition, the ~50 mM threshold for Tre to exhibit cooperative adsorption effects suggests that H-bond bridges may be important for Tre/DPPC interactions.

4.2 Experimental

4.2.1 Materials

1,2-dimyristoyl-*sn*-*glycero*-3-phosphoethanolamine (DPPC, powder, >99%) was purchased from Avanti Polar Lipids Inc. (Alabaster, Alabama). D-(+)-trehalose dihydrate from starch (Tre, powder, ≥99%) was purchased from Sigma-Aldrich (St. Louis, MO). HPLC grade chloroform (99.9%) was purchased from Fisher Scientific. All chemicals were used without further purification. Millipore water (resistivity of 18.2 MΩ) was used for all aqueous sample preparation.

4.2.2 Preparation of Samples

DPPC lipid stock solutions (0.7 mg/mL) were prepared in chloroform and sonicated for 10 minutes. Aqueous samples for VSFG measurements were prepared in Borosilicate Petri dishes. These Petri dishes were acid washed (50/50 vol. nitric/sulfuric) and rinsed with Millipore water before use. The DPPC/chloroform stock solution was spread on each subphase with a Hamilton glass microsyringe.

4.2.3 Vibrational Sum Frequency Generation

Vibrational sum frequency generation is a second order nonlinear spectroscopy technique. With this technique, only Raman and IR active molecules that are in a non-centrosymmetric environment can produce a SFG response. This specificity allows for the study of molecules at the surface without contributions from the bulk. To produce SFG signal, two incident laser sources—a tunable IR source and a fixed 800 nm visible source are combined in space and time at a surface. This creates a coherent nonlinear

polarization in molecules at the surface, which produces a SFG response at the sum of the two input frequencies. When the IR source is resonant with a vibrational mode of a species at the surface, the SF signal is resonantly enhanced.

The VSFG setup at Montana State University has been described in detail elsewhere.[176] Briefly, this system uses a Coherent Libra Ti:sapphire laser with a 85 fs pulse and a 1kHz repetition rate which produces 3.3 W of 800 nm light. An 80/20 beam splitter reflects 80% of the light into a Coherent OPerA Solo optical parametric amplifier to produce IR light. The 800 nm light and the IR light (3.4 μm) is focused onto the sample at 48° and 38°, respectively from surface normal. The SF response is collimated and isolated before being focused into a monochromator (SpectraPro-300i, Acton Research Corporation) and then dispersing onto a 1340 x 100 pixel CCD (PIXIS100B, Princeton Instruments).

4.2.4 Surface Tension

Surface tension measurements were done as described previously.[51] Briefly, a NIMA Langmuir trough (Model 302LL) equipped with a NIMA PS4 pressure sensor and a Micro Processor Interface 104, was used to preform measurements. Paper Wilhelmy plates (Brown Waite Engineering) were used to measure surface tension. The Langmuir trough barriers were closed at a speed of 10 cm^2/min.

Surface pressure (π) was measured as a function of surface area. The surface pressure is related to the surface tension of the underlying neat liquid phase (γ_0) and the surface tension that results from both the subphase and the surfactant monolayer (γ) as shown in Equation 4.1.

$$\Pi = \gamma_0 - \gamma \quad (4.1)$$

Excess free energy of mixing, ΔG^E_{mix}, can be calculated for ideal mixed monolayers containing two species that are restricted to the surface (Equation 4.2). In Equation 4.2, A_{12} is the actual area per molecule of a mixed monolayer, A_1 and A_2, are the area per molecule of a pure monolayer of one of the species in the mixed monolayer, and x_1 and x_2 are the mole fractions of each of the species in the mixed monolayer.[80-81]

$$\Delta G^E_{mix} = \int_{\pi_1}^{\pi_2} N_A(A_{12} - x_1A_1 - x_2A_2)d\pi \quad (4.2)$$

We can further simply this equation with two constraints. With species 1, DPPC, we assume DPPC is only species constrained to the aqueous/vapor interface because trehalose is not constrained to the surface. With moderate concentrations of trehalose, the surface tension is not differentiable from the surface tension of neat water. With these assumptions, Equation 4.2 becomes:

$$\Delta G^E_{mix} = \int_{\pi_1}^{\pi_2} N_A(A_{12} - A_1)d\pi \quad (4.3)$$

4.2.5 Differential Scanning Calorimetry

Differential scanning calorimetry (DSC) measurements were made using a TA Instruments Discovery (New Castle, DE). Vesicle solutions were put into Tzero pans and Tzero hermetic lids (TA Instruments) and sealed. Each sample was equilibrated to 20°C before heating by 0.5°C/min until 55°C to capture the transition temperature T_m of DPPC at approximately 41°C.

Vesicle solutions were made using standard protocols.[151] Briefly, a ~1 mg/ml solution of DPPC in chloroform was prepared in a round bottom flask. The chloroform

was evaporated off with a rotary evaporator with a bath temperature ~10°C greater than T_m of DPPC. This left behind a lipid film that was rehydrated with Millipore water and sonicated for 20 minutes in a bath ~10°C greater than the T_m. This vesicle solution was then mixed with trehalose solutions to result in 10 mM DPPC vesicle solution with the desired amount of trehalose. These solutions were left to equilibrate for a minimum of 20 minutes before use.

4.3 Results and Discussion

Trehalose is highly soluble in water (50 g/L). However, this solubility does not exclude Tre from being present at the surface. From Figure 4.1, Tre is VSFG active in the C-H stretch region when the bulk solution concentration reaches ~100 mM. Measurable VSFG signal requires Tre to be present in sufficiently high concentration(s) in the anisotropic interfacial environment. Provisional assignments can be made based on a combined DFT/FTIR study of anhydrous and dihydrated trehalose.[177] The peak at 2852 cm^{-1} is likely due to a C-H vibration from the ring carbons. The peak at 2878 cm^{-1} is potentially from the CH_2 asymmetric stretch or a C-H ring carbon. The 2940 cm^{-1} peak likely corresponds to a symmetric stretch of the CH_2 and the 2961 cm^{-1} peak in the PPP polarized spectrum is possibly a C-H stretch from a ring carbon with a hydrogen bond to water.

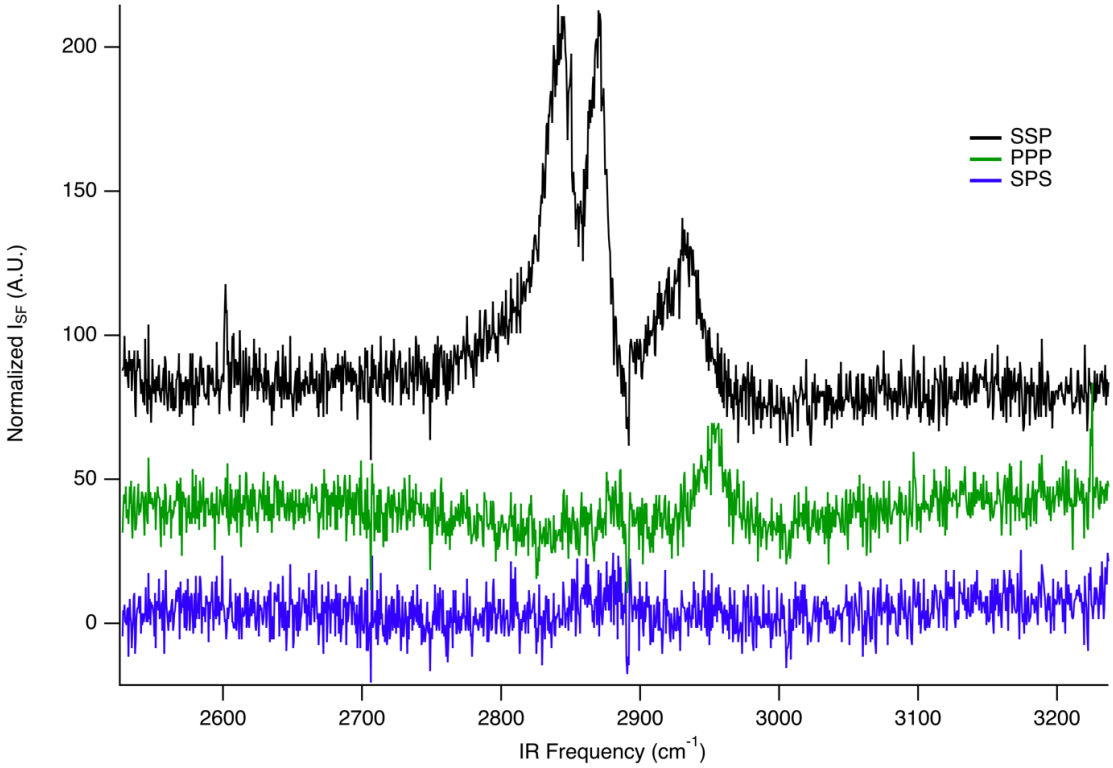

Figure 4.1 VSFG spectra of 100 mM Trehalose in three polarization combinations.

Figure 4.2 shows the VSFG spectra of DPPC monolayers at two different DPPC surface coverages, 55 $Å^2$/molecule and 40 $Å^2$/molecule. These surface coverages correspond to a 2-dimensional liquid condensed phase and a 2-dimensional solid phase, respectively. The symmetric stretch features at ~2870 cm^{-1} and ~2847 cm^{-1} correspond to the symmetric stretching modes of the methyl and methylene groups, respectively. Based on the literature assignments of Snyder *et. al.* these will also be referred to as the r^+ (methyl symmetric stretch) and d^+ (methylene symmetric stretch) peaks.[155]

In the SSP polarized data (top row) the SF intensity is a result of vibrational moments perpendicular to the sample surface. In the expanded, 55 $Å^2$/molecule SSP data (top left), the r^+ peak is lower in intensity than the d^+ peak with no and low Tre concentrations (0 and 1 mM) in the subphase. The low methyl symmetric stretch intensity

in comparison to a larger methylene symmetric stretch intensity is suggestive of DPPC molecules that are generally disordered in a floppy or tilted orientation. As the Tre concentration in the subphase is increased to higher concentration (10, 50 and 100 mM) the r^+ intensity increases and is greater than the signal from the methylene symmetric stretch indicating that the DPPC has become more conformationally ordered. A quantitative measure of the organization of the organic monolayer is often given by the r^+/d^+.[50, 156-158] These values are plotted in Figure 4.3. With the more expanded surface coverage (55 $Å^2$/molecules), this ratio increases with greater Tre in the subphase indicating that Tre induces greater organization within the DPPC monolayer. This result is consistent with the cooperative adsorption effects seen with other DPPC/monosaccharide interactions.[18, 51] Although we see an increase in the r^+/d^+ ratio at the 55 $Å^2$/molecule DPPC surface coverage, this ratio only reaches a value of 2.0, well below the upper limits of this ratio, with reports having ratios as high as 25 for tightly packed single chain Langmuir monolayers.[156]

Under SPS polarization conditions, the IR field probes vibrations having their IR transition moments parallel to the surface. In this polarization, with a surface coverage of 55 $Å^2$/molecule (middle left), the VSG signal grows in at ~2960 cm^{-1} with increasing trehalose concentration in the subphase. This peak is attributed to a CH_3 asymmetric stretch (r^-) and can result from structural and/or dynamic changes. For the spectra with lower concentrations of Tre, the r^- would expected to be larger for bent or disordered DPPC monolayers than for ordered monolayers, but rapid internal motion of the methyl group about its C_3 axis preferentially suppresses VSFG from r^-.[159] We propose that the

growth of this peak with higher Tre concentrations results from Tre cooperatively adsorbing to the lipid headgroup condensing of the lipids and restricting the methyl rotation.

In the PPP polarization combination, the moderately packed, 55 $Å^2$/molecule DPPC (left column, bottom) shows an increase in the r^- peak intensity with Tre concentrations greater than 10 mM. This increase corresponds to the flip in r^+ and d^+ intensity in the SSP polarized data at and above this same concentration.

The left column of Figure 4.2 shows spectra of DPPC at 40 $Å^2$/molecule in SSP, SPS, and PPP polarization combinations. At this surface coverage, DPPC is tightly packed as a 2-dimensional solid. In all polarization combinations, spectra show little variation due to Tre concentration. This behavior is attributed to fact that DPPC at this coverage already has very little conformational mobility so any interactions between cooperatively adsorbed Tre and DPPC headgroups will have little impact on lipid chain organization. This assessment is supported by the r^+/d^+ ratio for the SSP polarized spectra that shows little change at this coverage suggesting that Tre does not alter average orientation of the condensed DPPC monolayer.

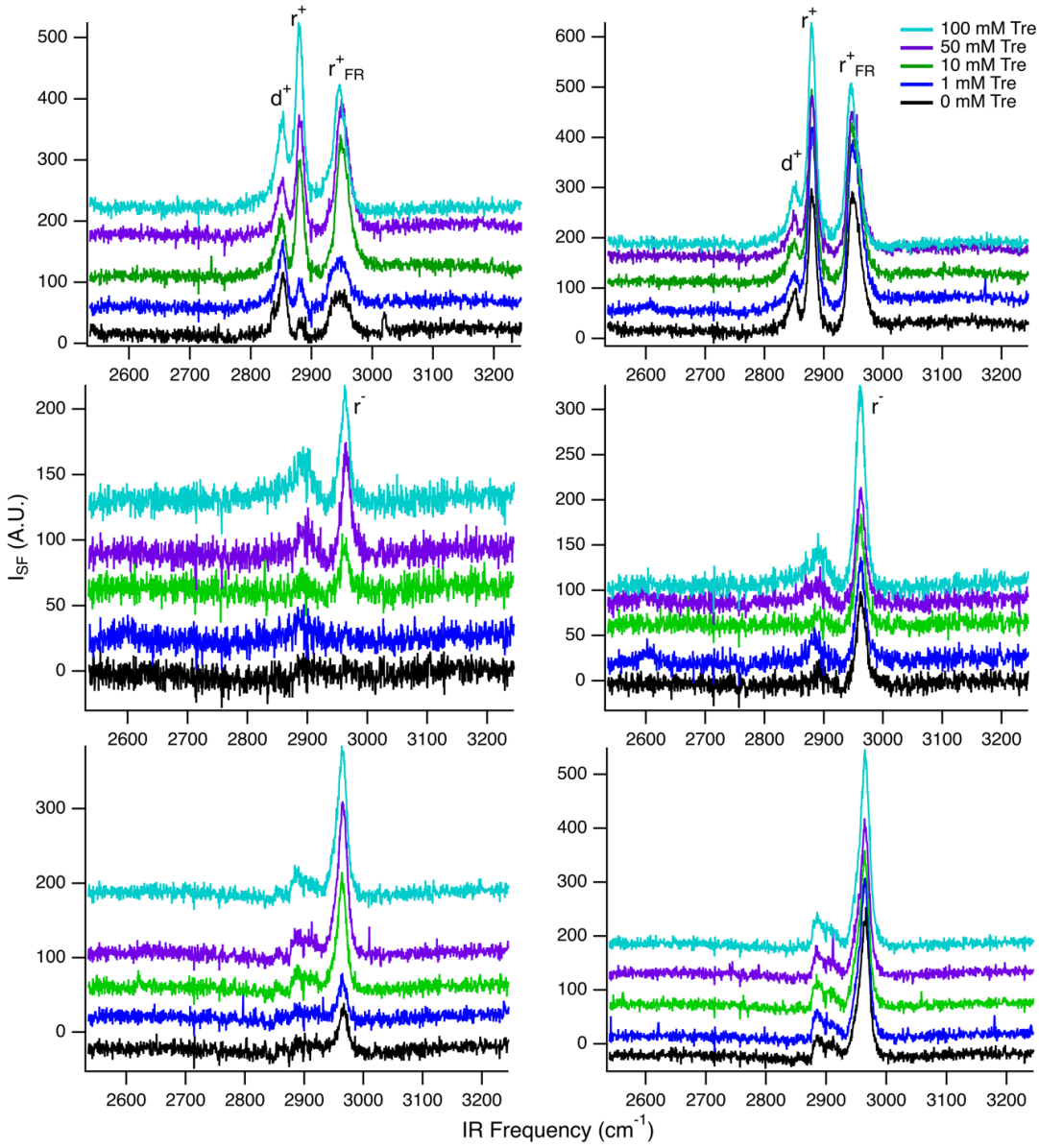

Figure 4.2 VSFG spectra of DPPC on different concentrations of Tre. The left column has DPPC at 55 Å^2/molecule and the right 40 Å^2/molecule. The top row is in SSP polarization, the middle SPS, and the bottom PPP.

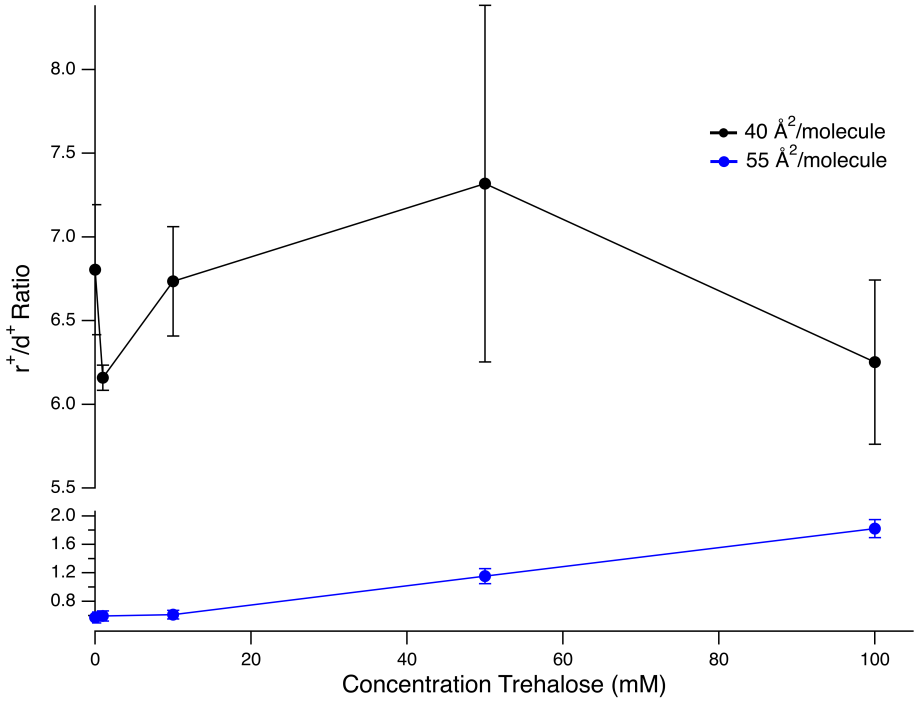

Figure 4.3 VSF r^+/d^+ intensity ratios for DPPC on Tre solutions

Tre's impact on monolayer behavior is examined further with π-Area isotherms. The isotherms show little deviation from each other at 55 $Å^2$/molecule where we see evidence of orientational changes in the VSFG spectra. The more concentrated 50 mM Tre subphase shows DPPC taking up a larger area per molecule. This result is likely due to interactions with the trehalose in the subphase causing a larger overall footprint for DPPC molecules. The 50 mM and 1 mM Tre data show a pronounced "bump" at 56 mN/m and 53 mN/m, respectively. This behavior has been observed in DPPC/DPPG mixtures with recombinant surfactant-associated protein C (SP-C)[153] and in DPPC/fibrinogen.[152] In these studies the bump has been attributed to the solute being 'squeezed' out of the insoluble monolayer.

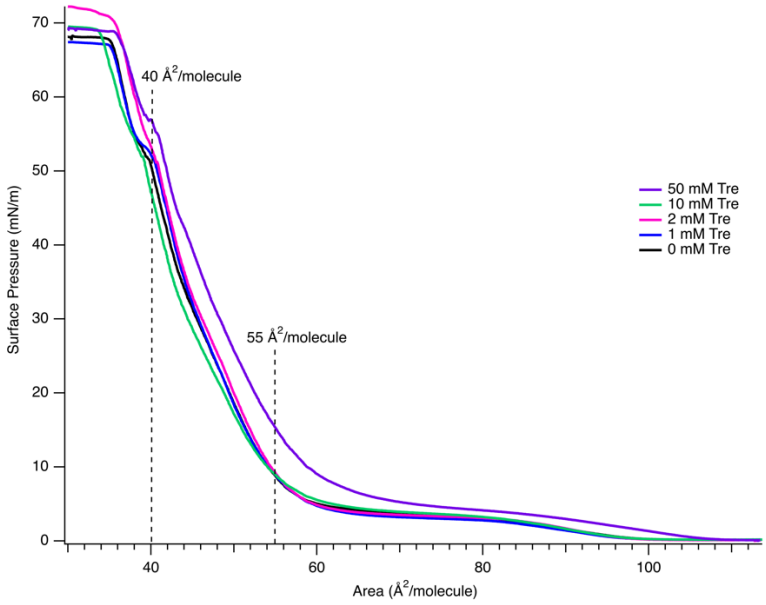

Figure 4.4 π-A isotherms of DPPC on trehalose solutions

Isotherm data were analyzed using excess free energy expressions shown in Equation 4.3. A negative excess free energy, ΔG^{EX}, in an ideal mixed monolayer with two surfactants restricted to the interface, indicates an attractive interaction between the two surfactants, resulting in a more compressed monolayer that is more stable than a pure isotherm.[81] In the case of trehalose and DPPC, trehalose is not constrained to the surface. With 50 mM Tre, excess free energy is positive. This behavior results from more expanded monolayers and also corresponds to a higher surface tension compared to the pure DPPC isotherm. An increase in surface tension could be a result of breaking the water hydrogen bonding network at the interface, possibly by replacing water because of trehalose-DPPC interactions.

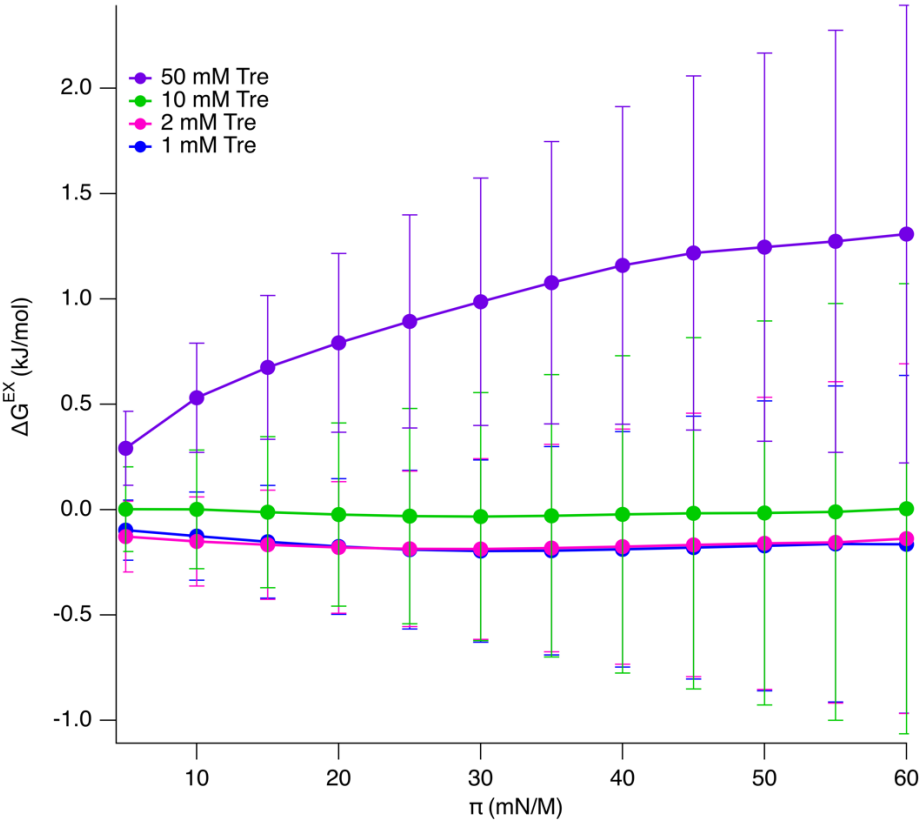

Figure 4.5 Excess free energy of mixing for DPPC on trehalose solutions.

Taken together, SFG and surface tension data paint a not altogether different picture describing Tre's interactions with DPPC monolayers. Changes in SFG vibrational intensities for expanded monolayers show clear evidence of Tre-induced changes in monolayer structure and organization starting with 10 mM Tre. However, surface tension data imply that Tre in solution has minimal impact on DPPC monolayer phase behavior at Tre concentrations up to 10 mM. Both data sets show that there needs to be enough Tre in the subphase for cooperative adsorption effects to occur. With these two methods, the initial concentration of Tre needed to see these effects differs but is likely to be between 10 and 50 for a ~55 $Å^2$/molecule monolayer. To further explore Tre cooperatively adsorbing to DPPC films, DSC measurements were performed using DPPC vesicles

containing aqueous solutions with varying amounts of dissolved Tre. With moderate, 50 mM Tre, the overall peak shape is the same, but the peak has broadened. As the concentration of Tre increases, the phase transition shifts to a higher temperature and a shoulder grows towards lower temperatures. Other molecules that exhibit this type of phase behavior on lipid bilayers are proton translocators.[84] Proton translocators, such as picric acid and 2,-4-Dinitrophenol, are known to interact with lipid bilayers, and this interaction appears in DSC data as growth of a shoulder in the parent transition peak at the low temperature side. The similar trends in the DSC data supports Tre forming H-bonds with the lipid monolayer.

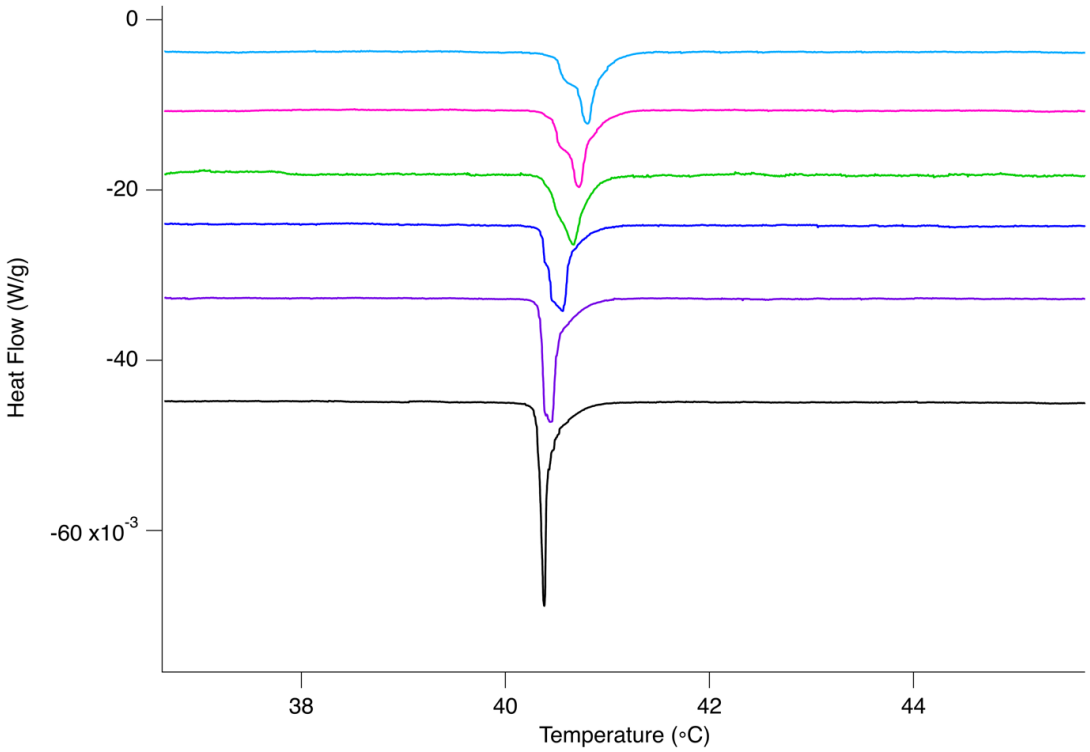

Figure 4.6 DSC measurements for DPPC vesicles in Tre solutions. All transitions are endothermic. The concentration of Tre in the subphase increases from 0 to 250 mM in increments of 50 mM from bottom (lowest concentration) to top (highest concentration).

4.4 Conclusions

The mechanism of cooperative adsorption was investigated in the model system of a DPPC monolayer on solutions of Millipore water containing Tre. Nonlinear optical spectroscopy was used to probe C-H vibrations at the aqueous/vapor interface from the DPPC monolayer. Using this optical technique, with moderate surface coverages of DPPC, Tre resulted in ordering of the DPPC monolayer when the subphase reached 10 mM Tre. The more tightly packed DPPC data showed little change from Tre in the subphase. In surface tension measurements, the Tre was little impacted by the Tre until 50 mM. These two measurements show agreement that there is a concentration threshold of Tre that needs to be met before Tre influences hydrated DPPC, but they do not agree on the amount of Tre. Thus, more experiments are needed between the 10 mM and 50 mM Tre concentration range to elucidate the initial concentration needed for cooperative adsorption interactions between Tre and DPPC. DSC measurements show data that is characteristic of molecules that facilitate the transport of protons across a membrane which suggests that hydrogen bonding between Tre and DPPC is a necessary component of Tre's bioprotective mechanism.

4.5 References

18. Burrows, S. M.; Gobrogge, E.; Fu, L.; Link, K.; Elliott, S. M.; Wang, H.; Walker, R., Oceanfilms-2: Representing Coadsorption of Saccharides in Marine Films and Potential Impacts on Modeled Marine Aerosol Chemistry. *Geophys. Res. Lett.* **2016**, *43*, 8306-8313.

50. Adams, E. M.; Verreault, D.; Jayarathne, T.; Cochran, R. E.; Stone, E. A.; Allen, H. C., Surface Organization of a Dppc Monolayer on Concentrated Srcl2 and Zncl2 Solutions. *Phys. Chem. Chem. Phys.* **2016**, *18*, 32345-32357.

51. Link, K. A.; Hsieh, C. Y.; Tuladhar, A.; Chase, Z.; Wang, Z. M.; Wang, H. F.; Walker, R. A., Vibrational Studies of Saccharide-Induced Lipid Film Reorganization at Aqueous/Air Interfaces. *Chem Phys* **2018**, *512*, 104-110.

80. Blume, A., Lipids at the Air–Water Interface. *ChemTexts* **2018**, *4*, 1-25.

81. Gzyl-Malcher, B.; Paluch, M., Studies of Lipid Interactions in Mixed Langmuir Monolayers. *Thin Solid Films* **2008**, *516*, 8865-8872.

84. Jain, M. K.; Wu, N. M., Effect of Small Molecules on the Dipalmitoyl Lecithin Liposomal Bilayer: Iii. Phase Transition in Lipid Bilayer. *J. Membr. Biol.* **1977**, *34*, 157-201.

93. Gil, A. M.; Belton, P. S.; and, V. F. S. A. P. A. M.; 1996, Spectroscopic Studies of Solid A-A Trehalose. *Elsevier*.

151. Gobrogge, C. A.; Kong, V. A.; Walker, R. A., Temperature-Dependent Partitioning of C152 in Binary Phosphatidylcholine Membranes and Mixed Phosphatidylcholine/Phosphatidylethanolamine Membranes. *J. Phys. Chem. B* **2017**, *121*, 7889-7898.

152. Kuo, R. R.; Chang, C. H.; Yang, Y. M.; Maa, J. R., Induced Removal of Dipalmitoyl Phosphatidylcholine by the Exclusion of Fibrinogen from Compressed Monolayers at Air/Liquid Interfaces. *J. Colloid Interface Sci.* **2003**, *257*, 108-115.

153. Amrein, M.; von Nahmen, A.; Sieber, M., A Scanning Force- and Fluorescence Light Microscopy Study of the Structure and Function of a Model Pulmonary Surfactant. *Eur. Biophys. J.* **1997**, *26*, 349-357.

155. MacPhail, R. A.; Strauss, H. L.; Snyder, R. G.; Elliger, C. A., Carbon-Hydrogen Stretching Modes and the Structure of *N*-Alkyl Chains. 2. Long, All-Trans Chains. *J. Phys. Chem.* **1984**, *88*, 334-341.

156. Can, S. Z.; Mago, D. D.; Walker, R. A., Structure and Organization of Hexadecanol Isomers Adsorbed to the Air/Water Interface. In *Langmuir*, 2006; Vol. 22, pp 8043-8049.

157. Walker, R. A.; Gruetzmacher, J. A.; Richmond, G. L., Phosphatidylcholine Monolayer Structure at a Liquid−Liquid Interface. In *J. Am. Chem. Soc.*, 1998; Vol. 120, pp 6991-7003.

158. Conboy, J. C.; Messmer, M. C.; Richmond, G. L., Dependence of Alkyl Chain Conformation of Simple Ionic Surfactants on Head Group Functionality as Studied by Vibrational Sum-Frequency Spectroscopy. *J. Phys. Chem. B* **1997**, *101*, 6724-6733.

159. Fourkas, J. T.; Walker, R. A.; Can, S. Z.; Gershgoren, E., Effects of Reorientation in Vibrational Sum-Frequency Spectroscopy. *J. Phys. Chem. C* **2007**, *111*, 8902-8915.

161. Schiffer, J. M.; Mael, L. E.; Prather, K. A.; Amaro, R. E.; Grassian, V. H., Sea Spray Aerosol: Where Marine Biology Meets Atmospheric Chemistry. *ACS Central Science* **2018**, *4*, 1617-1623.

162. Clark, G. A.; Henderson, J. M.; Heffern, C.; Akgün, B.; Majewski, J.; Lee, K. Y. C., Synergistic Interactions of Sugars/Polyols and Monovalent Salts with Phospholipids Depend Upon Sugar/Polyol Complexity and Anion Identity. *Langmuir* **2015**, *31*, 12688-12698.

163. Horta, B. A. C.; Perić-Hassler, L.; Hünenberger, P. H., Interaction of the Disaccharides Trehalose and Gentiobiose with Lipid Bilayers: A Comparative Molecular Dynamics Study. *Journal of Molecular Graphics and Modelling* **2010**, *29*, 331-346.

164. Pereira, C. S.; Hünenberger, P. H., The Influence of Polyhydroxylated Compounds on a Hydrated Phospholipid Bilayer: A Molecular Dynamics Study. *Molecular Simulation* **2008**, *34*, 403-420.

165. Tanaka, Y.; Takei, T.; Aiba, T.; Masuda, K.; Kiuchi, A.; Fujiwara, T., Development of Synthetic Lung Surfactants. *Journal of lipid research* **1986**, *27*, 475-485.

166. Crowe, J. H.; Oliver, A. E.; Comparative, F. T. I. a.; 2002, Is There a Single Biochemical Adaptation to Anhydrobiosis? *academic.oup.com*.

167. Crowe, L. M., Lessons from Nature: The Role of Sugars in Anhydrobiosis. *Comparative biochemistry and physiology. Part A, Molecular & integrative physiology* **2002**, *131*, 505-513.

168. Nagase, H.; Ueda, H.; Nakagaki, M., Effects of Sonication on the Lamellar Structures of L-Alpha-Dipalmitoyl Phosphatidylcholine(Dppc)/Saccharide/Water Systems. *Chemical & Pharmaceutical Bulletin* **1999**, *47*, 1355-1362.

169. Ohtake, S.; Schebor, C.; de Pablo, J. J., Effects of Trehalose on the Phase Behavior of Dppc–Cholesterol Unilamellar Vesicles. *Biochimica et Biophysica Acta (BBA) - Biomembranes* **2006**, *1758*, 65-73.

170. Lenné, T.; Bryant, G.; Holcomb, R.; Koster, K. L., How Much Solute Is Needed to Inhibit the Fluid to Gel Membrane Phase Transition at Low Hydration? *Biochimica et biophysica acta* **2007**, *1768*, 1019-1022.

171. del C Luzardo, M.; Amalfa, F.; Nuñez, A. M.; Díaz, S.; de Lopez, A. C. B.; Disalvo, E. A., Effect of Trehalose and Sucrose on the Hydration and Dipole Potential of Lipid Bilayers. *Biophysical Journal* **2000**, *78*, 2452-2458.

172. Márquez, M. J.; Romani, D.; Saud, S. D. J. o. K.; 2018, Structural and Vibrational Characterization of Anhydrous and Dihydrated Species of Trehalose Based on the Ftir and Ftraman Spectra and Dft Calculations. *Elsevier* **2018**, *30*, 229-249.

173. Interaction of Carbohydrates with Dry Dipalmitoylphosphatidylcholine. *Archives of Biochemistry and Biophysics* **1985**, *236*, 289-296.

174. Leekumjorn, S.; Sum, A. K., Molecular Dynamics Study on the Stabilization of Dehydrated Lipid Bilayers with Glucose and Trehalose. *The Journal of Physical Chemistry B* **2008**, *112*, 10732-10740.

175. Venable, R. M.; Skibinsky, A.; Pastor, R. W., Constant Surface Tension Molecular Dynamics Simulations of Lipid Bilayers with Trehalose. *Molecular Simulation* **2006**, *32*, 849-855.

176. Link, K. A.; Spurzem, G. N.; Tuladhar, A.; Chase, Z.; Wang, Z.; Wang, H.; Walker, R. A., Cooperative Adsorption of Glucuronic Acid to Dppc Monolayers Studied with Vibrational Sum Frequency Generation. *Journal of Physical Chemistry C* **2019**, *Submitted*.

177. Márquez, M. J.; Romani, D.; Saud, S. D. J. o. K.; 2018, Structural and Vibrational Characterization of Anhydrous and Dihydrated Species of Trehalose Based on the Ftir and Ftraman Spectra and Dft Calculations. *Elsevier*.

CHAPTER FIVE

LIPID/SACCHARIDE INTERFACE STUDIES WITH PE LIPIDS, SUCROSE, AND OCEAN-LIKE SUBPHASES FOLLOWED WITH CONCLUSIONS AND FUTURE DIRECTIONS

5.1 Introduction

The work presented in the previous chapters investigated cooperative adsorption mechanism in model systems relevant to those encountered in oceanic systems. Chapters 2-5 have each focused on different saccharides and little comparison has been made between saccharides. To compare saccharides, section 5.2 introduces an alternative way to correlate isotherm behavior with lipid organization using VSFG intensity ratios. Section 5.3 contains work with other saccharides that were screened to determine if they were promising candidates for more detailed studies of cooperative adsorption. These saccharides include xylose, sucrose, and glucose. Sucrose induced a small change in lipid phase transition temperature and was investigated more thoroughly with VSFG measurements. Also included in this section is the amino acid phenylalanine (Phe). Phe has been identified as a small molecule solute capable of rendering lipid bilayers more permeable to transport[109] and showed interesting preliminary DSC results in our laboratory. Section 5.4 describes preliminary experiments examining cooperative adsorption to DPPE monolayers where difference between DPPE and DPPC is that the former has a more accessible, positively charged amine on its headgroup. Section 5.5 describes experiments carried out just for fun. Specifically, experiments describe in this

section consider the opportunity for specific saccharide adsorption from solutions made from model sea salt solutions. Section 5.6 concludes other systems that were investigated, and this section is followed by conclusions for this research and future work to be done with cooperative adsorption.

5.2 Comparing Lipid Organization with Surface Tension Behavior

In the preceding chapters, π-A isotherms were presented that were acquired on a Langmuir Trough. Similarly, organization within lipid monolayers were inferred from relative intensities in VSFG spectra (r^+/d^+ ratios). Isotherm and SFG measurements were not compared directly. To determine if the r^+/d^+ intensity ratio from VSFG measurements and π-A isotherms from Langmuir trough measurements follow similar trends, the intensity ratios were plotted as an isotherm (Figure 5.1). For these VSFG isotherms, saccharides at a concentration of 100 mM were used.

The VSFG isotherm for DPPC on pure Millipore water is similar in shape to the representative Langmuir trough Millipore isotherm. The r^+/d^+ ratio for the Millipore case reached a maximum at 50 $Å^2$/ molecule after which the ratio does not change appreciably. With a 100 mM GA subphase, the ratio increases at lower surface coverages of DPPC with the steepest part of the slope between 70 and 60 $Å^2$/ molecule compared with 55 and 50 $Å^2$/ molecule for the Millipore VSFG isotherm. The increase in ratio for the GA containing isotherm at more disperse lipid coverage is evidence that GA facilitates ordering in the DPPC monolayer, further supporting the cooperative adsorption hypothesis. The GU r^+/d^+ 'isotherm' shows different behavior. Data show some increase

in the ratio as the DPPC surface coverage increases, but this increase does not have the steep slope characteristic of the other VSFG isotherms. This result suggests that high concentrations of GU might reach adsorption saturation with relatively expanded DPPC monolayers.

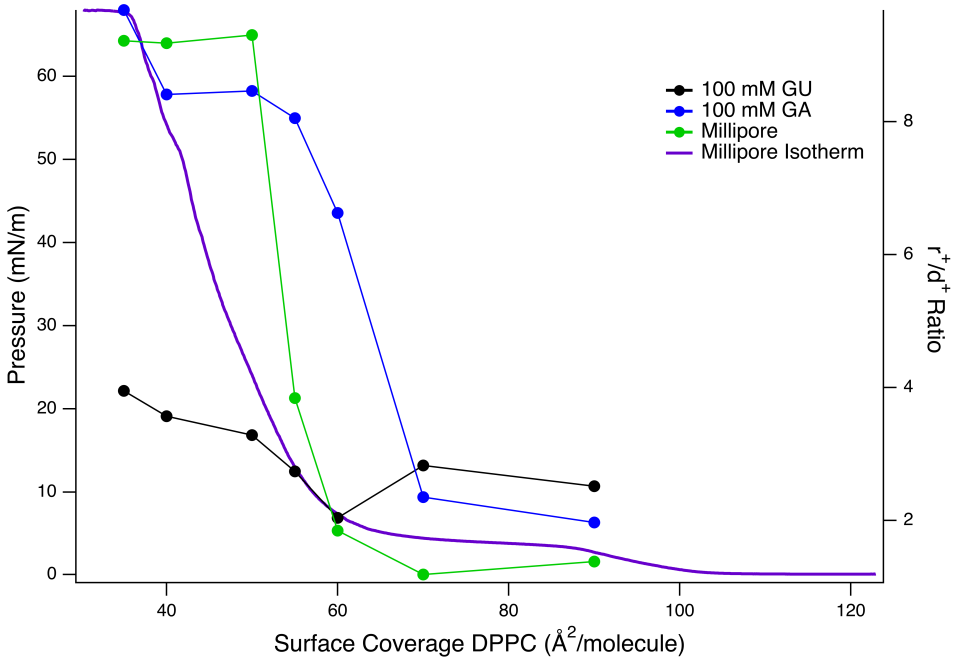

Figure 5.1 π-A isotherm of DPPC on Millipore water (purple) and r^+/d^+-A isotherms from VSFG measurements on Millipore water and solutions with 100 mM GA or GU.

5.3 Initial Investigations into Other Saccharides

Additional saccharides (Figure 5.2) were screened with DSC measurements to look for evidence of dehydration in the lipid membranes that would manifest in the DSC data as an additional peak or distinctive shoulder on the main transition. DSC heat flow vs. temperature plots in Figure 5.2 show the impact of glucose, sucrose, and xylose on DPPC bilayer transition temperature. The overall shape of the transition is unchanged by

these sugars and also show no evidence of a second peak. The only notable change between these sugars is that the vesicles containing sucrose exhibited a slightly lower T_m (Figure 5.3).

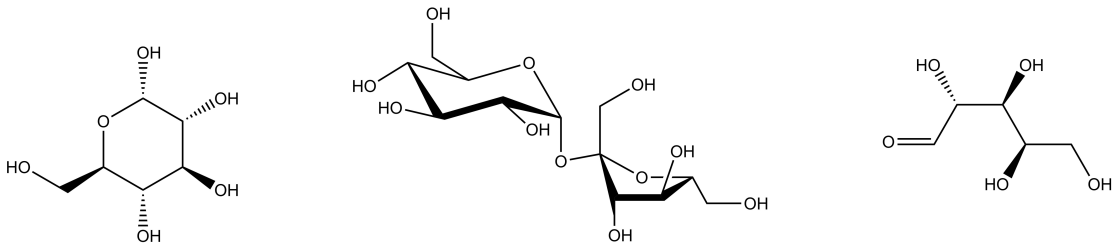

Figure 5.2 Molecular structures of glucose, sucrose and xylose.

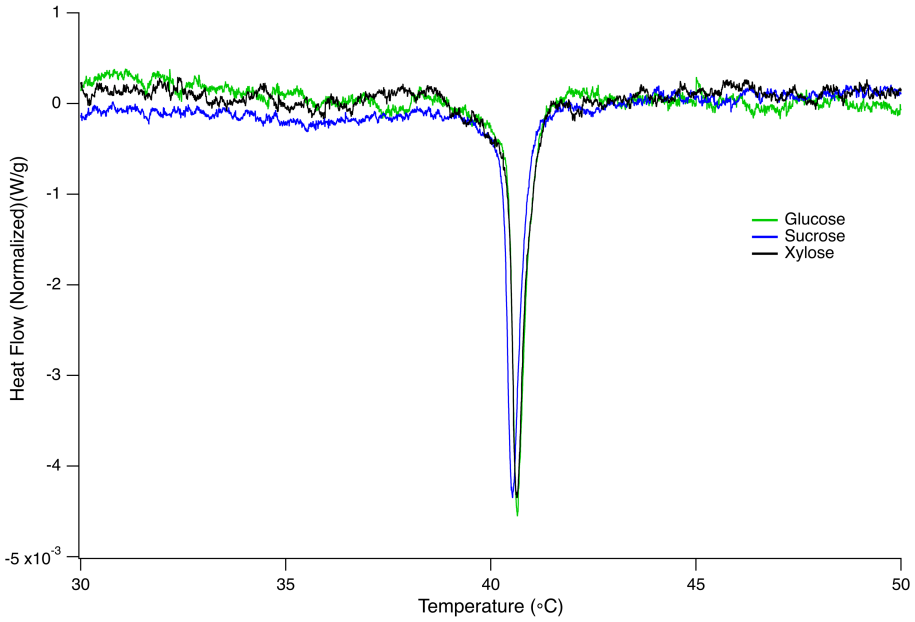

Figure 5.3 DSC heat flow vs. temperature plots for glucose, sucrose, and xylose.

Of the saccharides reported in Figure 5.3, only sucrose showed evidence of association with the lipid membrane. Consequently, cooperative adsorption of sucrose to

DPPC films was investigated more thoroughly with VSFG measurements (Figure 5.4). At tightly packed 40 $Å^2$/ molecule the VSFG intensity is similar over the range of concentrations of sucrose in the subphase. The r^+/d^+ ratio is a semi-quantitative measure of the relative lipid ordering in the DPPC monolayer. For tightly packed DPPC monolayers (40 $Å^2$/ molecule), the addition of sucrose results in a slight decrease in the DPPC ordering until sucrose reaches a concentration of 100 mM. A similar decrease in order is seen in more expanded DPPC monolayers (55 $Å^2$/ molecule). Based on these preliminary data, sucrose does show strong affinity for the lipid monolayer.

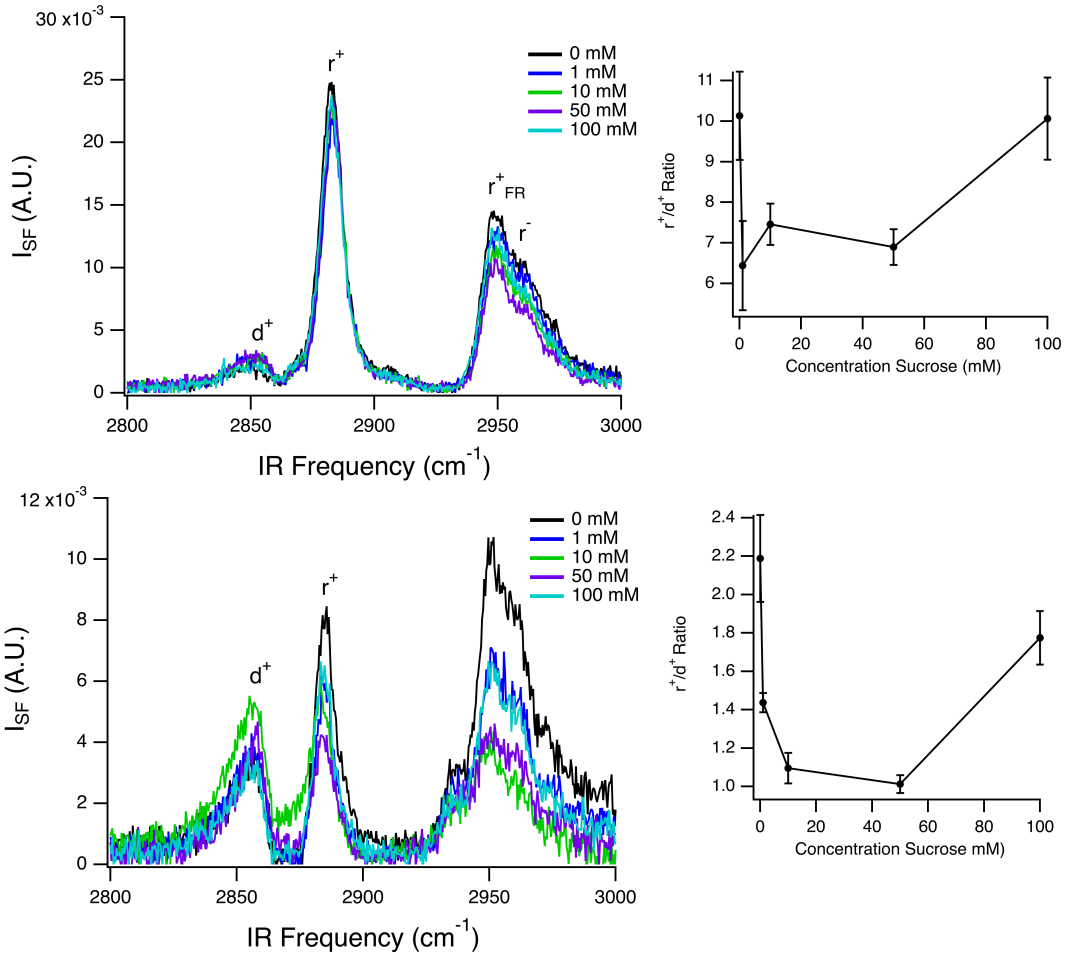

Figure 5.4 VSFG measurements of DPPC at 40 Å^2/ molecule data (top) and 55 Å^2/ molecule data (bottom) on solutions containing sucrose. Corresponding r^+/d^+ ratios are in the right column.

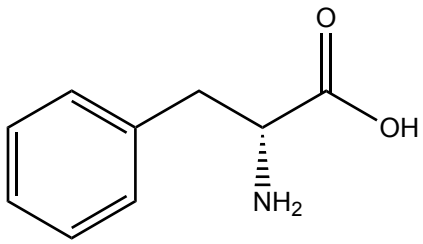

Figure 5.5 Molecular structure of phenylalanine.

In addition to these saccharides, the amino acid, phenylalanine (Phe) (Figure 5.5) was screened with DSC measurements. We chose to study Phe because Vaida *et. al.* reported that Phe increases membrane permeability.[109] In DSC experiments performed in our laboratory and presented in Figure 5.6, DPPC bilayers rehydrated in Millipore water (right) solution show some broadening with increasing Phe concentrations. With the 100 mM of Phe sample, the broadening in the heat flow vs. temperature occurs at lower temperatures, similar to the DPPC phase transition behavior with DPPC/trehalose. On the left in Figure 5.6, the DPPC was rehydrated in a 10 mM phosphate buffer. With the buffer present, the broadening in the heat flow vs. temperature data is even more pronounced at 100 mM Phe, with the broadening becoming more of a side peak instead of homogenous broadening. This broadening behavior with higher concentrations of Phe suggests that Phe is an interesting candidate deserving more investigation. The amplified broadening with buffer present is consistent with published synergistic effects between cations and sugars.[51, 146, 162]

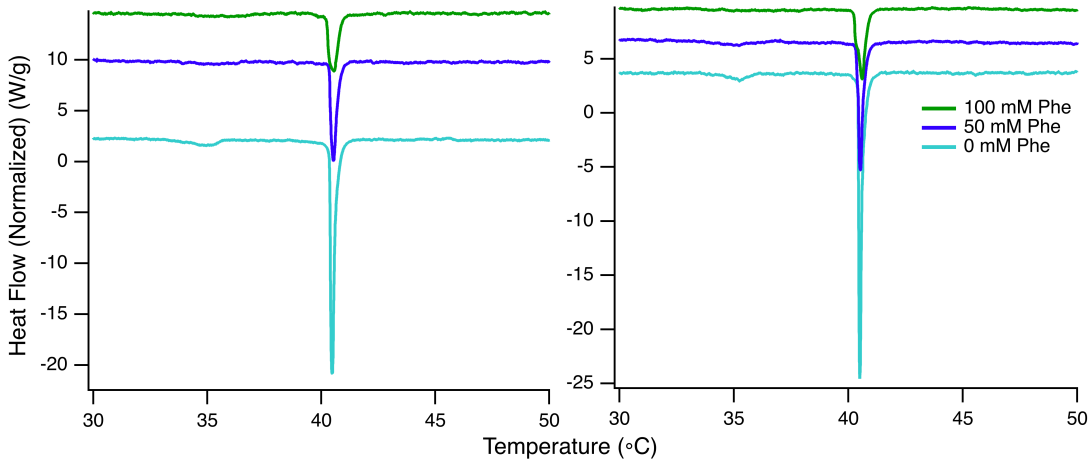

Figure 5.6 DSC measurements of DPPC with solutions containing Phe. On the left the DPPC was rehydrated in Millipore and on the right the Phe was rehydrated in a 10 mM phosphate buffer.

Another saccharide that was investigated was n-acetyl-d-glucosamine (NADG) (Figure 5.7). This saccharide was initially chosen because of its similarity to glucosamine, but with C-H groups that were more likely to be VSFG active. Surface tension data (Figure 5.9) and VSFG measurements (Figure 5.8) provide some evidence that NADG is weakly surface active by itself. NADG's ability to adsorb cooperatively to lipid monolayers was not explored further in this work.

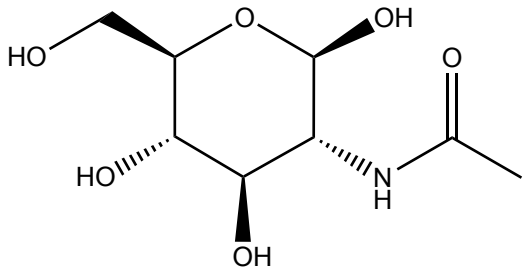

Figure 5.7 Molecular structure of NADG

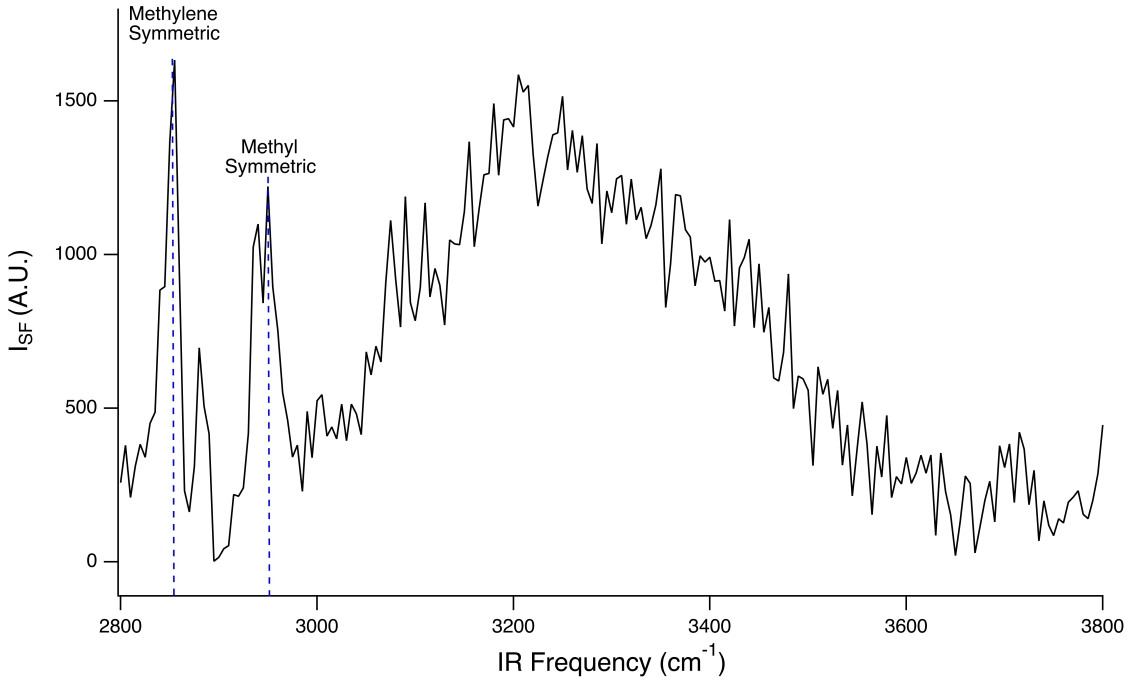

Figure 5.8 VSFG spectra of NADG.

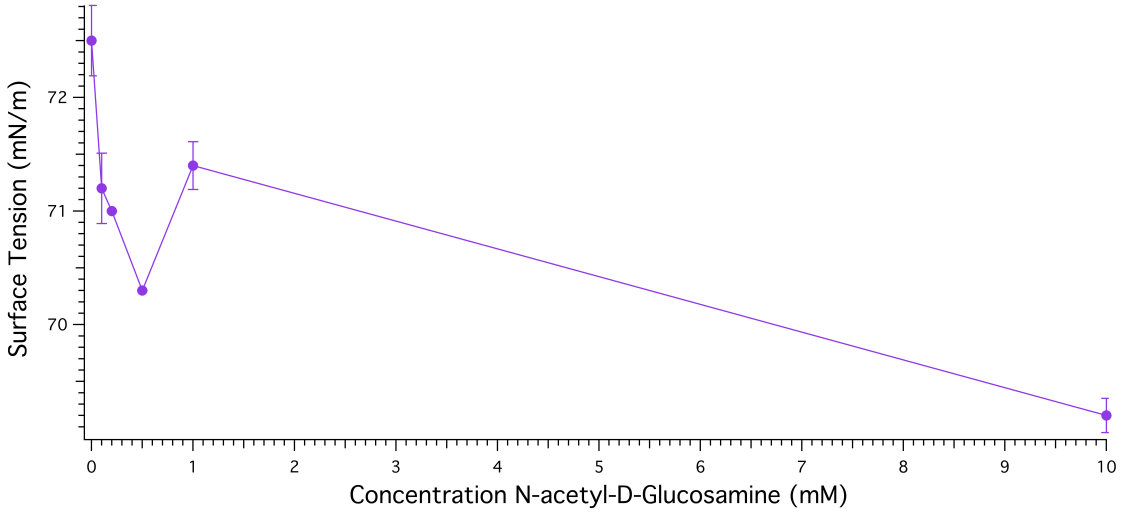

Figure 5.9 Surface tension of solutions of NADG

5.4 DMPE

Results presented in Chapters 2-4 used DPPC monolayers to test the limits of cooperative adsorption. This choice was motivated in part by DPPC's prevalence in environmental and biological settings. Phosphocholines (PC), such as DPPC, are zwitterionic, with a phosphate group and a quaternary amine, providing the negatively charged and positively charged regions, respectively. The positive charge on the quaternary amine is relatively inaccessible given the three methyl and one methylene group surrounding the nitrogen atom. This protection did not prevent the negatively charged glucuronic acid (GU) from cooperatively adsorbing to DPPC monolayers as reported in Chapter 3. The GU result raised a question about how charged saccharides, especially the negatively charged GU, might interact with a more accessible, positively charge sites in lipid monolayers.

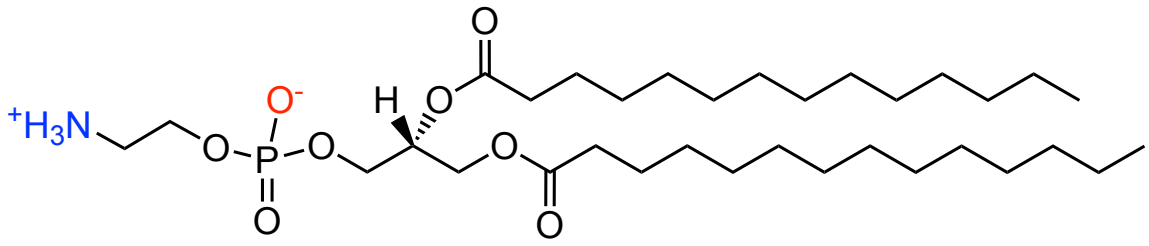

Figure 5.10 Molecular structure of DMPE

In order to test the hypothesis that a more accessible cationic charge would promote cooperative adsorption by anionic solutes, a phosphatidylethanolamine, DMPE, was chosen (Figure 5.10). Phosphatidylethanolamines (PE) have a primary amine instead of the quaternary amine found in PCs. In PEs, the positive charge on the nitrogen group is more accessible and interacts more strongly with its surroundings as evidenced by

consistently higher gel-to-liquid crystalline transition temperatures for lipids having equivalent acyl chains. Methods used to investigate DMPE included VSFG, both at MSU and at PNNL, and DSC measurements.

SSP spectra were acquired from DMPE monolayers at various surface coverages adsorbed to aqueous solutions with different concentrations of GU. The ratios reported in Figure 5.11 show little difference in the r^+/d^+ ratio in expanded 55 $Å^2$/ molecule. This result is surprising because GU is negatively charged, and the GA is positively charged. Even with the more accessible primary amine group, GU does not induce more ordering in the lipid monolayer than GA. This trend also generally carries over to the 40 $Å^2$/ molecule surface coverage, with the ratios differing more between saccharide species, but overall the ratios follow the same decrease and plateau with the addition of saccharide. The decrease in ordering of the tightly packed monolayer does not fit a cooperative adsorption mechanism. A possible reason for the DMPE to be little affected by the saccharides is that the primary amine associates closely with the phosphate group on adjacent DMPE molecules and this creates a strong self-assembly among DMPE, leaving little space for saccharide association.

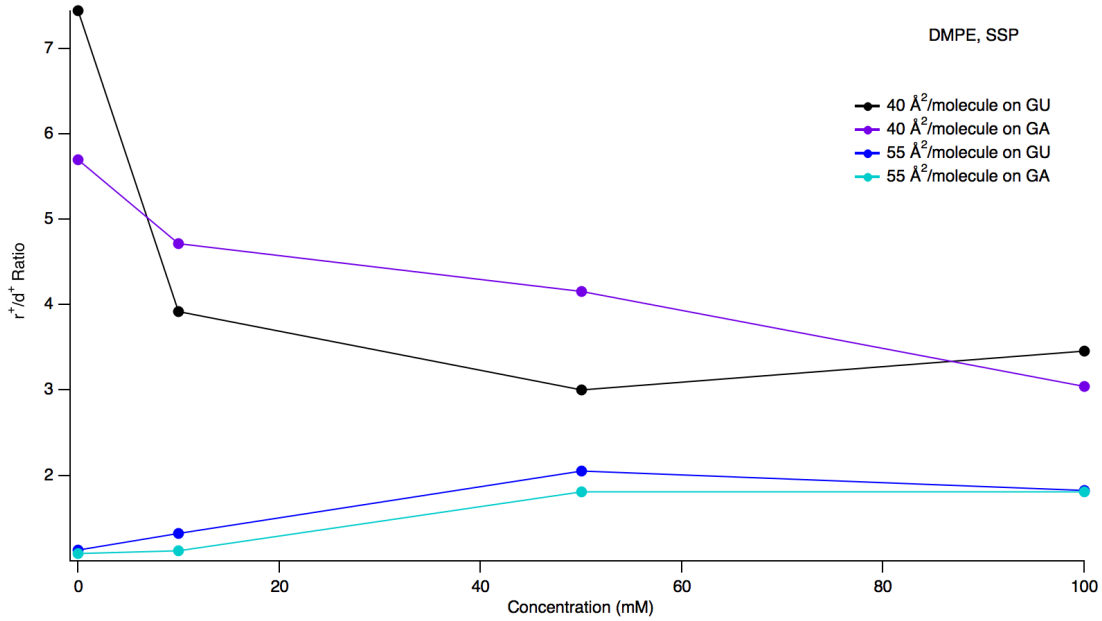

Figure 5.11 VSFG r^+/d^+ ratio for DPPC monolayers on various concentrations of GA or GU in the subphase.

DSC measurements of DMPE vesicles rehydrated in 25 mM GU are plotted in Figure 5.12. The solutions were spiked with additional GU and allowed to equilibrate for 8 hours before taking measurements. The transition temperature of the solutions increased with additional amounts of added GU, but the overall peak shape was similar between samples.

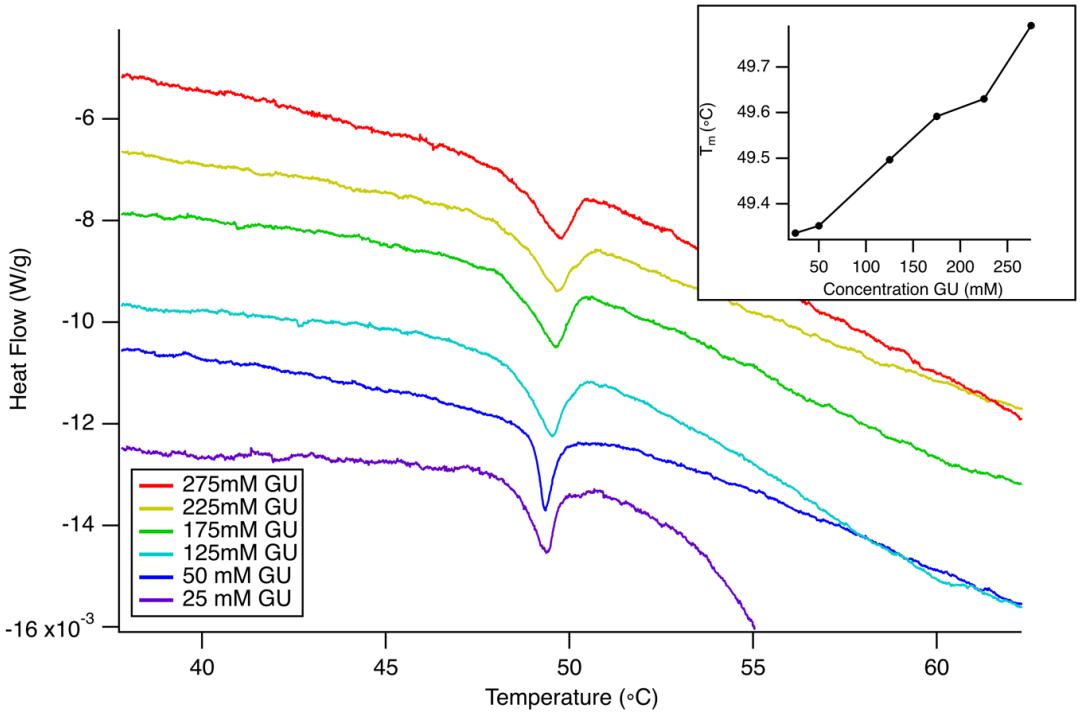

Figure 5.12 DSC measurements of DPPC with solutions containing GU.

5.5 Ocean as a Subphase

The main driving force of the research presented in this thesis has always been to better understand organic accumulation in sea spray aerosols. For the fundamental studies presented, Millipore water or carbonate buffer systems were used as the subphase. To explore more ocean-like subphases, experiments were done using Instant Ocean® sea salt and Mediterranean Sea salt (La Baleine). Instant Ocean® is a synthetic blend of salts that is sold commercially to make ideal marine environments in aquariums. The ions in Instant Ocean® are listed in Table 5.1.[178] La Baleine Mediterranean Sea salt is commercially available as a food additive in grocery stores. Naturally sourced sea salt is

harvested from sea water dried in sunlight, so the salt content is representative of the location whence it was gathered, but the exact blend of ions in this sea salt is unknown.

Table 5.1 Ion concentrations for Instant Ocean® sea salt. Adapted from Adams *et.al.*[178]

Cation	**Concentration (mol/L)**	**Anion**	**Concentration (mol/L)**
Na^+	0.4521	Cl^-	0.5315
K^+	0.0104	SO_4^{2-}	0.0267
Mg^{2+}	0.0530	HCO_3^-	0.0032
Ca^{2+}	0.0096	Br^-	6.75×10^{-4}
Sr^{2+}	9.64×10^{-5}	F^-	5.11×10^{-5}

To prepare solutions of sea salt, the instructions provided by Instant Ocean® were used. Briefly, the sea salt was prepared at room temperature in Millipore. The sea salt was added and dissolved until the specific gravity read 1.020 with a hydrometer. The solution was then left stirring with a loose cover for 24 hours to equilibrate dissolved oxygen/carbon dioxide. The final pH of the La Baleine sea salt solution was 6.7. The final pH of the Instant Ocean® was 8.4. Saccharides were used at a concentration of 100 mM in the sea salt solutions.

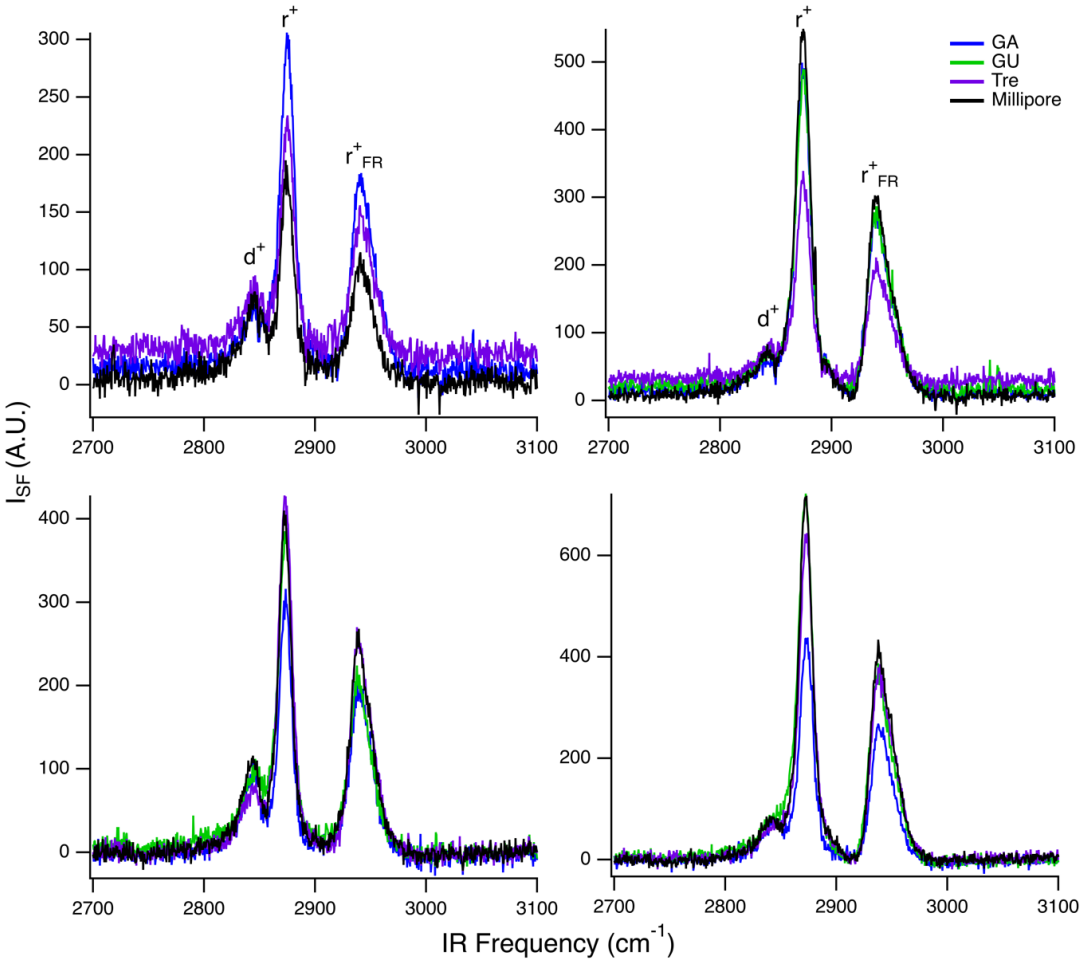

Figure 5.13 VSFG spectra of DPPC on Instant Ocean (top row) and Mediterranean Sea salt (bottom row). The left column has a DPPC surface coverage of 55 Å^2/ molecule and the right column has a tightly packed DPPC monolayer at 40 Å^2/ molecule. All saccharides solutions were 100 mM.

The VSFG spectra in Figure 5.13 all have very little intensity in d^+ (methylene symmetric stretch) compared to the r^+ intensity (methyl symmetric stretch). The low d^+ intensity is opposite some of the behaviors with these lipids on Millipore/saccharide solutions that have a methylene intensity greater than the methyl intensity at low saccharide concentrations with expanded 55 Å^2/molecule monolayers (See Figures 2.6, 3.4, and 4.2). This result suggests a relatively well ordered DPPC regardless of whether

or not saccharides are present in the subphase. This result is likely due to a condensing effect from the ions in the sea salt. The salt is well in abundance of the saccharide concentration in the solution (Instant Ocean® is 0.5 M Na^+),[178] which is characteristic in the subsurface, bulk ocean, but not of the sea surface microlayer that can have 16x more saccharide concentration than sodium. The limits tested here were more representative of the bulk ocean and the VSFG data show that lipid monolayer reorganization is not strongly saccharide dependent as quantified by the r^+/d^+ ratios in Figure 5.14. These r^+/d^+ ratios show no systematic correlation between saccharide identity and DPPC organization.

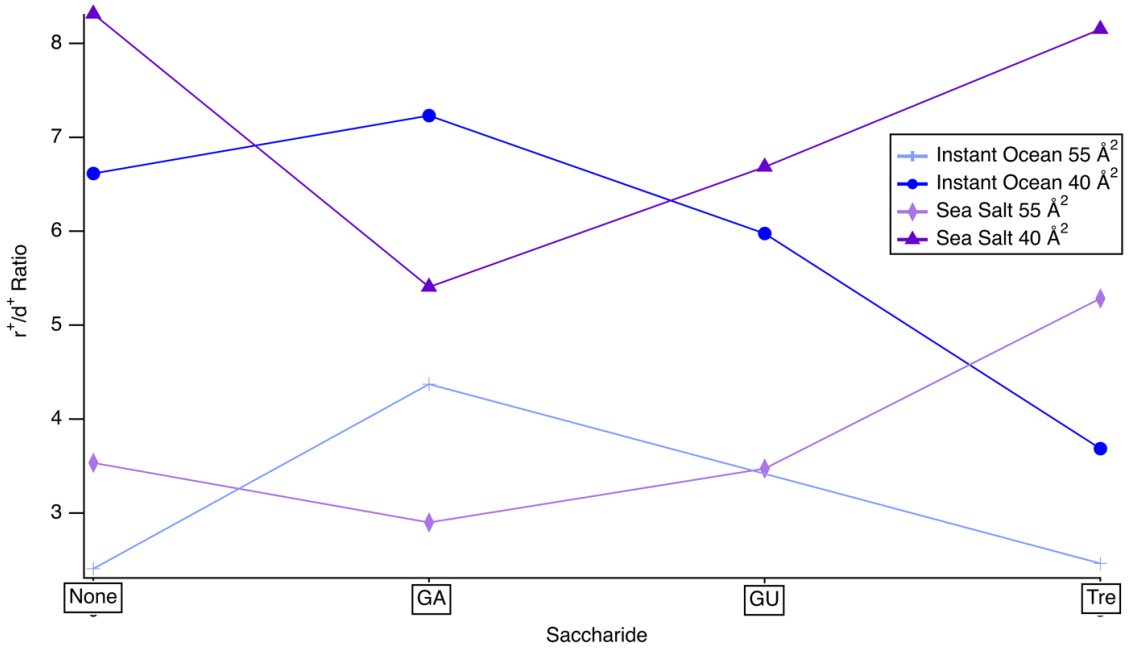

Figure 5.14 VSFG r^+/d^+ ratios for DPPC on different saccharide containing solutions.

In addition to testing cooperative adsorption on the sea salt solutions, trehalose's surface activity was also tested as a function of sea salt type. For both sea salt solutions,

trehalose was VSFG active. The VSFG intensity was greater for trehalose on Instant Ocean®, which had a higher pH at 8.4, than on the Mediterranean Sea salt at pH 6.7.

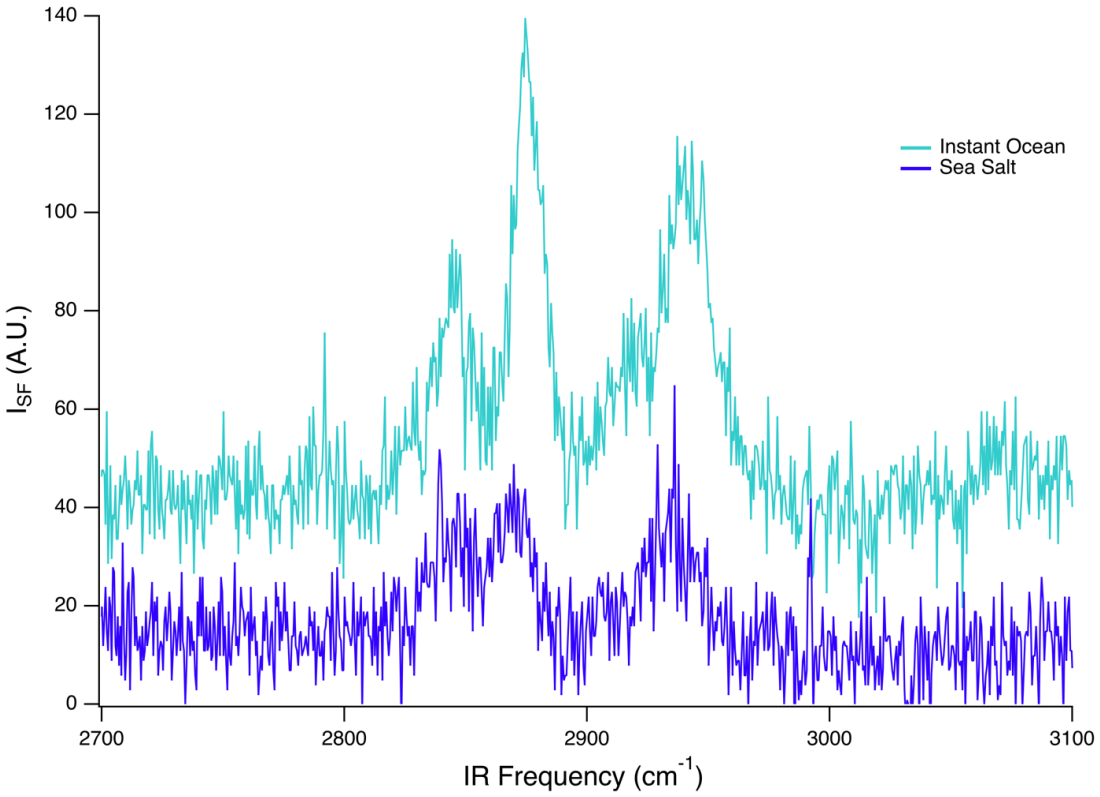

Figure 5.15 VSFG spectra of trehalose on sea salt solutions.

DSC experiments were carried out with DPPC vesicles rehydrated with Instant Ocean®. In these experiments, the DPPC did not show a 'ripple phase' transition. High salt concentrations appear to inhibit this pretransition. A similar decrease in the pretransition has been reported for increasing concentrations of pyrimidine analogue.[179] The DPPC phase change from the ordered gel state to the more disordered liquid gel state is at a higher temperature than in Millipore by 0.76°C. The heat flow vs. temperature curve is also broadened by the presence of salt as compared to a DPPC isotherm in

Millipore water and no clear shoulder appears on the main peak's low temperature side as is seen with Tre/DPPC isotherms in Millipore water. (Figure 4.6) This result suggests that salt hydrates the vesicles and prevents two subsets of vesicles from forming. The transition temperature T_m increases slightly with Tre concentration in the sea salt solutions suggesting that Tre has some interaction with the DPPC bilayers.

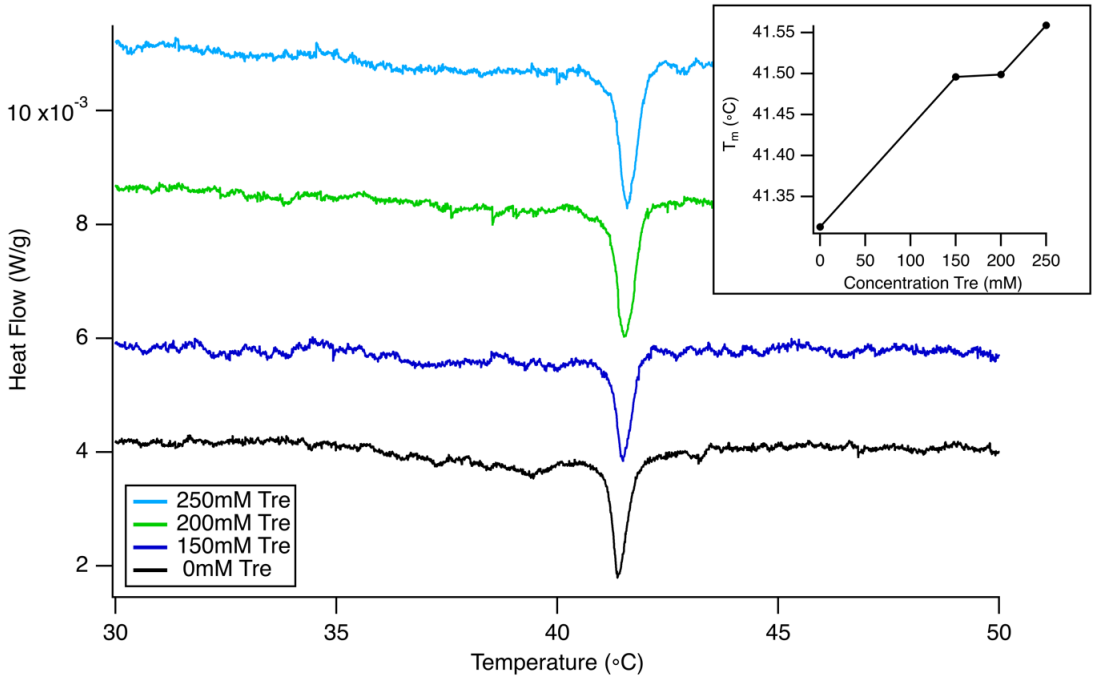

Figure 5.16 DSC measurements of DPPC rehydrated with Instant Ocean® as a function of Tre concentration.

5.6 Conclusions

Work presented in this thesis examined cooperative adsorption between lipids and saccharides as a possible mechanism to explain increased organic content in sea spray aerosols (SSA). Nonlinear optical spectroscopy was used to study the effect saccharides have on the organization of lipid molecules at the aqueous/vapor interface. These results were supported with surface tension measurements to gain additional insight into cooperative effects between the lipid monolayer and saccharides in solution and differential scanning calorimetry measurements to study the interaction between saccharides and lipid bilayers.

Initial work focused on the interaction between glucosamine (GA), the monomer unit of chitin, and DPPC, a main component of lung surfactant. For the DPPC/GA system, vibrational sum frequency generation (VSFG) data showed GA induced ordering in DPPC monolayers regardless of the charge on the GA. This effect was evident with both positively charged GA in Millipore and neutral GA in pH 9 carbonate buffer. Both of the experimental conditions resulted in an increase in the r^+/d^+ intensity ratio with both tightly packed and moderately packed DPPC monolayers. From DPPC isotherms on GA/buffer solutions, the saccharide/buffer ion combination amplified lipid expansion which was dependent on GA concentration and not buffer pH. This work also included initial studies on glucuronic acid's (GU) effects on lipid monolayers, with both GA and GU resulting in the phase transition for DPPC bilayers to require more energy with the saccharides present. These results add support to the cooperative adsorption hypothesis as a mechanism for saccharide accumulation at interfaces.

The research in Chapter 3 expands on the initial results from the GU/DPPC system. For moderately packed DPPC monolayers on GU/Millipore water solutions, GU causes reordering in DPPC monolayers as evident with VSFG data that show a flip in intensity from the methylene symmetric stretch (d^+) to the methyl symmetric stretch (r^+) as a function of GU concentration. With tightly packed DPPC monolayers and with DPPC monolayers on GU/buffer solutions, the GU causes less organizational change on the DPPC monolayers likely because of saturation and competitive effects with buffer ions. This VSFG result from the C-H stretching region was supported with VSFG data from the O-H vibrational stretch region for water. These VSFG experiments were coupled with surface tension measurements and DSC measurements, that added support to the VSFG results with GU resulting in a dehydration effect on lipid bilayers in Millipore that is mitigated by the presence of buffers. The results from this chapter show that in limited cases, anions such as GU, can cause structural changes to DPPC monolayers and bilayers that supports the cooperative adsorption hypotheses. In the cases of tightly packed lipid monolayers and high buffer concentrations, cooperative adsorption effects are limited.

Chapter 4 focused on the effects of a disaccharide, trehalose (Tre) on DPPC monolayers and bilayers. Similar to the results in Chapter 4, VSFG with Tre in the subphase resulted in a flip in the r^+/d^+ ratio for moderately expanded, 55 $Å^2$/molecule, DPPC monolayers. This finding is consistent with the cooperative adsorption hypothesis. The more tightly packed, 40 $Å^2$/molecule DPPC monolayers were less affected by Tre. Langmuir trough measurements showed few changes in the lipid monolayer for Tre

concentrations less than 50 mM which was quantified in the Gibbs free energy data. DSC measurements with Tre exhibited a growth of a lower temperature side peak in the main phase transition curve which was amplified with high Tre concentration. These results support a picture of Tre having low reorganization effects on DPPC monolayers until the Tre concentration in the subphase increases to about 50 mM.

Taken in its entirety, work presented in this thesis helps resolve the hypothesis of cooperative adsorption, that describes an interaction between insoluble molecules at the surface and soluble molecules in the bulk phase, in which, the surface molecules draw the soluble molecules to the surface through noncovalent interactions. The results presented in this research show support for this mechanism with some restrictions. In the case of DPPC monolayers, cooperative adsorption is a more effective mechanism when the DPPC monolayer is not tightly packed into a two-dimensional solid, although this may be a result in the limitation of using surfactants as a probe instead of the saccharides themselves. Cooperative adsorption effects are more evident with higher concentrations of saccharides in the subphase which is a promising result for SSA accumulation because the sea surface microlayer has up to a 16x enrichment in saccharides compared to sodium.[20]

5.7 Future Directions

There are a number of unresolved questions concerning the systems in this work that merit revision and additional attention. First, the DMPE saccharide experiments would benefit from surface tension measurements to determine if DMPE is unaffected

from the monosaccharides or if different, lower surface coverages should be used for VSFG studies. If the DMPE is already tightly packed at 40 and 55 $Å^2$/molecule, lower surface coverages may provide a better test system.

The DSC measurements of phenylalanine, particularly with buffer, show some interesting effects that would benefit from a deeper look including DSC measurements with higher Phe concentrations coupled with surface tension measurements and VSFG measurements.

To find direct evidence of cooperative adsorption, VSFG measurements of surface active saccharides, such as Tre and NADG with deuterated DPPC would be ideal. If C-H symmetric stretches from either of these saccharides were present with deuterated DPPC, that would tell us about the saccharides at the interface and a concentration dependent study could tell us about the relative amount of saccharide is at the surface. For this study, lower surface coverages such as 60 $Å^2$/ molecule, may be more useful to see cooperative adsorption effects because a 40 $Å^2$/ molecule, tightly packed system, might not show as pronounced effect.

5.8 References

20. Jayarathne, T., et al., Enrichment of Saccharides and Divalent Cations in Sea Spray Aerosol During Two Phytoplankton Blooms. *Environ. Sci. Technol.* **2016**, *50*, 11511-11520.

51. Link, K. A.; Hsieh, C. Y.; Tuladhar, A.; Chase, Z.; Wang, Z. M.; Wang, H. F.; Walker, R. A., Vibrational Studies of Saccharide-Induced Lipid Film Reorganization at Aqueous/Air Interfaces. *Chem Phys* **2018**, *512*, 104-110.

109. Perkins, R.; Vaida, V., Phenylalanine Increases Membrane Permeability. *Journal of the American Chemical Society* **2017**, *139*, 14388-14391.

146. Schill, S. R.; Burrows, S. M.; Hasenecz, E. S.; Stone, E. A.; Bertram, T. H., The Impact of Divalent Cations on the Enrichment of Soluble Saccharides in Primary Sea Spray Aerosol. *Atmosphere* **2018**, *9*, 476-417.

162. Clark, G. A.; Henderson, J. M.; Heffern, C.; Akgün, B.; Majewski, J.; Lee, K. Y. C., Synergistic Interactions of Sugars/Polyols and Monovalent Salts with Phospholipids Depend Upon Sugar/Polyol Complexity and Anion Identity. *Langmuir* **2015**, *31*, 12688-12698.

178. Adams, E.; Allen, H., Palmitic Acid on Salt Subphases and in Mixed Monolayers of Cerebrosides: Application to Atmospheric Aerosol Chemistry. *Atmosphere* **2013**, *4*, 315-336.

179. Pili, B.; Bourgaux, C.; Meneau, F.; Couvreur, P.; Ollivon, M., Interaction of an Anticancer Drug, Gemcitabine, with Phospholipid Bilayers. *Journal of Thermal Analysis and Calorimetry* **2009**, *98*, 19-28.

REFERENCES CITED

1. FitzGibbon, J.; Mensah, K. O., Climate Change as a Wicked Problem: An Evaluation of the Institutional Context for Rural Water Management in Ghana. *SAGE Open* **2012**, *2*, 2158244012448487.

2. Sun, J.; Yang, K., *The Wicked Problem of Climate Change: A New Approach Based on Social Mess and Fragmentation*, 2016; Vol. 8, p 1312.

3. Hansen, J.; Ruedy, R.; Sato, M.; Lo, K., Global Surface Temperature Change. *Reviews of Geophysics* **2010**, *48*.

4. Team, G., Giss Surface Temperature Analysis (Gistemp). NASA Goddard Institute for Space Studies, 2019.

5. Blunden, J., D. S. Arndt, and G. Hartfield , Eds., 2018: State of the Climate in 2017. Bull. Amer. Meteor. Soc., 99 (8), Si–S310, doi:10.1175/2018BAMSStateoftheClimate.1.

6. Derksen, C.; Brown, R., Spring Snow Cover Extent Reductions in the 2008–2012 Period Exceeding Climate Model Projections. *Geophysical Research Letters* **2012**, *39*.

7. Robinson, D. A.; Frei, A., Seasonal Variability of Northern Hemisphere Snow Extent Using Visible Satellite Data. *The Professional Geographer* **2000**, *52*, 307-315.

8. Gardner, A. S., et al., A Reconciled Estimate of Glacier Contributions to Sea Level Rise: 2003 to 2009. *Science* **2013**, *340*, 852-857.

9. Jacob, T.; Wahr, J.; Pfeffer, W. T.; Swenson, S., Recent Contributions of Glaciers and Ice Caps to Sea Level Rise. *Nature* **2012**, *482*, 514.

10. Cavalieri, D. J.; Parkinson, C. L., Arctic Sea Ice Variability and Trends, 1979&Ndash;2010. *The Cryosphere* **2012**, *6*, 881-889.

11. Kwok, R.; Rothrock, D. A., Decline in Arctic Sea Ice Thickness from Submarine and Icesat Records: 1958–2008. *Geophysical Research Letters* **2009**, *36*.

12. Rothrock, D. A.; Yu, Y.; Maykut, G. A., Thinning of the Arctic Sea-Ice Cover. *Geophysical Research Letters* **1999**, *26*, 3469-3472.

13. Laxon, S. W., et al., Cryosat-2 Estimates of Arctic Sea Ice Thickness and Volume. *Geophysical Research Letters* **2013**, *40*, 732-737.

14. Kwok, R.; Cunningham, G. F., Variability of Arctic Sea Ice Thickness and Volume from Cryosat-2. *Philosophical Transactions of the Royal Society A: Mathematical, Physical and Engineering Sciences* **2015**, *373*, 20140157.

15. Nerem, R. S.; Beckley, B. D.; Fasullo, J. T.; Hamlington, B. D.; Masters, D.; Mitchum, G. T., Climate-Change–Driven Accelerated Sea-Level Rise Detected in the Altimeter Era. *Proceedings of the National Academy of Sciences* **2018**, *115*, 2022-2025.

16. Usgcrp *Climate Science Special Report: Fourth National Climate Assessment, Volume I*; U.S. Global Change Research Program: Washington, DC, USA, 2017; p 470.

17. *A National Strategy for Advancing Climate Modeling*; The National Academies Press: Washington, DC, 2012, p 294.

18. Burrows, S. M.; Gobrogge, E.; Fu, L.; Link, K.; Elliott, S. M.; Wang, H.; Walker, R., Oceanfilms-2: Representing Coadsorption of Saccharides in Marine Films and Potential Impacts on Modeled Marine Aerosol Chemistry. *Geophys. Res. Lett.* **2016**, *43*, 8306-8313.

19. Wang, S.; Maltrud, M. E.; Burrows, S. M.; Elliott, S. M.; Cameron-Smith, P., Impacts of Shifts in Phytoplankton Community on Clouds and Climate Via the Sulfur Cycle. *Global Biogeochemical Cycles* **2018**, *32*, 1005-1026.

20. Jayarathne, T., et al., Enrichment of Saccharides and Divalent Cations in Sea Spray Aerosol During Two Phytoplankton Blooms. *Environ. Sci. Technol.* **2016**, *50*, 11511-11520.

21. Meskhidze, N.; Xu, J.; Gantt, B.; Zhang, Y.; Nenes, A.; Ghan, S. J.; Liu, X.; Easter, R.; Zaveri, R., Global Distribution and Climate Forcing of Marine Organic Aerosol: 1. Model Improvements and Evaluation. *Atmos Chem Phys* **2011**, *11*, 11689-11705.

22. Fossum, K. N., et al., Summertime Primary and Secondary Contributions to Southern Ocean Cloud Condensation Nuclei. *Sci. Rep.* **2018**, *8*, 13844.

23. Forestieri, S. D.; Staudt, S. M.; Kuborn, T. M.; Faber, K.; Ruehl, C. R.; Bertram, T. H.; Cappa, C. D., Establishing the Impact of Model Surfactants on Cloud Condensation Nuclei Activity of Sea Spray Aerosol Mimics. **2018**, *18*, 10985-11005.

24. Quinn, P. K.; Coffman, D. J.; Johnson, J. E.; Upchurch, L. M.; Bates, T. S., Small Fraction of Marine Cloud Condensation Nuclei Made up of Sea Spray Aerosol. *Nature Geoscience* **2017**, *10*, 674-679.

25. DeMott, P. J., et al., Sea Spray Aerosol as a Unique Source of Ice Nucleating Particles. *Proceedings of the National Academy of Sciences of the United States of America* **2016**, *113*, 5797-5803.

26. DeMott, P. J., et al., Ice Nucleation by Particles Containing Long-Chain Fatty Acids of Relevance to Freezing by Sea Spray Aerosols. *Environmental science. Processes & impacts* **2018**, *20*, 1559-1569.

27. DeMott, P. J.; Hill, T. C. J. *Marine Ice Nuclei Collections – Magic (Magic-in) Final Campaign Summary*; DOE ARM Climate Research Facility, Pacific Northwest National Laboratory; Richland, Washington: Feb 01, 2016.

28. Wilson, T. W., et al., A Marine Biogenic Source of Atmospheric Ice-Nucleating Particles. *Nature* **2015**, *525*, 234-238.

29. Rosenfeld, D.; Zhu, Y.; Wang, M.; Zheng, Y.; Goren, T.; Yu, S., Aerosol-Driven Droplet Concentrations Dominate Coverage and Water of Oceanic Low-Level Clouds. *Science* **2019**, *363*, eaav0566-11.

30. Han, Z. W.; Li, J. W.; Yao, X. H.; Tan, S. C., A Regional Model Study of the Characteristics and Indirect Effects of Marine Primary Organic Aerosol in Springtime over East Asia. *Atmos Environ* **2019**, *197*, 22-35.

31. McCoy, D. T.; Burrows, S. M.; Wood, R.; Grosvenor, D. P.; Elliott, S. M.; Ma, P. L.; Rasch, P. J.; Hartmann, D. L., Natural Aerosols Explain Seasonal and Spatial Patterns of Southern Ocean Cloud Albedo. *Science Advances* **2015**, *1*, e1500157-e1500157.

32. Carslaw, K. S., et al., Large Contribution of Natural Aerosols to Uncertainty in Indirect Forcing. *Nature* **2013**, *503*, 67-+.

33. Rosenfeld, D.; Lohmann, U.; Raga, G. B.; O'Dowd, C. D.; Kulmala, M.; Fuzzi, S.; Reissell, A.; Andreae, M. O., Flood or Drought: How Do Aerosols Affect Precipitation? *Science* **2008**, *321*, 1309-1313.

34. Fröhlich-Nowoisky, J., et al., Bioaerosols in the Earth System: Climate, Health, and Ecosystem Interactions. *Atmospheric Research* **2016**, *182*, 346-376.

35. Karl, T. R.; Trenberth, K. E., Modern Global Climate Change. *Science* **2003**, *302*, 1719.

36. Russell, L. M.; Hawkins, L. N.; Frossard, A. A.; Quinn, P. K.; Bates, T. S., Carbohydrate-Like Composition of Submicron Atmospheric Particles and Their Production from Ocean Bubble Bursting. *Proc. Natl. Acad. Sci. U. S. A.* **2010**, *107*, 6652-6657.

37. Burrows, S. M.; Ogunro, O.; Frossard, A. A.; Russell, L. M.; Rasch, P. J.; Elliott, S. M., A Physically Based Framework for Modeling the Organic Fractionation of Sea Spray Aerosol from Bubble Film Langmuir Equilibria. *Atmos Chem Phys* **2014**, *14*, 13601-13629.

38. Cunliffe, M.; Engel, A.; Frka, S.; Gašparović, B.; Guitart, C.; Murrell, J. C.; Salter, M.; Stolle, C.; Upstill-Goddard, R.; Wurl, O., Sea Surface Microlayers: A Unified Physicochemical and Biological Perspective of the Air–Ocean Interface. *Progress in Oceanography* **2013**, *109*, 104-116.

39. Grythe, H.; Strom, J.; Krejci, R.; Quinn, P.; Stohl, A., A Review of Sea-Spray Aerosol Source Functions Using a Large Global Set of Sea Salt Aerosol Concentration Measurements. *Atmos Chem Phys* **2014**, *14*, 1277-1297.

40. Hawkins, L. N.; Russell, L., Polysaccharides, Proteins, and Phytoplankton Fragments: Four Chemically Distinct Types of Marine Primary Organic Aerosol Classified by Single Particle Spectromicroscopy. *Adv Meteorol* **2010**, *2010*, 14.

41. Bhattacharyya, L.; Rohrer, J. S., *Applications of Ion Chromatography for Pharmaceutical and Biological Products*; Hoboken, N.J. : John Wiley & Sons, Inc.: Hoboken, N.J., 2012.

42. Bichsel, Y.; von Gunten, U., Formation of Iodo-Trihalomethanes During Disinfection and Oxidation of Iodide-Containing Waters. *Environmental Science & Technology* **2000**, *34*, 2784-2791.

43. Jewison, T., et al., Ymdb: The Yeast Metabolome Database. *Nucleic acids research* **2012**, *40*, D815-20.

44. Ramirez-Gaona, M.; Marcu, A.; Pon, A.; Guo, A. C.; Sajed, T.; Wishart, N. A.; Karu, N.; Djoumbou Feunang, Y.; Arndt, D.; Wishart, D. S., Ymdb 2.0: A Significantly Expanded Version of the Yeast Metabolome Database. *Nucleic acids research* **2017**, *45*, D440-d445.

45. Nakahara, H.; Lee, S.; Shoyama, Y.; Shibata, O., The Role of Palmitic Acid in Pulmonary Surfactant Systems by Langmuir Monolayer Study: Lipid–Peptide Interactions. *Soft Matter* **2011**, *7*, 11351-11359.

46. HUNT, J. H.; GUYOTSIONNEST, P.; Shen, Y. R., Observation of C-H Stretch Vibrations of Monolayers of Molecules Optical Sum-Frequency Generation. *Chemical physics letters* **1987**, *133*, 189-192.

47. Walker, R. A.; Gruetzmacher, J. A.; Richmond, G. L., Phosphatidylcholine Monolayer Structure at a Liquid−Liquid Interface. *Journal of the American Chemical Society* **1998**, *120*, 6991-7003.

48. Ma, G.; Allen, H. C., Dppc Langmuir Monolayer at the Air−Water Interface: Probing the Tail and Head Groups by Vibrational Sum Frequency Generation Spectroscopy. *Langmuir* **2006**, *22*, 5341-5349.

49. Adams, E. M.; Casper, C. B.; Allen, H. C., Effect of Cation Enrichment on Dipalmitoylphosphatidylcholine (Dppc) Monolayers at the Air-Water Interface. *J. Colloid Interface Sci.* **2016**, *478*, 353-364.

50. Adams, E. M.; Verreault, D.; Jayarathne, T.; Cochran, R. E.; Stone, E. A.; Allen, H. C., Surface Organization of a Dppc Monolayer on Concentrated Srcl2 and Zncl2 Solutions. *Phys. Chem. Chem. Phys.* **2016**, *18*, 32345-32357.

51. Link, K. A.; Hsieh, C. Y.; Tuladhar, A.; Chase, Z.; Wang, Z. M.; Wang, H. F.; Walker, R. A., Vibrational Studies of Saccharide-Induced Lipid Film Reorganization at Aqueous/Air Interfaces. *Chem Phys* **2018**, *512*, 104-110.

52. Pan, X.; Yang, F.; Chen, S.; Zhu, X.; Wang, C., Cooperative Effects of Zwitterionic–Ionic Surfactant Mixtures on the Interfacial Water Structure Revealed by Sum Frequency Generation Vibrational Spectroscopy. *Langmuir* **2018**, *34*, 5273-5278.

53. Bulk Contributions Modulate the Sum-Frequency Generation Spectra of Interfacial Water on Model Sea-Spray Aerosols. **2017**, 1-41.

54. Jubb, A. M.; Hua, W.; Allen, H. C., Environmental Chemistry at Vapor/Water Interfaces: Insights from Vibrational Sum Frequency Generation Spectroscopy. *Annual Review of Physical Chemistry* **2012**, *63*, 107-130.

55. Zhang, T.; Brantley, S. L.; Verreault, D.; Dhankani, R.; Corcelli, S. A.; Allen, H. C., Effect of Ph and Salt on Surface-Pka of Phosphatidic Acid Monolayers. *Langmuir* **2017**, acs.langmuir.7b03579-34.

56. Shultz, M. J.; Schnitzer, C.; Simonelli, D.; Baldelli, S., Sum Frequency Generation Spectroscopy of the Aqueous Interface: Ionic and Soluble Molecular Solutions. *Int Rev Phys Chem* **2000**, *19*, 123-153.

57. Velarde, L.; Zhang, X. Y.; Lu, Z.; Joly, A. G.; Wang, Z.; Wang, H. F., Communication: Spectroscopic Phase and Lineshapes in High-Resolution Broadband Sum Frequency Vibrational Spectroscopy: Resolving Interfacial Inhomogeneities of “Identical" Molecular Groups. *J. Chem. Phys.* **2011**, *135*, 241102.

58. Wang, H.-F., Sum Frequency Generation Vibrational Spectroscopy (Sfg-Vs) for Complex Molecular Surfaces and Interfaces: Spectral Lineshape Measurement and Analysis Plus Some Controversial Issues. *Progress in Surface Science* **2016**, *91*, 155-182.

59. Wang, H.-F.; Gan, W.; Lu, R.; Rao, Y.; Wu, B.-h., Quantitative Spectral and Orientational Analysis in Surface Sum Frequency Generation Vibrational Spectroscopy (Sfg-Vs). *International Reviews in Physical Chemistry* **2005**, *24*, 191-256.

60. Wang, H.-F.; Velarde, L.; Gan, W.; Fu, L., Quantitative Sum-Frequency Generation Vibrational Spectroscopy of Molecular Surfaces and Interfaces: Lineshape, Polarization, and Orientation. **2015**, *66*, 189-216.

61. Wang, H. F.; Gan, W.; Lu, R.; Rao, Y.; Wu, B. H., Quantitative Spectral and Orientational Analysis in Surface Sum Frequency Generation Vibrational Spectroscopy (Sfg-Vs). **2005**, *24*, 191-256.

62. Zhang, Z.; Guo, Y.; Lu, Z.; Velarde, L.; Wang, H. F., Resolving Two Closely Overlapping -Cn Vibrations and Structure in the Langmuir Mono Layer of the Long-Chain Nonadecanenitrile by Polarization Sum Frequency Generation Vibrational Spectroscopy. *J. Phys. Chem. C* **2012**, *116*, 2976-2987.

63. Zhang, D.; Gutow, J.; Physical, K. E. T. J. o.; 1994, Vibrational Spectra, Orientations, and Phase Transitions in Long-Chain Amphiphiles at the Air/Water Interface: Probing the Head and Tail Groups by Sum Frequency …. *ACS Publications*.

64. Lambert, A. G.; Davies, P. B.; Neivandt, D. J., Implementing the Theory of Sum Frequency Generation Vibrational Spectroscopy: A Tutorial Review. *Applied Spectroscopy Reviews* **2005**, *40*, 103-145.

65. Hung, K.-K.; Stege, U.; Hore, D. K., Ir Absorption, Raman Scattering, and Ir-Vis Sum-Frequency Generation Spectroscopy as Quantitative Probes of Surface Structure. *Applied Spectroscopy Reviews* **2014**, *50*, 351-376.

66. Shen, Y. R., Surface-Properties Probed by 2nd-Harmonic and Sum-Frequency Generation. **1989**, *337*, 519-525.

67. Shen, Y. R., Basic Theory of Surface Sum-Frequency Generation. *Journal of Physical Chemistry C* **2012**, *116*, 15505-15509.

68. Ye, S.; Noda, H.; Morita, S.; Kohei Uosaki, a.; Osawa, M., Surface Molecular Structures of Langmuir−Blodgett Films of Stearic Acid on Solid Substrates Studied by Sum Frequency Generation Spectroscopy. *Langmuir* **2003**, *19*, 2238-2242.

69. Ye, S.; Osawa, M., Molecular Structures on Solid Substrates Probed by Sum Frequency Generation (Sfg) Vibration Spectroscopy. *Chemistry Letters* **2009**, *38*, 386-391.

70. Bain, C. D., Sum-Frequency Vibrational Spectroscopy of the Solid/Liquid Interface. *Journal of the Chemical Society, Faraday Transactions* **1995**, *91*, 1281-16.

71. Ohno, P. E.; Wang, H. F.; Geiger, F. M., Second-Order Spectral Lineshapes from Charged Interfaces. *Nat. Commun.* **2017**, *8*, 1032.

72. Ohno, P. E.; Wang, H. F.; Paesani, F.; Skinner, J. L.; Geiger, F. M., Second-Order Vibrational Lineshapes from the Air/Water Interface. *J. Phys. Chem. A* **2018**, *122*, 4457-4464.

73. Liu, W.; Fu, L.; Wang, Z.; Sohrabpour, Z.; Li, X.; Liu, Y.; Wang, H. F.; Yan, E. C. Y., Two Dimensional Crowding Effects on Protein Folding at Interfaces Observed by Chiral Vibrational Sum Frequency Generation Spectroscopy. *Phys. Chem. Chem. Phys.* **2018**, *20*, 22421-22426.

74. Lu, Z.; Karakoti, A.; Velarde, L.; Wang, W. N.; Yang, P.; Thevuthasan, S.; Wang, H. F., Dissociative Binding of Carboxylic Acid Ligand on Nanoceria Surface in Aqueous Solution: A Joint in Situ Spectroscopic Characterization and First-Principles Study. *J. Phys. Chem. C* **2013**, *117*, 24329-24338.

75. Mifflin, A. L., et al., Accurate Line Shapes from Sub-1 Cm(-1) Resolution Sum Frequency Generation Vibrational Spectroscopy of Alpha-Pinene at Room Temperature. *J. Phys. Chem. A* **2015**, *119*, 1292-1302.

76. Olenick, L. L.; Chase, H. M.; Fu, L.; Zhang, Y.; McGeachy, A. C.; Dogangun, M.; Walter, S. R.; Wang, H. F.; Geiger, F. M., Single-Component Supported Lipid Bilayers Probed Using Broadband Nonlinear Optics. *Phys. Chem. Chem. Phys.* **2018**, *20*, 3063-3072.

77. Velarde, L.; Wang, H.-F., Capturing Inhomogeneous Broadening of the –Cn Stretch Vibration in a Langmuir Monolayer with High-Resolution Spectra and Ultrafast Vibrational Dynamics in Sum-Frequency Generation Vibrational Spectroscopy (Sfg-Vs). *Journal of Chemical Physics* **2013**, *139*, 084204.

78. Vaughn, J., Ultrafast Pulse Shaping. In *Ultrafast Optics Textbook*, Trebino, R., Ed. Internet, 2015.

79. Aston, M. S., The Study of Surfactant Monolayers by Surface Pressure?Area Measurement. *Chemical Society Reviews* **1993**, *22*, 67-5.

80. Blume, A., Lipids at the Air–Water Interface. *ChemTexts* **2018**, *4*, 1-25.

81. Gzyl-Malcher, B.; Paluch, M., Studies of Lipid Interactions in Mixed Langmuir Monolayers. *Thin Solid Films* **2008**, *516*, 8865-8872.

82. Kodama, M.; Kuwabara, M.; Seki, S., Sucessive Phase-Transition Phenomena and Phase Diagram of the Phosphatidylcholine-Water System as Revealed by Differential Scanning Calorimetry. *Biochim. Biophys. Acta, Biomembr.* **2002**, 567-570.

83. McElhaney, R. N., The Use of Differential Scanning Calorimetry and Differential Thermal-Analysis in Studies of Model and Biological-Membranes. *Chem Phys Lipids* **1982**, *30*, 229-259.

84. Jain, M. K.; Wu, N. M., Effect of Small Molecules on the Dipalmitoyl Lecithin Liposomal Bilayer: Iii. Phase Transition in Lipid Bilayer. *J. Membr. Biol.* **1977**, *34*, 157-201.

85. Riske, K. A.; Barroso, R. P.; Vequi-Suplicy, C. C.; Germano, R.; Henriques, V. B.; Lamy, M. T., Lipid Bilayer Pre-Transition as the Beginning of the Melting Process. *Biochim. Biophys. Acta* **2009**, *1788*, 954-963.

86. Cutro, A. C.; Disalvo, E. A.; Frías, M. A., Effects of Phenylalanine on the Liquid-Expanded and Liquid-Condensed States of Phosphatidylcholine Monolayers. *Lipid Insights* **2019**, *12*, 117863531882092-9.

87. Adamczewski, P.; Tsoukanova, V., Phenylalanine Intercalation Parameters for Liquid-Disordered Phase Domains – a Membrane Model Study. **2018**, 1-8.

88. Feng, R.-J.; Li, X.; Zhang, Z.; Lu, Z.; Guo, Y., Spectral Assignment and Orientational Analysis in a Vibrational Sum Frequency Generation Study of Dppc Monolayers at the Air/Water Interface. *Journal of Chemical Physics* **2016**, *145*, 244707-12.

89. Casper, C. B.; Verreault, D.; Adams, E. M.; Hua, W.; Allen, H. C., Surface Potential of Dppc Monolayers on Concentrated Aqueous Salt Solutions. *J. Phys. Chem. B* **2016**, *120*, 2043-52.

90. Casillas-Ituarte, N. N.; Chen, X.; Castada, H.; Allen, H. C., Na(+) and Ca(2+) Effect on the Hydration and Orientation of the Phosphate Group of Dppc at Air-Water and Air-Hydrated Silica Interfaces. *J. Phys. Chem. B* **2010**, *114*, 9485-9495.

91. LIS, L. J.; LIS, W. T.; PARSEGIAN, V. A.; RAND, R. P., Adsorption of Divalent Cations to a Variety of Phosphatidylcholine Bilayers. *Biochemistry* **1981**, *20*, 1771-1777.

92. LIS, L. J.; PARSEGIAN, V. A.; RAND, R. P., Binding of Divalent Cations to Dipalmitoylphosphatidylcholine Bilayers and Its Effect on Bilayer Interaction. *Biochemistry* **2002**, *20*, 1761-1770.

93. Gil, A. M.; Belton, P. S.; and, V. F. S. A. P. A. M.; 1996, Spectroscopic Studies of Solid A-A Trehalose. *Elsevier*.

94. Becker, A.; Schloder, P.; Steele, J. E.; Wegener, G., The Regulation of Trehalose Metabolism in Insects. *Experientia* **1996**, *52*, 433-9.

95. Elbein, A. D.; Carroll, D.; Pastuszak, I.; Pan, Y. T., New Insights on Trehalose: A Multifunctional Molecule. *Glycobiology* **2003**, *13*, 17R-27R.

96. Zhang, H.; Fan, Q.; Wang, Y. E.; Neal, C. R.; Zuo, Y. Y., Comparative Study of Clinical Pulmonary Surfactants Using Atomic Force Microscopy. *Biochim Biophys Acta* **2011**, *1808*, 1832-42.

97. Ma, G.; Allen, H. C., New Insights into Lung Surfactant Monolayers Using Vibrational Sum Frequency Generation Spectroscopy. *Photochemistry and Photobiology* **2006**, *82*, 1517-1529.

98. Nag, K.; Perez-Gil, J.; Ruano, M. L.; Worthman, L. A.; Stewart, J.; Casals, C.; Keough, K. M., Phase Transitions in Films of Lung Surfactant at the Air-Water Interface. *Biophysical journal* **1998**, *74*, 2983-2995.

99. Kulovesi, P.; Telenius, J.; Koivuniemi, A.; Brezesinski, G.; Vattulainen, I.; Holopainen, J. M., The Impact of Lipid Composition on the Stability of the Tear Fluid Lipid Layer. *Soft Matter* **2012**, *8*, 5826-5834.

100. Mathers, W., Evaporation from the Ocular Surface. *Experimental Eye Research* **2004**, *78*, 389-394.

101. Plant, A. L., Supported Hybrid Bilayer Membranes as Rugged Cell Membrane Mimics. *Langmuir* **1999**, *15*, 5128-5135.

102. Sackmann, E., Supported Membranes: Scientific and Practical Applications. *Science* **1996**, *271*, 43-48.

103. Borden, M. A.; Longo, M. L., Oxygen Permeability of Fully Condensed Lipid Monolayers. *Journal of Physical Chemistry B* **2004**, *108*, 6009-6016.

104. Scholl, F. A.; Morais, P. V.; Gabriel, R. C.; Schoning, M. J.; Siqueira, J. R.; Caseli, L., Carbon Nanotubes Arranged as Smart Interfaces in Lipid Langmuir-Blodgett Films Enhancing the Enzymatic Properties of Penicillinase for Biosensing Applications. *Acs Applied Materials & Interfaces* **2017**, *9*, 31054-31066.

105. Kucerka, N.; Dushanov, E.; Kholmurodov, K. T.; Katsaras, J.; Uhrikova, D., Calcium and Zinc Differentially Affect the Structure of Lipid Membranes. *Langmuir* **2017**, *33*, 3134-3141.

106. Ciumac, D.; Campbell, R. A.; Xu, H.; Clifton, L. A.; Hughes, A. V.; Webster, J. R. P.; Lu, J. R., Implications of Lipid Monolayer Charge Characteristics on Their Selective Interactions with a Short Antimicrobial Peptide. *Colloids and Surfaces B-Biointerfaces* **2017**, *150*, 308-316.

107. Joondan, N.; Jhaumeer-Laulloo, S.; Caumul, P., Effect of Chain Length on the Micellization, Antibacterial, Dppc Interaction and Antioxidant Activities of L-3,4-Dihydroxyphenylalanine (L-Dopa) Esters. *Journal of Surfactants and Detergents* **2015**, *18*, 1095-1104.

108. Griffith, E. C.; Perkins, R. J.; Telesford, D. M.; Adams, E. M.; Cwiklik, L.; Allen, H. C.; Roeseova, M.; Vaida, V., Interaction of L-Phenylalanine with a Phospholipid

Monolayer at the Water-Air Interface. *Journal of Physical Chemistry B* **2015**, *119*, 9038-9048.

109. Perkins, R.; Vaida, V., Phenylalanine Increases Membrane Permeability. *Journal of the American Chemical Society* **2017**, *139*, 14388-14391.

110. Doxastakis, M.; Sum, A. K.; de Pablo, J. J., Modulating Membrane Properties: The Effect of Trehalose and Cholesterol on a Phospholipid Bilayer. *Journal of Physical Chemistry B* **2005**, *109*, 24173-24181.

111. Burrows, S. M.; Ogunro, O.; Frossard, A. A.; Russell, L. M.; Rasch, P. J.; Elliott, S. M., A Physically Based Framework for Modeling the Organic Fractionation of Sea Spray Aerosol from Bubble Film Langmuir Equilibria. *Atmospheric Chemistry and Physics* **2014**, *14*, 13601-13629.

112. Wilson, T. W., et al., A Marine Biogenic Source of Atmospheric Ice-Nucleating Particles. *Nature* **2015**, *525*, 234-+.

113. Aller, J. Y.; Radway, J. C.; Kilthau, W. P.; Bothe, D. W.; Wilson, T. W.; Vaillancourt, R. D.; Quinn, P. K.; Coffman, D. J.; Murray, B. J.; Knopf, D. A., Size-Resolved Characterization of the Polysaccharidic and Proteinaceous Components of Sea Spray Aerosol. *Atmospheric Environment* **2017**, *154*, 331-347.

114. Ault, A. P., et al., Size-Dependent Changes in Sea Spray Aerosol Composition and Properties with Different Seawater Conditions. *Environmental Science & Technology* **2013**, *47*, 5603-5612.

115. O'Dowd, C. D.; De Leeuw, G., Marine Aerosol Production: A Review of the Current Knowledge. *Philosophical Transactions of the Royal Society a-Mathematical Physical and Engineering Sciences* **2007**, *365*, 1753-1774.

116. Quinn, P. K.; Bates, T. S.; Schulz, K. S.; Coffman, D. J.; Frossard, A. A.; Russell, L. M.; Keene, W. C.; Kieber, D. J., Contribution of Sea Surface Carbon Pool to Organic Matter Enrichment in Sea Spray Aerosol. *Nature Geoscience* **2014**, *7*, 228-232.

117. Burrows, S. M.; Gobrogge, E.; Fu, L.; Link, K.; Elliott, S. M.; Wang, H. F.; Walker, R., Oceanfilms-2: Representing Coadsorption of Saccharides in Marine Films and Potential Impacts on Modeled Marine Aerosol Chemistry. *Geophysical Research Letters* **2016**, *43*, 8306-8313.

118. Adams, E. M.; Casper, C. B.; Allen, H. C., Effect of Cation Enrichment on Dipalmitoylphosphatidylcholine (Dppc) Monolayers at the Air-Water Interface. *Journal of Colloid and Interface Science* **2016**, *478*, 353-364.

119. Ferber, U. M.; Kaggwa, G.; Jarvis, S. P., Direct Imaging of Salt Effects on Lipid Bilayer Ordering at Sub-Molecular Resolution. *European Biophysics Journal with Biophysics Letters* **2011**, *40*, 329-338.

120. Ghosh, S. K.; Castorph, S.; Konovalov, O.; Salditt, T.; Jahn, R.; Holt, M., Measuring Ca2+ Induced Structural Changes in Lipid Monolayers: Implications for Synaptic Vesicle Exocytosis. *Biophysical Journal* **2012**, *102*, 1394-1402.

121. Kewalramani, S.; Hlaing, H.; Ocko, B. M.; Kuzmenko, I.; Fukoto, M., Effects of Divalent Cations on Phase Behavior and Structure of a Zwitterionic Phosphlipid (Dmpc) Monolayer at the Air-Water Interface. *Journal of Physical Chemistry Letters* **2010**, *1*, 489-495.

122. Lin, W.; Clark, A. J.; Paesani, F., Effects of Surface Pressure on the Properties of Langmuir Monolayers and Interfacial Water at Model Sea Spray Aerosol Surfaces. *Langmuir* **2015**, *31*, 2147-2156.

123. Bichsel, Y.; vonGunten, U., Formation of Iodo-Trihalomethanes During Disinfection and Oxidation of Iodide Containing Waters. *Environmental Science and Technology* **2000**, *34*, 2784-2791.

124. Rohrer, J. S., *Applications of Ion Chromatography for Parmaceutical and Biological Products*, 1st ed.; John Wiley and Sons, Inc., 2012, p 457.

125. Adams, E. M.; Verreault, D.; Jayarathne, T.; Cochran, R. E.; Stone, E. A.; Allen, H. C., Surface Organization of a Dppc Monolayer on Concentrated Srcl2 and Zncl2 Solutions. *Physical Chemistry Chemical Physics* **2016**, *18*, 32345-32357.

126. Aston, M. S., The Study of Surfactant Monolayers by Surface Pressure Area Measurement. *Chemical Society Reviews* **1993**, *22*, 67-71.

127. Velarde, L.; Wang, H. F., Capturing Inhomogeneous Broadening of the -Cn Stretch Vibration in a Langmuir Monolayer with High-Resolution Spectra and Ultrafast Vibrational Dynamics in Sum-Frequency Generation Vibrational Spectroscopy (Sfg-Vs). *Journal of Chemical Physics* **2013**, *139*.

128. Gobrogge, C. A.; Blanchard, H. S.; Walker, R. A., Temperature-Dependent Partitioning of Coumarin 152 in Phosphatidylcholine Lipid Bilayers. *Journal of Physical Chemistry B* **2017**, *121*, 4061-4070.

129. Gobrogge, C. A.; Walker, R. A., Quantifying Solute Partitioning in Phosphatidylcholine Membranes. *Analytical Chemistry* **2017**, *89*, 12587-12595.

130. Avanti_Polar_Lipids Liposome Preparation. https://avantilipids.com/tech-support/liposome-preparation/

131. Kozak, M.; Domka, L.; Jurga, S., Interactions of Cationic Surfactantswith Dppc. *Journal of Thermal Analysis and Calorimetry* **2007**, *88*, 395-399.

132. Mansour, H. M.; Zografi, G., Relationships between Equilibrium Spreading Pressure and Phase Equilibria of Phospholipid Bilayers and Monolayers at the Air-Water Interface. *Langmuir* **2007**, *23*, 3809-3819.

133. McConlogue, C. W.; Malamud, D.; Vanderlick, T. K., Interaction of Dppc Monolayers with Soluble Surfactants: Electrostatic Effects of Membrane Perturbants. *Biochimica Et Biophysica Acta-Biomembranes* **1998**, *1372*, 124-134.

134. Clark, G. A.; Henderson, J. M.; Heffern, C.; Akgün, B.; Majewski, J.; Lee, K. Y. C., Synergistic Interactions of Sugars/Polyols and Monovalent Salts with Phospholipids Depend Upon Sugar/Polyol Complexity and Anion Identity. *Langmuir* **2015**, *31*, 12688-12698.

135. Macphail, R. A.; Strauss, H. L.; Snyder, R. G.; Elliger, C. A., C-H Stretching Modes and the Structure of Normal Alkyl Chains .2. Long, All-Trans Chains *Journal of Physical Chemistry* **1984**, *88*, 334-341.

136. Snyder, R. G.; Strauss, H. L.; Elliger, C. A., C-H Stretching Modes and the Structure of Normal Alkyl Chains . 1. Long Disordered Chains *Journal of Physical Chemistry* **1982**, *86*, 5145-5150.

137. Can, S. Z.; Mago, D. D.; Walker, R. A., Structure and Organization of Hexadecanol Isomers Adsorbed to the Air/Water Interface. *Langmuir* **2006**, *22*, 8043-8049.

138. Walker, R. A.; Gruetzmacher, J. A.; Richmond, G. L., Phosphatidylcholine Monolayer Structure at a Liquid-Liquid Interface. *Journal of the American Chemical Society* **1998**, *120*, 6991-7003.

139. Can, S. Z.; Chang, C. F.; Walker, R. A., Spontaneous Formation of Dppc Monolayers at Aqueous/Vapor Interfaces and the Impact of Charged Surfactants. *Biochimica Et Biophysica Acta-Biomembranes* **2008**, *1778*, 2368-2377.

140. Kodama, M.; Kuwabara, M.; Seki, S., Successive Phase-Transition Phenomena and Phase Diagram of the Phosphatidylcholine-Water System as Revealed by Differential Scanning Calorimetry. *Biochimica et Biophysica Acta (BBA) - Biomembranes* **1982**, *689*, 567-570.

141. Minami, H.; Inoue, T., Dehydration of Hydrated Bilayer of Dipalmitoylphosphatidylcholine Caused by Beryllium Ion: Evidence from a Differential Scanning Calorimetry of Bilayer Phase Transition. *Journal of Colloid and Interface Science* **1998**, *206*, 338-341.

142. Pham, D. Q., et al., Biological Impacts on Carbon Speciation and Morphology of Sea Spray Aerosol. *ACS Earth Space Chem.* **2017**, *1*, 551-561.

143. Facchini, M. C., et al., Primary Submicron Marine Aerosol Dominated by Insoluble Organic Colloids and Aggregates. *Geophys. Res. Lett.* **2008**, *35*.

144. Elliott, S., et al., Does Marine Surface Tension Have Global Biogeography? Addition for the Oceanfilms Package. *Atmosphere* **2018**, *9*, 216-232.

145. Ahmed, S. N.; Brown, D. A.; London, E., On the Origin of Sphingolipid/Cholesterol-Rich Detergent-Insoluble Cell Membranes: Physiological Concentrations of Cholesterol and Sphingolipid Induce Formation of a Detergent-Insoluble, Liquid-Ordered Lipid Phase in Model Membranes. *Biochemistry* **1997**, *36*, 10944-10953.

146. Schill, S. R.; Burrows, S. M.; Hasenecz, E. S.; Stone, E. A.; Bertram, T. H., The Impact of Divalent Cations on the Enrichment of Soluble Saccharides in Primary Sea Spray Aerosol. *Atmosphere* **2018**, *9*, 476-417.

147. Reddy, S. K.; Thiraux, R.; Wellen Rudd, B. A.; Lin, L.; Adel, T.; Joutsuka, T.; Geiger, F. M.; Allen, H. C.; Morita, A.; Paesani, F., Bulk Contributions Modulate the Sum-Frequency Generation Spectra of Water on Model Sea-Spray Aerosols. *Chem* **2018**, *4*, 1629-1644.

148. Ebben, C. J.; Ault, A. P.; Ruppel, M. J.; Ryder, O. S.; Bertram, T. H.; Grassian, V. H.; Prather, K. A.; Geiger, F. M., Size-Resolved Sea Spray Aerosol Particles Studied by Vibrational Sum Frequency Generation. *The Journal of Physical Chemistry A* **2013**, *117*, 6589-6601.

149. Can, S. Z.; Mago, D. D.; Esenturk, O.; Walker, R. A., Balancing Hydrophobic and Hydrophilic Forces at the Water/Vapor Interface: Surface Structure of Soluble Alcohol Monolayers. *The Journal of Physical Chemistry C* **2007**, *111*, 8739-8748.

150. Esenturk, O.; Walker, R. A., Surface Vibrational Structure at Alkane Liquid/Vapor Interfaces. *J Chem Phys* **2006**, *125*, 174701.

151. Gobrogge, C. A.; Kong, V. A.; Walker, R. A., Temperature-Dependent Partitioning of C152 in Binary Phosphatidylcholine Membranes and Mixed Phosphatidylcholine/Phosphatidylethanolamine Membranes. *J. Phys. Chem. B* **2017**, *121*, 7889-7898.

152. Kuo, R. R.; Chang, C. H.; Yang, Y. M.; Maa, J. R., Induced Removal of Dipalmitoyl Phosphatidylcholine by the Exclusion of Fibrinogen from Compressed Monolayers at Air/Liquid Interfaces. *J. Colloid Interface Sci.* **2003**, *257*, 108-115.

153. Amrein, M.; von Nahmen, A.; Sieber, M., A Scanning Force- and Fluorescence Light Microscopy Study of the Structure and Function of a Model Pulmonary Surfactant. *Eur. Biophys. J.* **1997**, *26*, 349-357.

154. Snyder, R. G.; Strauss, H. L.; Elliger, C. A., Carbon-Hydrogen Stretching Modes and the Structure of N-Alkyl Chains. 1. Long, Disordered Chains. *J. Phys. Chem.* **1982**, *86*, 5145-5150.

155. MacPhail, R. A.; Strauss, H. L.; Snyder, R. G.; Elliger, C. A., Carbon-Hydrogen Stretching Modes and the Structure of *N*-Alkyl Chains. 2. Long, All-Trans Chains. *J. Phys. Chem.* **1984**, *88*, 334-341.

156. Can, S. Z.; Mago, D. D.; Walker, R. A., Structure and Organization of Hexadecanol Isomers Adsorbed to the Air/Water Interface. In *Langmuir*, 2006; Vol. 22, pp 8043-8049.

157. Walker, R. A.; Gruetzmacher, J. A.; Richmond, G. L., Phosphatidylcholine Monolayer Structure at a Liquid−Liquid Interface. In *J. Am. Chem. Soc.*, 1998; Vol. 120, pp 6991-7003.

158. Conboy, J. C.; Messmer, M. C.; Richmond, G. L., Dependence of Alkyl Chain Conformation of Simple Ionic Surfactants on Head Group Functionality as Studied by Vibrational Sum-Frequency Spectroscopy. *J. Phys. Chem. B* **1997**, *101*, 6724-6733.

159. Fourkas, J. T.; Walker, R. A.; Can, S. Z.; Gershgoren, E., Effects of Reorientation in Vibrational Sum-Frequency Spectroscopy. *J. Phys. Chem. C* **2007**, *111*, 8902-8915.

160. Jain, M. K.; Wu, N. M., Effect of Small Molecules on the Dipalmitoyl Lecithin Liposomal Bilayer: Iii. Phase Transition in Lipid Bilayer. *The Journal of Membrane Biology*, *34*, 157-201.

161. Schiffer, J. M.; Mael, L. E.; Prather, K. A.; Amaro, R. E.; Grassian, V. H., Sea Spray Aerosol: Where Marine Biology Meets Atmospheric Chemistry. *ACS Central Science* **2018**, *4*, 1617-1623.

162. Clark, G. A.; Henderson, J. M.; Heffern, C.; Akgün, B.; Majewski, J.; Lee, K. Y. C., Synergistic Interactions of Sugars/Polyols and Monovalent Salts with Phospholipids Depend Upon Sugar/Polyol Complexity and Anion Identity. *Langmuir* **2015**, *31*, 12688-12698.

163. Horta, B. A. C.; Perić-Hassler, L.; Hünenberger, P. H., Interaction of the Disaccharides Trehalose and Gentiobiose with Lipid Bilayers: A Comparative Molecular Dynamics Study. *Journal of Molecular Graphics and Modelling* **2010**, *29*, 331-346.

164. Pereira, C. S.; Hünenberger, P. H., The Influence of Polyhydroxylated Compounds on a Hydrated Phospholipid Bilayer: A Molecular Dynamics Study. *Molecular Simulation* **2008**, *34*, 403-420.

165. Tanaka, Y.; Takei, T.; Aiba, T.; Masuda, K.; Kiuchi, A.; Fujiwara, T., Development of Synthetic Lung Surfactants. *Journal of lipid research* **1986**, *27*, 475-485.

166. Crowe, J. H.; Oliver, A. E.; Comparative, F. T. I. a.; 2002, Is There a Single Biochemical Adaptation to Anhydrobiosis? *academic.oup.com*.

167. Crowe, L. M., Lessons from Nature: The Role of Sugars in Anhydrobiosis. *Comparative biochemistry and physiology. Part A, Molecular & integrative physiology* **2002**, *131*, 505-513.

168. Nagase, H.; Ueda, H.; Nakagaki, M., Effects of Sonication on the Lamellar Structures of L-Alpha-Dipalmitoyl Phosphatidylcholine(Dppc)/Saccharide/Water Systems. *Chemical & Pharmaceutical Bulletin* **1999**, *47*, 1355-1362.

169. Ohtake, S.; Schebor, C.; de Pablo, J. J., Effects of Trehalose on the Phase Behavior of Dppc–Cholesterol Unilamellar Vesicles. *Biochimica et Biophysica Acta (BBA) - Biomembranes* **2006**, *1758*, 65-73.

170. Lenné, T.; Bryant, G.; Holcomb, R.; Koster, K. L., How Much Solute Is Needed to Inhibit the Fluid to Gel Membrane Phase Transition at Low Hydration? *Biochimica et biophysica acta* **2007**, *1768*, 1019-1022.

171. del C Luzardo, M.; Amalfa, F.; Nuñez, A. M.; Díaz, S.; de Lopez, A. C. B.; Disalvo, E. A., Effect of Trehalose and Sucrose on the Hydration and Dipole Potential of Lipid Bilayers. *Biophysical Journal* **2000**, *78*, 2452-2458.

172. Márquez, M. J.; Romani, D.; Saud, S. D. J. o. K.; 2018, Structural and Vibrational Characterization of Anhydrous and Dihydrated Species of Trehalose Based on the Ftir and Ftraman Spectra and Dft Calculations. *Elsevier* **2018**, *30*, 229-249.

173. Interaction of Carbohydrates with Dry Dipalmitoylphosphatidylcholine. *Archives of Biochemistry and Biophysics* **1985**, *236*, 289-296.

174. Leekumjorn, S.; Sum, A. K., Molecular Dynamics Study on the Stabilization of Dehydrated Lipid Bilayers with Glucose and Trehalose. *The Journal of Physical Chemistry B* **2008**, *112*, 10732-10740.

175. Venable, R. M.; Skibinsky, A.; Pastor, R. W., Constant Surface Tension Molecular Dynamics Simulations of Lipid Bilayers with Trehalose. *Molecular Simulation* **2006**, *32*, 849-855.

176. Link, K. A.; Spurzem, G. N.; Tuladhar, A.; Chase, Z.; Wang, Z.; Wang, H.; Walker, R. A., Cooperative Adsorption of Glucuronic Acid to Dppc Monolayers Studied with Vibrational Sum Frequency Generation. *Journal of Physical Chemistry C* **2019**, *Submitted*.

177. Márquez, M. J.; Romani, D.; Saud, S. D. J. o. K.; 2018, Structural and Vibrational Characterization of Anhydrous and Dihydrated Species of Trehalose Based on the Ftir and Ftraman Spectra and Dft Calculations. *Elsevier*.

178. Adams, E.; Allen, H., Palmitic Acid on Salt Subphases and in Mixed Monolayers of Cerebrosides: Application to Atmospheric Aerosol Chemistry. *Atmosphere* **2013**, *4*, 315-336.

179. Pili, B.; Bourgaux, C.; Meneau, F.; Couvreur, P.; Ollivon, M., Interaction of an Anticancer Drug, Gemcitabine, with Phospholipid Bilayers. *Journal of Thermal Analysis and Calorimetry* **2009**, *98*, 19-28.